PD-LJ-76-132
REVISED

(12)

physical dynamics, inc.

X-RAY LASER APPLICATIONS STUDY

SEMIANNUAL TECHNICAL REPORT
APRIL 1976 - OCTOBER 1976

CONTRACT N00173-76-C-0151
ARPA ORDER 2694

NOVEMBER 1976

SPONSORED BY
DEFENSE ADVANCED RESEARCH PROJECTS AGENCY
MATERIALS SCIENCES DIVISION
ARLINGTON, VA 22209

UNCLASSIFIED

SECURITY CLASSIFICATION OF THIS PAGE (When Data Entered)

REPORT DOCUMENTATION PAGE		READ INSTRUCTIONS BEFORE COMPLETING FORM
1. REPORT NUMBER	2. GOVT ACCESSION NO.	3. RECIPIENT'S CATALOG NUMBER
4. TITLE (and Subtitle) X-Ray Laser Application Study		5. TYPE OF REPORT & PERIOD COVERED Semiannual April 1976 - October 1976
		6. PERFORMING ORG. REPORT NUMBER PD-LJ-76-132
7. AUTHOR(s) S. Jorna, et al.		8. CONTRACT OR GRANT NUMBER(s) N00173-76-C-0151 ARPA Order 2694
9. PERFORMING ORGANIZATION NAME AND ADDRESS Physical Dynamics, Inc. P. O. Box 556 La Jolla, CA 92038		10. PROGRAM ELEMENT, PROJECT, TASK AREA & WORK UNIT NUMBERS
11. CONTROLLING OFFICE NAME AND ADDRESS Defense Advanced Research Projects Agency Arlington, VA 22209		12. REPORT DATE November 1976 13. NUMBER OF PAGES 207
14. MONITORING AGENCY NAME & ADDRESS(if different from Controlling Office) Naval Research Laboratory Interaction Physics Branch Optical Sciences Division Washington, D.C. 20375		15. SECURITY CLASS. (of this report) Unclassified 15a. DECLASSIFICATION/DOWNGRADING SCHEDULE

16. DISTRIBUTION STATEMENT (of this Report)

DISTRIBUTION STATEMENT A
Approved for public release;
Distribution Unlimited

17. DISTRIBUTION STATEMENT (of the abstract entered in Block 20, if different from Report)

18. SUPPLEMENTARY NOTES

19. KEY WORDS (Continue on reverse side if necessary and identify by block number)

x-ray laser applications
x-ray sources

20. ABSTRACT (Continue on reverse side if necessary and identify by block number)

This report is concerned with potential applications of x-ray lasers. The program is supported by ARPA and monitored by NRL. Applications considered in detail are ESCA (electron spectroscopy for chemical analysis), x-ray holography, production of micro-electronic circuitry by lithography, x-ray microscopy, metallurgical uses, medico-radiology, radiation chemistry, and effect on nuclear decay rates. The relative merits of x-ray lasers over presently available sources such as synchrotrons and laser plasma sources are also being studied under this program.

DD FORM 1 JAN 73 1473 EDITION OF 1 NOV 65 IS OBSOLETE

UNCLASSIFIED

(14) PD-LJ-76-132

REVISED

(6) # X-RAY LASER APPLICATIONS STUDY.

(9) SEMIANNUAL TECHNICAL REPORT,

APRIL 1976 — OCTOBER 1976

(10) PRINCIPAL INVESTIGATOR: S. JORNA

PHYSICAL DYNAMICS, INC.
P. O. Box 556
LA JOLLA, CA 92038

(15) CONTRACT N00173-76-C-0151,
ARPA ORDER-2694

(11) NOVEMBER 1976

(12) 209 p.

SPONSORED BY
DEFENSE ADVANCED RESEARCH PROJECTS AGENCY
MATERIALS SCIENCES DIVISION
ARLINGTON, VA 22209

PREFACE

Potential applications of x-ray lasers cover many areas in physics, chemistry, and technology. This variegation is reflected in the present study to which several workers have contributed. The contributors to this part of the study were:

Dr. N. A. Bailey, Radiology Department, University of California, San Diego

Dr. J. Galligan, Department of Metallurgy, University of Connecticut, Storrs

Dr. C. G. Gardner, Southwest Research Institute, Texas

Dr. J. Hirth, Department of Metallurgical Engineering, Ohio State University

Dr. S. Jorna, Physical Dynamics, Inc., La Jolla, California

Dr. R. Mueller, Department of Electrical Engineering, University of Minnesota, Minneapolis

Dr. D. A. Shirley, Chemistry Department, University of California, Berkeley

Dr. W. Smith, Physics Department, University of Connecticut

Dr. P. A. Sullivan, Hughes Research Laboratories, Malibu, California

Dr. J. K. Thomas, Chemistry Department and Radiation Laboratory, University of Notre Dame, Indiana

Dr. G. T. Trammell, Physics Department, Rice University, Texas

ABSTRACT

This report is concerned with potential applications of x-ray lasers. The relative merits of x-ray lasers with respect to presently available sources for the various applications are also discussed.

TABLE OF CONTENTS

SUMMARY AND CONCLUSIONS

In this study on potential applications of x-ray lasers we have attempted to answer the question: "Suppose an x-ray laser can be built, what are its most likely applications?" In answering this question we have for the most part assumed that a laser can be built to specifications suitable for each application. The only constraints that have been imposed on the parameters are those governed by the physical processes giving rise to lasing. This is not to imply that these requirements will be easy to meet. For example (Section 1), from the Larmor radiation condition it follows that the lifetime of an inverted state is about $10^{-15}\ \lambda_{\text{Å}}^2$, where $\lambda_{\text{Å}}$ is the wavelength in Ångstroms, so that a 1 Å (12 keV) transition requires a power of 2 W per atom. Taking the traveling wave scheme suggested by Shipman (1967) as an example, a natural design for the lasing material is a 1 cm long thread of 1 μm in diameter and density 10^{20} atoms/cm^3. The power requirement is then 10^{12} W corresponding to an energy requirement of 10^{12} × 30 psec (the time taken by the light to travel 1 cm) = 30 J. These are realizable numbers and since, furthermore, other laser schemes mentioned in Section 1 depend on longer-lived metastable states with reduced power requirements, it seems reasonable to assume for some applications a 1 Å laser beam of 1 μm diameter and collimation of the order of 0.1 mrad. The losses in converting pump energy first into x-ray energy and then into lasing energy will, of course, raise the energy requirement further.

Justification for the development of a new tool must inevitably involve a determination of whether already existing resources can do the job as well. Some space has, therefore, been devoted (Section 2) to a description of alternative sources. The most promising of these is the electron synchrotron or electron storage ring. Some of the bigger machines provide a continuum

of radiation from < 1 Å to > 1000 Å with intensities comparable to, and in some instances higher than, those obtainable from more conventional sources. Synchrotron light has the further merits of being highly polarized and of emerging as a beam that is well-collimated, at least in one plane. Further, its intensity is well-defined in terms of the machine parameters, a quality that renders this beam particularly attractive for detector calibration. Some of its features are in fact so closely related to those expected from an x-ray laser that in our assessment of some laser applications we have been guided markedly by the uses to which synchrotron radiation has already been put. The question now, of course, arises: what then are the unique qualities of an x-ray laser beam likely to be? These are discussed fully in the various parts of this report. Briefly, they should be intensity, beam diameter, monochromaticity, pulse length and coherence. Monochromaticity, for example, is of great importance to the study of the chemical state of elements. X-ray lasers by the very process of lasing will yield extremely narrow lines, whereas synchrotron radiation, being continuous, must first be monochromatized by methods generally limited by natural linewidths. The intensity of light from an x-ray laser will be orders of magnitude higher than synchrotron radiation when measured in W/cm^2-Å at a single wavelength and over a small area. However, for exposing fine-grain media over large areas a broad spectrum of synchrotron radiation may contribute to the exposure and result in an effectively shorter exposure time. Also, the proposed use of a helical wiggler (Kincaid 1976) may increase the brightness of synchrotron radiation from an electron storage ring by several orders of magnitude at a single wavelength. Also, the x-ray laser beam

is highly collimated in both planes. It is these unique attributes that together have motivated this search for applications of x-ray lasers.

In Sections 3-12 are described the main areas in which x-ray lasers may conceivably be useful. The order of presentation is largely arbitrary and was dictated more by when each topic was studied than by any predetermined arrangement by importance. We shall deviate here from that plan to present first those areas of application where an x-ray laser will be an especially useful tool.

In Electron Spectroscopy for Chemical Analysis (ESCA; Section 6) the kinetic energy distribution of electrons generated near the surface by an incident flux of x-rays is studied to determine the elemental composition (and chemical state) of the surface of a specimen. The electrons may be produced as photoelectrons (conventional ESCA) or as Auger electrons, emitted when holes are filled. The main difficulties with most x-ray sources in current usage are their lack of intensity and, for determining chemical shifts less than $\sim$1 eV, the minimum linewidth ($\sim$1 eV) of the radiation. The lack of intensity leads to long exposure times needed to acquire accurate information. The linewidth, limited by the natural linewidth for conventional x-ray tubes and by the monochromator pass-band when synchrotron radiation is used, sets a lower limit on the resolvable chemical shifts which in, say, some carbon compounds is a small fraction of an eV. An x-ray laser would provide photon fluxes orders of magnitude higher than even the highest-current electron storage rings. Even a single laser pulse could with suitable detectors and data acquisition techniques provide a complete electron spectrum (often requiring days of conventional

operation). Linewidths of 0.1-0.01 eV, produced by gain narrowing, should lead to the precise determination of core-level chemical shifts in molecules containing more than one atom of the same element in slightly different chemical environments. Several examples of the usefulness of such information to catalysis, metallurgy, and the study of organic compounds are given in Section 6.5.1. A further advantage of great potential significance is the possibility of exploiting the laser beam's small diameter in microprobe analysis. Such Selected Area Electron Spectroscopy could be applied to the analysis of fracture surfaces of high-strength alloys as two-phase composite materials. A number of microprobe shots of the specimen's surface followed by electron microscope magnification could yield information on the surface distribution of elements and their chemical state. But the beam's small diameter may also be one of its drawbacks. The high fluxes calculated for a typical laser could destroy the sample. Estimates of damage thresholds and some ways around this problem are given in Section 6.2. Absorption spectroscopy requires tunability so that an absorption edge can be straddled. The high intensity of the laser radiation makes the photon mixing scheme suggested by Eisenberger and McCall (1971) entirely feasible. Tunability over energies of the order of eV's therefore should present no problem.

In summary, the features that render an x-ray laser particularly attractive for ESCA work are the high radiation intensity and narrow linewidth. Coherence (except for the link between coherence length and linewidth) and a high degree of collimation do not appear to be requirements. Because only one core-level peak of any element needs to be observed (no

significant further information is obtained from deeper levels) it is unnecessary to employ photon energies exceeding 1 keV (for neon E_B = 870 eV). On the other hand, for optimum analytical capability, the photons must not be much less energetic. A 10 Å laser would thus be adequate.

High-resolution lithography (Section 3) is one of the more promising applications. For resolution better than 1 μm to be obtained the contact print must be recorded on grainless media whose sensitivity varies from 10-1000 mJ/cm^2 in the 5-100 Å wavelength range. Negative resists, in which polymerization is induced by the radiation, have the highest sensitivity but this is accompanied by a decrease in resolution resulting from chain reactions. A lower limit on the useful wavelength is likely to be set by the range of secondary or photo-electrons. For the typical positive resist PMMA (polymethyl methacrylate) 1 keV photo-electrons have a range of about 0.05 μm, increasing approximately as the square of the photo-electron energy. The useful wavelength will then be limited for sub-micron work to $\lambda \gtrsim 5$ Å. One of lithography's main applications is the replication of micro-electronic components with linewidths down to 0.1 μm which would utilize wavelengths in the 5-50 Å range. Examples of particular micro-electronic devices are discussed in Section 3.6. The advantages of such devices are essentially two-fold: the closer tolerances make possible closer spacing of active elements and the fabrication of more complex circuitry with less material and fewer interconnections, resulting in increased reliability and lower cost per function; the closer element spacing is also of more fundamental significance in that the reduced linewidths allow improved device performance, e.g., logic gates with

speed power products of 0.01 pJ and surface transducers operating at higher frequencies than hitherto possible, extending into the 10 GHz region with 0.1 μm linewidths (above 10 GHz the material properties limit the performance of SAW devices). Losses in integrated optics will, of course, also be less with increased edge smoothness (∿0.05 μm) because of reduced scattering.

The application of conventional sources has been disappointing primarily because the low sensitivity of the resist material requires inordinately long exposures. These range from tens of minutes to as long as many hours. Further, the resolution with these sources is limited by geometrical distortion, a function of the gap between the mask and substrate (S), and by penumbral blurring which depends in addition on the angular extension of the source. Penumbral blurring can be reduced by decreasing the size of the source or by increasing the source-mask separation (D). Both cures lessen the effective flux on the mask: the former because of power dissipation limitations, the latter by the $1/D^2$ decrease in x-ray flux. Ideally, then, one needs a beam of high intensity and excellent collimation. The x-ray laser would provide just such a beam, with the additional advantage that the wavelength could be tailored to the absorption characteristics of the mask and resist materials. As a simple example, a beam divergence of a mrad yields a negligible geometric distortion of 10^{-3} times the mask-substrate gap and a penumbral blurring of 10^{-4} S/D for a μm diameter beam.

The short pulse emitted from an x-ray laser may have sufficient intensity to expose the resist material in one pulse but it will introduce a thermal spike in the mask and substrate. The intensity must be controlled

in order to prevent materials damage. Also the small beam diameter must be expanded to cover approximately a 1 to 10 cm diameter area for many lithography applications.

Turning now to metallurgical applications (Section 5), we must distinquish between surface and volume studies. The study of metal surfaces does not require penetration and radiation in the 10 Å regime probably suffices. Volume studies require penetration: for example, mm penetration in copper requires a wavelength of 1 Å, in platinum 0.5 Å radiation is required. In surface studies a small diameter laser beam would be particularly useful in the accurate determination of dislocation cell structure (important in studies on the effect of wear on metal surfaces) and crack formation as we have already mentioned. For small depth gauging of this kind it is often useful to operate near an absorption edge, and monochromaticity becomes an asset in discriminating against fluorescence. In this respect the laser should be preferable to a synchrotron whose radiation when monochromatized inevitably contains the higher orders. Filtering leads to additional intensity loss emphasizing still further the laser's advantage. Monochromatic radiation (at wavelengths straddling an absorption edge) is also useful for studying the presence of voids by differential absorption, and in quality control of infrared mirrors by comparison of diffraction line shapes. For these applications the main requirements should be intensity, beam size, and wavelength (< 1 Å for penetration studies). Coherence and intensity become prime requisites for the holographic determination of the size and shape of interior flaws and their orientation with respect to other structures. Of course, the wavelength must again be short enough for penetration.

Holography (Section 7) has been widely mentioned as an application of x-ray laser radiation. We have already referred to its use in imaging internal structures in metals, a concept that can, of course, be extended to the examination of biological (cf., Section 4) and other materials, provided the wavelength be chosen to provide enough penetration and sufficient contrast. But the most intriguing promise of x-ray holography has been the possible direct visualization in three dimensions of the structure of complex biological molecules. This calls for a resolution of the order of Ångstroms and multiple exposures with alignment precision to similar tolerances. The most severe argument against its feasibility is the required radiation load on the object molecule brought about by the resolution requirement and the finite size and separation of the detector elements. This raises the photon fluxes to such high levels that the object under investigation will almost certainly be destroyed. By-passing this problem by the use of spherical reference waves assumes the existence of zone plates with Ångstrom resolution. But the holographic production of such plates requires an Ångstrom-sized source which itself might then as well be used to image the object directly by contact or projection microscopy (Section 10). An exception is phase objects which do not lend themselves readily to such techniques. In that case the imaging becomes essentially phase contrast microscopy. Holography on atomic dimensions may, nevertheless, be feasible when the radiation load is distributed over a large number of identical object distributions as with holograms of two-dimensional periodic structures.

Microscopy (Section 10) should be a fruitful area of application. In the absence of refractory elements the basic techniques are, of course,

contact and projection (pinhole) radiography. Several examples have already been mentioned. The laser would have advantages over other x-ray sources in intensity and beam collimation. High intensity allows short exposure times so that the movement of, say, a biological specimen does not lead to image degradation. Good beam collimation implies that the resolution limit is set by Fresnel diffraction rather than by finite source effects. The study of biological specimens would probably require wavelengths of 10 Å or higher to achieve sufficient contrast. At 10 Å the half-value layer is about 0.5 cm for air and about 5 μm for C. This means that the specimen can be examined in vivo without stringent vacuum requirements, but, also, that the resolution is limited to about 0.02 μm, the minimum Fresnel fringe width for these parameters. Ten Å is in any case as low as one wants to go in wavelength because of the increased range of photo-electrons (∿1 μm at 10 kV) at higher photon energies. Realizing that the resolution would be limited to about 0.01 μm with the image magnified by electron microscopy, we preceive that the advantages of an x-ray laser beam over other x-ray sources are its intensity and collimation, and over an electron microscope the possibility of in vivo visualization of structures the size of fine detail in viruses which are beyond the range of optical microscopy. The greater penetration of x rays also means that thicker specimens can be examined than with an electron microscope.

Medical radiography (Section 4) is an interesting candidate for x-ray laser applications. Discussed are differential absorption measurements to obtain the distribution of elements in various organs (e.g., iodine in the thyroid gland, osteoporosity), holographic imaging for the localization of,

say, tumor masses, and rapid elemental analysis of cells by microphotometry and fluorescence. Except for the last-named, these applications all require penetration through cm of tissue, and hence photon energies well in excess of 10 keV.

In the area of radiochemistry (Section 9) the main attributes of x-ray laser radiation will be the short pulse times (10^{-15} - 10^{-12} sec) and the high intensity. Short pulse times will be useful for the observation of very short-lived chemical species such as higher excited states and for the measurement of rapid initial reaction rates where chemical species are highly concentrated. Rapid relaxation processes, such as solvation, could also be studied in the sub-picosecond regime. Intensity must be high to produce sufficient linear energy transfer and hence chemical change. Reasonable penetration through sample containers requires operating wavelengths shorter than 1 Å (H.V.L. for H_2O at 1 Å ≃ 1 mm). It is in principle possible to dissociate compounds with the aid of x rays. This might be used, for example, to produce hydrogen and oxygen from water. However, the expected inefficiency of x-ray production by a laser is such that this does not appear to be economically worthwhile for fuel production.

The remaining sections of this report contain a number of further possible applications none of which by itself would justify the building of a laser, but which are deemed of sufficient interest for inclusion. Inelastic scattering of x-rays from metal surfaces can yield very accurate information about the location of Fermi surfaces. Synchrotron radiation has been used in the 8 Å region, but only weak signals were obtained. For statistically more significant work higher photon fluxes such as would be provided by an x-ray laser are required in the 1 - 10 Å regime. The

possibility of producing heavy ions in high charge states at low temperature could have an important impact on the quality of ion beams. Often such ions are produced in Saha equilibria at high temperatures with significant transverse velocities which limit the achievable beam quality. The production of ions with small transverse velocities (cold ions) should yield beams of greatly reduced divergence, an important factor for long distance propagation.

It is clear that x-ray lasers would be useful in a variety of disciplines. There are a number of disadvantages, however. These vary with the application. If we assume that a 1 - 10 TW laser is required for a pump, the resulting installation is not only going to be expensive (10^6 - 10^7) but also exceedingly bulky. It is, therefore, unlikely that the laser will have economic applications in industry in the near term. Rather, as for the synchrotron, the installation should be set up for use by many groups. Even then, most applications would probably be in the fundamental research program areas rather than applied technology such as x-ray lithography for microcircuit fabrication. The bulkiness of the device precludes its use in the field, a significant restriction for some metallurgical uses. The intensity, as we have seen, may be undesirably high if the beam's small diameter is to be fully exploited. Techniques for overcoming this problem, perhaps with beam splitters, need further study. Also, the pulse repetition rate, set by that of the pump, may be undesirably low resulting in a lower time-integrated flux than can be obtained from a synchrotron, say.

It does not appear that x-ray laser radiation will have special advantages over synchrotron radiation in the study by x-ray diffraction

of crystals down to sizes of the order of 0.1 mm. To cover the sample the laser beam must be allowed to expand from a 1 μm initial diameter to 0.1 mm. The intensity loss of four orders of magnitude reduces the beam intensity to that obtainable from some of the more energetic storage rings. Coherence may also not be an important advantage as phase information can be obtained, at least in principle, by the three-wavelength procedure discussed by Herzenberg and Lau (1967). The short pulse time, however, may be important in studying crystal imperfections because of the freezing of lattice vibrations. For diffraction studies on microscopic crystals the μm diameter beam of a laser and the great intensity could be advantages. Potential problems are mounting the specimen and the ability of the structure to withstand the radiation load. On the latter point, the surprisingly high radiation tolerance of some organic crystals to monochromatized synchrotron radiation is encouraging. These matters will be considered in greater detail in a subsequent report.

1. INTRODUCTION

In a study on the applications of x-ray lasers it seems natural to discuss some of the concepts that have been proposed for the actual construction of such devices. Before one can reasonably assess possible areas of application, it is useful to have some idea of plausible parameters such as beam size, degree of collimation, intensity, wavelength, etc., for eventual x-ray lasers. Many schemes have been proposed. Some are more realistic than others, and we will confine ourselves in this brief survey to the more extensively analyzed ones. We will avail ourselves freely of the extensive review recently prepared by Waynant and Elton (1975) and the references given therein.

1.1 Pumping Requirements

A rough idea of the magnitude of the difficulties facing a builder of x-ray lasers is already gained by calculating the pump power requirements for producing an inverted population between two core electronic states (Schawlow and Townes 1958). This is readily obtained from the rate equations for an atom which spontaneously emits photons into a particular mode (A) at a rate R. If $N_{2,n}$ is the occupation number of the atom n in its excited state (2) and $N_{1,n}$ the corresponding occupation number of the lower state (1), the rate of change of the photon population n due to spontaneous and stimulated emission and stimulated absorption is just

$$\frac{dn}{dt} = -\alpha n + \sum_{k=1}^{N} R(N_{2,k} - N_{1,k})n + \sum_{k=1}^{N} RN_{2,k} , \qquad (1)$$

where $-\alpha n$ is the loss rate due to scattering processes, etc., and the summation is over all atoms. Usually we may neglect the rate of spontan-

eously emitted photons because n is large, and if we also assume that R does not depend on k, laser action takes place for dn/dt > 0 or

$$R\Delta N > \alpha \ . \tag{2}$$

To calculate R let the radiative lifetime of an atom be τ so that τ^{-1} photons are emitted spontaneously per second per atom. We are interested in photons emitted into a particular mode in a frequency interval $\Delta\nu$ so that we must divide τ^{-1} by the number of modes there are in $\Delta\nu$, the spontaneous line width of the atom. There is a discrete mode in each h^3 volume of phase space so that the number of modes required is given by

$$\int \frac{dp\ dq}{h^3} = \frac{4\pi}{3}\left(\frac{h\nu}{c}\right)^3 \frac{V}{h^3} \ , \tag{3}$$

where V is the volume containing the photons. The number of photons radiating into $\Delta\nu$ in one mode is therefore

$$R = \frac{c^3}{4\pi\tau V\nu^2\Delta\nu} \ . \tag{4}$$

More accurately, there is a factor of order unity multiplying Equation (3) whose value depends on the line shape. From Equation (2) the laser condition becomes

$$g \equiv \frac{c^3(\Delta N/V)}{4\pi\tau\nu^2\Delta\nu} > \alpha \ . \tag{5}$$

The left hand side is essentially c times the gain cm^{-1} so that if we take 100 small gain lengths for reasonable operation, the required inversion density for a length ℓ of the lasing column is

$$N^* > 100 \frac{4\pi\tau\Delta\nu}{\lambda^2 \ell} . \tag{6}$$

An estimate for τ follows from Larmor's expression for the average power P_L radiated by a dipole oscillating at frequency ω:

$$P_L = \frac{1}{3} \frac{e^2\omega^4}{c^3} |x|^2 , \tag{7}$$

with x the displacement. This is balanced by the rate at which the energy of the harmonic oscillator changes. Thus

$$\frac{1}{2} m\omega^2 \frac{d}{dt} |x|^2 = -\frac{1}{3} \frac{e^2\omega^4}{c^3} |x|^2 , \tag{8}$$

corresponding to a decay rate

$$\gamma = - \frac{1}{|x|^2} \frac{d}{dt} |x|^2 = \frac{2r_0}{3c} \omega^2 , \tag{9}$$

where $r_0 = e^2/mc^2 = 2.8 \times 10^{-13}$ cm is the classical electron radius. In terms of the wavelength λ this yields in convenient units

$$\tau \simeq \frac{2}{\gamma} \simeq 10^{-15} [\lambda(\mathring{A})]^2 . \tag{10}$$

This expression is only approximately valid to the extent that there are oscillations in a growth period. This means $\gamma << \omega$ which corresponds to assuming that the wavelength of the radiation is much larger than r_0. We note from Equations (6) and (10) that the wavelength dependence cancels (except through its presence in $\Delta\nu$) and the gain condition becomes (cf., Duguay 1973, Chapline and Wood 1975)

$$N^* \gtrsim \frac{\Delta\nu}{\ell} \; 10^{18} \; \text{cm}^{-3} \tag{11}$$

with $\Delta\nu$ in eV and ℓ in cm. We have denoted by N^* the net population inversion density ($\Delta N/V$); if the levels 1 and 2 have statistical weights g_1 and g_2 this is modified to $N^*V \equiv N_2 - (g_2/g_1)N_1$. The minimum linewidth $\Delta\nu$ depends on the temperature and density of the lasing medium. For instance, in cold matter $\Delta\nu$ is governed mainly by Auger auto-ionization, while at high density and temperature Stark broadening may dominate while at low density Doppler broadening sets the lower limit (Griem 1964, 1974).

It is now possible to assess the difficulties that must be overcome before x-ray lasing can be achieved. A serious handicap is the absence of efficient reflectors at x-ray wavelengths which means that the needed amplification must occur in one pass through the medium and one must rely on superradiance (Dicke 1954, 1964), or amplified spontaneous emission (Allen and Peters 1970, 1971). Due to the short lifetime ($10^{-15} \; \lambda_{\text{Å}}^2$) the pumping power is exceedingly high; a 12 keV (1Å) transition requires a pumping power of $(1.2 \times 10^4)(1.6 \times 10^{-19})/10^{-15} \simeq 2$ W/atom. For gain the inversion density must be of the order of $10^{18}/\ell \; \text{cm}^{-3}$ for a typical $\Delta\nu = 1$ eV

(Auger width) in cold matter. In the travelling wave scheme in which the laser amplifies its own spontaneous emission (Shipman 1967, Chapline and Wood 1975) the pump power requirement is given as

$$P_{pump} = h\nu N^* \frac{d^2 c}{\varepsilon} , \qquad (12)$$

which is just the requirement that the total energy requirement $h\nu N^* V$ be supplied in the time ℓ/c with a pumping efficiency ε. In the diffraction limit $d = (\lambda\ell)^{\frac{1}{2}}$ this corresponds to $P_{pump} \simeq 1GW$ with $\Delta\nu = 1$ eV and $\varepsilon = 10^{-3}$. For $\ell = 1$ cm this would yield a 1 μm x-ray beam at 1 Å with a divergence measured in fractions of a mrad. Because of matching and focusing inefficiencies one obtains the more realistic figure of 1 TW for pumping a 10 Å laser. Photo-electric absorption, of course, sets a further constraint on the maximum gain and amplifying length achievable in practice.

1.2 Lasing Schemes

Duguay (1973) considers direct pumping with x-rays harder than the K-shell ionization energy of copper (9 keV), relying on inversion due to the different cross-sections for creating K-shell and L-shell vacancies (Duguay and Rentzepis 1967, Stankevich 1970). Comparison with the much smaller photoionization cross-section leads to a power flux requirement for copper of 10^{17} W/cm^2 which can just be reached with present-day terawatt lasers (10 J in 10 psec) focused down to a 30 μm spot. This estimate does not allow for conversion inefficiencies in the conversion of infrared to x radiation (Malozzi et al. 1973).

To suppress Auger autoionization it has been proposed to utilize the longer lifetimes of metastable states of low-Z materials such as lithium

in a two-step process (Drake et al. 1969, Mahr and Roeder 1974, Vekhov et al. 1975). Typically, a high-intensity laser produces a plasma whose x-radiation preferentially photoionizes a K-shell electron producing highly-excited atoms in the 1s 2s state but which is not sufficiently energetic to undergo Auger autoionization. Since the effective metastability time of the ion in the lasing medium can be much longer than the Auger lifetime, reduced pumping powers become feasible. The required inversion density only achieves acceptable levels in the absence of depleting processes such as collisional de-excitation. Since these are bound to occur, gain is inevitably reduced and one must remain skeptical about metastable lasing. Another scheme (Wood et al. 1973, 1974) depends on rapid adiabatic decompression and cooling of a laser-heated fiber to produce an inversion by collisional recombination. Collisional recombination is expected to dominate over radiative recombination leading to preferential population of the higher states. A full computer calculation must verify this scheme. This also applies to other proposed methods for which the calculations have often ignored such physical processes as hydrodynamics, pump coupling, possible excitation of instabilities, radiative recombination, etc.

Several other schemes for producing population inversion have been cited in the literature. Examples are electron collisional excitation of rare gas excimers (Rhodes 1974, Lorents 1974), ion lasers by electron collisions (Elton 1975, Andrews 1975), atom-ion resonance charge transfer (Louisell et al. 1975, Scully et al. 1973, Vinogradov and Sobelman 1973), free-electron lasers (Pantell et al. 1968, Madey 1971, Madey et al. 1973), etc. Many of these schemes can only be expected to penetrate into the VUV

region, while others remain speculative due to inadequate computer modeling. This applies also to the free-electron laser in which lasing is expected from the stimulated emission by transitions between electron continuum states, a process closely related to traveling-wave amplifiers (Motz and Nalsurnura 1960), and the backscattered Compton photons from relativisitc electron beams which as polarized monochromatic x-rays have found research applications (Sinclair et al. 1969). Unfortunately, the gain for these processes is a strong function of the wavelength of the emitted wavelength and it appears doubtful that intense x-ray sources can be produced by this approach (cf., Kroll 1975). More particularly, the increase in the frequency of the incident light is due to the energy of the electrons in the beam. For a collinear collision with the incident laser beam directed oppositely to the electron beam, the frequency of the scattered photons ω_2 is related to the frequency of the incident photons ω_1 and the energy of the electrons E by

$$\omega_2 \simeq 4\,\omega_1 (E/mc^2)^2 = 16\,\omega_1\,[E(MeV)]^2 \ .$$

The effective gain, α, for the scattered radiation has been expressed by Pantell et al. (1968) in terms of the photon density, n_f, the electron density of the beam, n_e, and the width of the energy scatter of the beam electrons. They find

$$\alpha \simeq 0.7\, r_0^2 \left(\frac{E}{\Delta}\right) \left(\frac{\hbar\omega_2}{\Delta}\right) \lambda_1 \lambda_2^2\, n_e n_f \ ,$$

where r_0 is the classical electron radius e^2/mc^2. As an example, take (cf., Molchanov 1972) $\hbar\omega_1 = 1.17$ eV and $n_f = 2 \times 10^{22}$ cm^{-3} for a neodynium glass laser and for the electrons E = 2 MeV, $E/\Delta = 10^5$ and $n_e = 2 \times 10^{13}$ cm^{-3} corresponding to a beam current density of about 10^5 A/cm^2. These values yield a gain of 2.2 cm^{-1} at a wavelength of $\sim$170 Å. These and other schemes for obtaining x-ray lasing action have been treated and documented in full by Waynant and Elton (1976).

1.3 Parametric Up-Conversion

A technique which should be mentioned here that has produced coherent short wavelength radiation is that of up-converting signals from infrared or visible sources by exploiting nonlinearities in crystals or phase matching in metal vapors (Harris and Miles 1971, 1973). For sufficiently strong driving fields the dielectric constant and hence the polarization of many media becomes a function of the field strength. Since metal vapors have inversion symmetry, it is clear that the polarization can only be an odd function of the field so that only odd harmonics are produced. Since the conversion efficiency in such parametric processes is a function of the driving intensity (Bloom et al. 1975), it must be expected that one cannot penetrate very far into the x-ray wavelength region by this procedure, although tripling efficiencies approaching 40 percent can be achieved. In the region of 900 Å, about the shortest wavelength obtained so far, the efficiency is down to about 10^{-7}. Schemes reaching down into the soft x-ray regime have been proposed by Harris (1973) with an efficiency of 10^{-7} to 177 Å. Nevertheless, since the beam quality and coherence of the driving beam are maintained, the output beams in this region and down to 400-500 Å

will provide early testing of some applications now thought of in connection with x-ray laser beams such as holography and x-ray microscopy. Tunability can be obtained with photon mixing (Eisenberger and McCall 1971). An early example of a vacuum ultraviolet hologram is that described by Bjorklund et al. (1974) which shows features on the order of 800 Å. A difficulty which will remain with these non-lasing schemes is, however, the lack of intensity. This implies long exposure times of photoresist materials and only shallow modulation. Thus, any zone plates manufactured with these beams will only provide moderate image contrast. A further disadvantage is the large diameter of the emerging beam which precludes its use as a scanning microscope. Since the driving pulse sets the pulse width of the emerging beam, applications involving sub-pico second times which have been mentioned in connection with x-ray lasers are also excluded. Some typical output data that have been achieved in VUV holography experiments have been given by Bjorklund (1974). These experiments were carried out at the ninth harmonic of the 1.06 μm Nd:YAG laser line or at 1182 Å with pulses of 12 psec duration and an estimated coherence length of 0.4 cm. The available energy per pulse was about 0.3 μJ corresponding to 1.5 μW average power at a repetition rate of 5/sec. The recording medium was polymethyl methacrylate (PMMA) used extensively in electron beam lithography (Herzog et al. 1972) and as a positive resist material to x-ray radiation (Spears and Smith 1972). Coated layers of PMMA 1400 Å thick on quartz flats were then exposed to the interference pattern produced by the incident VUV beam and its reflection off a front surface mirror (Al + MgF_2 coating). Typical exposure times needed to modulate the PMMA were on the

order of 1000 sec involving superposition of fringe patterns produced by 5000 pulses. The minimum energy flux has been found to be 0.1 $\mu J/cm^2$ to obtain a fringe spacing of 836 Å with only moderate aspect ratio. Similar experiments were carried out for recording Fraunhofer holograms of μm sized spheres viewed with an electron microscope but image contrast remained poor. The use of the high-power lasers (1-100 TW) now being designed for laser fusion work should yield greater output resulting in reduced exposure times and improved image contrast, however, rendering this approach to coherent x-radiation extremely useful for testing some future applications of x-ray lasers.

1.4 X-Ray Laser Parameters

For the purpose of studying applications it is useful to have some guide as to the likely parameters of a future x-ray laser. In the near future pumping powers of short-pulsed lasers will probably be limited to the TW regime, i.e., 1 J in 1 psec or 10 J in 10 psec. In the interesting wavelength range of 10-1 Å the mode of operation will be that of amplified spontaneous emission with pulse lengths ranging from 10^{-13} - 10^{-15} sec (Duguay 1973). The active medium will be less than a cm in length and of the order of a μm in diameter, corresponding to a beam divergence measured in fractions of a mrad. The spatial coherence will be limited to a few thousand wavelengths at best while the temporal coherence will be set by the amount of gain narrowing that occurs. The line width may, however, be expected to be narrower than most conventional sources which normally have $\Delta\lambda/\lambda \simeq 10^{-4}$; the line width of the Al K_α line at 8.3 Å, for instance has a line width of 0.9 eV (Siegbahn 1972). The lasing medium in many suggested schemes will be a highly ionized, medium-Z plasma.

2. ALTERNATIVE SOURCES OF X RADIATION

For certain applications intensity and/or line width are important considerations, for others the combination of beam diameter and intensity is paramount. For any of these applications sources other than x-ray laser may be suitable. We will therefore review briefly the parameter ranges covered by such alternative sources as x-ray tubes, electron storage rings, and laser-driven plasmas.

2.1 Conventional Sources

The conventional source of x-rays is a point source created by electron bombardment of a target. A typical target for high power applications is a rotating aluminum target capable of dissipating 10 kW over a target area of about 0.1 cm^2. This produces 0.11 W/sr or a flux of 70 $\mu W/CM^2$ at a 40 cm distance at the Al K_α wavelength of 8.3 Å. Shorter wavelengths are produced by copper (K_α = 1.54 Å) and molybdenum (K_α = 0.71 Å) targets with a 0.1 cm^2 target area, accelerating voltage 50 kV, and electron beam current of 20 m A. These yield monoenergetic photon fluxes at the specimen of 10^{10} photons/cm^2sec or 13 $\mu W/cm^2$ at 1.54 Å and 28 $\mu W/cm^2$ at 0.71 Å. Typical line widths of these sources $\Delta\lambda/\lambda$ are in the range of 10^{-4} - 10^{-5}. More specifically, the inherent width of Al K_α line is approximately 0.9 eV which corresponds to $\Delta\lambda/\lambda \simeq 6 \times 10^{-4}$. Linewidth is of crucial importance in photoelectron spectroscopy where it is frequently desirable to measure chemical shifts to a fraction of an eV [Siegbahn (1967, 1972)]. More detailed information of conventional x-ray and XUV sources is given by Garton (1959, 1966), Samson (1967), and Balloffet et al. (1961). For a brief discussion of fine-focus x-ray tubes see Section 10.2.2.

2.2 Synchrotron Radiation

Synchrotrons have long been a useful tool for nuclear physicists in the study of the interaction between high energy electrons (or protons) and matter and as sources of γ rays in photonuclear studies. As the particles go along their circular orbits the centripetal acceleration causes them to lose energy in the form of radiation at a rate set by the Lorentz invariant relativistic generalization of Larmor's result for an accelerated charge

$$P = \frac{2}{3}\frac{e^2}{m^2c^3}\frac{dp_\mu}{d\tau}\frac{dp_\mu}{d\tau} \quad , \tag{1}$$

where m is the mass of the charge e, $\tau = t/\gamma$ is the proper time, and p_μ is the momentum-energy four-vector. For a rotational frequency ω in a circular accelerator, this leads to the result obtained by Liénard (1898)

$$P = \frac{2}{3}\frac{e^2c}{R^2}\beta^4\gamma^4 \quad , \tag{2}$$

since $\omega = v/R$ with R the orbit radius, $\beta = v/c$, and $\gamma = E/m_oc^2$ in terms of the particle energy E and its rest mass m_o. Clearly, electrons radiate far more effectively than protons. The energy loss per revolution per particle is just $P \times (2\pi R/v)$ or in convenient units

$$E\ (\text{keV/rev}) = 88.5[E(\text{Gev})]^4/R(\text{m}) \quad . \tag{3}$$

For a typical installation (NINA, GB) the electron energy E = 4 GeV and R = 20.77 m so that

$$\Delta E \simeq 1\ \text{Mev/rev} \quad . \tag{4}$$

The upper limit on the particle energy is set by the radiofrequency power which can make up for this radiative loss. This restricts operation to the 5 - 15 GeV range.

As a consequence of the relativistic motion of the charged particle, its radiation pattern changes from the sine-squared angular distribution of radiation from an accelerating dipole to one that is confined to a narrow cone around the forward direction of the motion. From the calculations of Schwinger (1946, 1949), the halfwidth of the angular distribuiton at half intensity is approximately given by

$$\Theta_{1/2} \simeq m_o c^2/E = 1/\gamma \qquad (5)$$

for wavelengths near the peak of the intensity versus wavelength curve. For E = 4 GeV, this yields for an electron synchrotron $\Theta_{1/2} \simeq 10^{-4}$ rad. Because the radiation is so narrowly confined to the forward direction an observer receives a pulse of radiation whenever the tangent to the orbit sweeps past at a rate

$$\nu' \sim \gamma c/R \quad . \qquad (6)$$

Because the emitting particle is moving towards the observer at relativistic speed, the actual frequency seen by the observer is Doppler shifted by $1/(1-\beta) \sim \gamma^2$. Consequently, the frequency detected by the observer is

$$\nu \sim \gamma^3 \, c/R \quad . \qquad (7)$$

Due to irregularities in the electron orbital velocity and betatron oscillations, the actual spectrum is a continuum with Eq. (7) giving the cut-off frequency. For $E \approx 4$ GeV($\gamma \sim 8000$) and $R = 20.77$ m, $\nu \sim 7 \times 10^{18}$ sec^{-1} corresponding to a wavelength of about 0.4 Å. A more detailed calculation by Tomboulian and Hartman (1956) yields for the critical wavelength

$$\lambda_c(A^o) = \frac{5.59\, R\,(m)}{[E(GeV)]^3} \quad , \tag{8}$$

or 1.8 Å for NINA at 4 GeV.

Unfortunately, in practice the narrow collimation of the radiation in the plane of the synchrotron orbit is lost as the particles orbit, though the strong angular dependence of the radiation above and below this plane remains. The detailed expressions for the instantaneous power radiated per sec per radian per unit wavelength have been obtained by Tomboulian and Hartman (1956). For our purposes it is sufficient to list the expression for the total power radiated into all angles at a given wavelength λ as

$$P(\lambda)(W/Å) = 7.5 \times 10^{-8} \frac{[E(GeV)]^7}{[R(m)]^3} G(y) \quad , \tag{9}$$

where $(y = \lambda_c/\lambda)$

$$G(y) = y^3 \int_y^\infty K_{5/3}(x)dx \tag{10}$$

is plotted in Codling (1973, p. 549). The maximum value of G is about unity, occuring near $\lambda = \lambda_c$.

Thus we can calculate the approximate output of a typical synchrotron such as NINA (E = 4 GeV, R = 20.77 m). The expressions given until now are for single electrons and to yield the total radiation power they must be multiplied by the number of accelerated particles (N) given by the average circulating current (I). For NINA, I = 20 mA and

$$N = \frac{1.3 \times 10^{8}}{\eta} I(\text{mA}) R(\text{m}) \quad , \tag{11}$$

where η is the duty cycle which ranges from as low as 0.1 at short wavelengths up to about 0.5 in the 100 Å regime (Codling 1973). For $\eta = 1/2$ we obtain for NINA that $N \sim 10^{11}$ electrons.

2.2.1 Synchrotron Flux at 100 Å and 1 Å

Let us calculate some typical outputs for NINA at 100 Å and 1 Å. From Table 2.1 the performance of other operational mechines can be similarly calculated. Equations (9) and (10) ($G \sim 10^{-4}$) yield for $N = 10^{11}$ and $\eta = 1/2$ so that the power emitted per Å at 100 Å is 0.7 W/Å corresponding to 3.5×10^{16} photons emitted per second per Å at 100 Å wavelength. The usable flux is much less than this because it is emitted around the entire orbit and the radiation at 100 Å must be separated from the rest of the spectrum. Also safety considerations restrict proximity to the tangent point on the orbit to distances (D) of tens of meters. Ignoring monochromator efficiency for the moment (see Section 2.4), we suppose that the beam is transversely collimated by a slit of width t at a distance D from the radiating volume. The fraction of radiation passing through the slit is then $t/2\pi D$. For t = 2 cm and D = 30 m this implies a loss factor of 10^{-4}. Vertical

Table 2.1. Important parameters for some electron storage rings and synchrotrons used as x-ray sources.

Accelerator	Energy (GeV)	Radius (m)	λ_c (Å)	Average Current (mA)
Synchrotrons				
DESY				
(Hamburg)	7.5	31.7	0.4	45
(Bonn)	2.3	7.7	3.5	27.5
Yerevan (USSR)	6.1	26	0.6	22
NINA				
(Daresbury)	4.0†	20.77	1.8	20
Storage Rings				
SPEAR				
(Palo Alto)	3.0	13	2.7	30
TANTALUS I				
(Stoughton)	0.24	0.65	263	40
SURF II				
(Washington, D.C.)	0.24	0.8	344	∿50

†maximum energy now 5 GeV

collimation leads to a much smaller loss because of the narrow emittance angle. For instance, at 100 Å about 1/2 of the radiation falls within a vertical angle of 0.7 mrad. Therefore, at 30 m the radiation flux passing through a 2 cm × 2 cm slit is about 2×10^{12} photons/sec Å or 40 μW/Å. The further loss introduced by the monochomator depends on wavelength and design. At 1 Å a similar calculation yields a total photon flux of approximately ($\eta = 0.1$) 4×10^{18} photons/sec Å or 8 kW/Å. The various losses reduce this to 800 mW/Å for the above configuration. Actually, the vertical radiation half-angle is now 0.1 mrad so that most of the radiation in the vertical plane will be intercepted by a slit of height 0.6 cm. The power flux density at the slit is then $\sim$ 600m W/cm^2 Å. For a line width of 1 eV which is achievable with line sources and monochromators, this corresponds to 60 μW/cm$^2 10^{-4}$ Å. This is quite comparable to the output for conventional x-ray tubes, and Parratt (1959) has pointed out that synchrotrons have intensity advantages over these sources at 1 Å if the synchrotron energy exceeds 4 GeV. At 1 Å, the DESY machine in Hamburg (E = 7.5 GeV, R = 31.7 m, I = 6 mA) has proved to be superior to conventional high powered x-ray sources in diffraction studies (Rosenbaum et al. 1971).

2.2.2 Advantages and Disadvantages of Synchrotron Radiation

Synchrotron radiation has the further merit of being highly plane polarized with the electric vector parallel to the orbital plane. In addition the degree of polarization can be accurately calculated from the known machine parameters. This is particularly important at wavelengths less than 1000 Å where only inefficient polarization can be

achieved by reflection due to low reflectivities (Samson 1967). Knowledge of the degree of polarization enables the radiation to be used in the study of anistropic crystals. Reflectance measurements with light polarized in different directions relative to the optic axis leads to the determination of effective optical constants in various directions (Godwin 1969, Klucker et al. 1971, Bammes et al. 1972). In photoelectron spectroscopy where the angular distribution of emitted electrons has been related to the structure of crystals (Fadley and Bergström 1971) a highly polarized beam should be advantageous. In the 600-900 Å range the polarization properties of synchrotron radiation have been used to explore the plasma resonance of aluminum (plasma frequency 15 eV). Since the plasmon is a longitudinal oscillation, a p component at non-normal incidence is required. The decay of the plasmon excited in this way was indeed observed by Steinmann and Skibowski (1966) as an increase in the photoemission for the p component at 830 Å.

The continuous wavelength coverage at high intensity from 1000 Å to 1 Å is an important advantage of synchrotron radiation, especially for studying sharp resonances in atomic and molecular photoionization continua and exciton structures in solids. For the unambiguous determination of absorption cross sections at particular wavelengths, however, a continuum source has a decided disadvantage. This is because of the difficulty when using a monochromator of separating the scattered light and higher-order contributions from the first-order component. This can be done only moderately well by using selective reflection. The problem of order sorting is even worse for grazing incidence spectrometers due to the inevitable appearance of harmonic multiples. In this connection the

inevitable hard x-ray components in the bigger machines can lead to rapid ruination of reflection gratings when one wants to work with the softer x-ray components. A further disadvantage of storage rings as a source of x-radiation is the high vacuum requirement ($< 10^{-7}$ Torr), although this is useful for some surface studies where a high vacuum is required at the irradiated sample. Conventional electron bombardment x-ray sources operate at a vacuum of 10^{-4} Torr and may suffer from oil backstreaming leading to possible target contamination.

A tunable x-ray laser would appear to suffer from none of these problems. It would produce intense radiation of extremely narrow line-width in a well-collimated beam.

2.2.3 Applications of Synchrotron Radiation

In the soft x-ray regime synchrotron radiation has been found useful in studying fluorescence K emission spectra of C, B, and Be at 45 Å, 67 Å, and 114 Å, respectively (Feser et al. 1971). Depending on whether the removed core electron is replaced with one from the valence or the conduction band, the density of states of the valence or conduction bands can be determined. While such studies can often be carried out more efficiently with electron beams, whose cross section for excitation of fluorescence is greater, than with photons, x-rays have the advantage over electrons in the study of organic materials because they produce less surface damage. The difficulty with the synchrotron continuum, however, is again the unwanted presence of hard x-ray components which leads to intense scattered short wavelength radiation. The tunable x-ray laser would, of course, have no such problem.

A number of other application areas for synchrotron radiation have been suggested or are in progress (Codling 1973). We recount these

briefly here as many can be carried out much more directly and with greater precision with a tunable x-ray laser.

Elango et al. (1970) have correlated the emission of visible radiation with F center alkali halides produced by synchrotron radiation in the 300-80 Å wavelength range. The study of adsorbed layers, important for instance in semiconductor behavior, should be facilitated by analyzing the change in XUV reflectivities and photoemission yields by probing with x-radiation (Peavey and Lichtman 1971). The narrow linewidth and high intensity of x-ray laser should be an advantage over synchrotron radiation.

The high degree of polarization of synchrotron radiation has led Skibowski et al. (1968) to study the transmittance and reflectance of aluminum films as a function of p and s polarization. They have found a pronounced dependence near the aluminum plasma frequency of 835 Å and ascribe the dip in thin film transmittance for the p component to the excitation of plasmons (Ferrell and Stern 1962, Ejiri and Sasaki 1966). Resolution was limited by the monochromator and the slit width (0.5 mm) used to about 3 Å at 800 Å. Further improvement could not be obtained because of the uncertain size and motion of the electron beam. Clearly, considerable improvement in resolution to determine more accurately the line shape of the radiation decay of optically excited plasmons would be possible with an x-ray laser beam which would not require further monochromatization.

An important application of synchrotron radiation has been the construction of a scanning x-ray microscope by Horowitz and Howell (1972). The radiation was focused by an x-ray condensing mirror and collimated by a 2 μm pinhole in 100 μm of gold. At an operating wavelength of 5 Å diffraction sets an approximate limit of $L = d^2/\lambda$ or about 0.8 cm on the specimen-

objective distance. The depth of field, limited by the horizontal beam convergence, amounts to 0.1 cm, significantly larger than that of ordinary microscopy. The target characteristics are measured by the characteristic fluorescent x-rays. Resolution is set by the size of the pinhole ($\sim$ 2 μm). Improved resolution could be obtained with smaller pinholes but at the expense of exposure time which for a given image quality varies inversely as the square of the resolution size. The sample thickness that can be probed is set by the penetration of the primary and the absorption of the fluorescent radiation. In the range considered (2-20 Å) this thickness is limited to 10-100 μm for unit density material. The x-ray fluorescent spectra produced by characteristic K radiation are relatively simple leading to good discrimination among the elements. It is thus possible to analyze the element content of μm-sized areas with element separation limited mainly by Thomson scattering from air molecules and the sample. The authors indicate that concentrations of particular elements down to 10^{-6} to 10^{-9} gm/cm^2 at a resolution of 2 μm should be detectable. A further advantage is the absence of vacuum requirements and the ability, therefore, of examining structures <u>in vivo</u>. It is clear that an x-ray laser has all the advantages of synchrotron radiation while not requiring such intensity reducing devices as a monochromator, filter, and pinhole.

Another important application of synchrotron radiation is for x-ray lithography, which has been recently demonstrated (Spiller et al. 1976, Fay and Trotel 1976). The collimation of synchrotron radiation was shown to be especially useful since 1 μm wide lines could be replicated with negligible geometric distortion with a mask-to-substrate gap(s) up to 1 mm.

For this application no monochromator was used but the monochromaticity of an x-ray laser may be useful for enhancing the absorption characteristics of the mask and resist materials.

2.3 Laser-Driven Plasma Sources

A highly efficient method for converting infrared radiation into intense coherent x radiation is a plasma irradiated by an intense laser. Extensive investigations have been made into the generation of x-rays at the focus of high-power laser beams (cf., e.g., Fawcett et al. 1966, Basov et al. 1967, Basov et al. 1969, Jaeglé et al. 1971, Yamanaka et al. 1972, Mead et al. 1972, Malozzi et al. 1972, Kliwer 1973). The radiation emitted by such plasmas covers the wide range of $\lesssim 1$ to $\gtrsim 100$ keV and consists of a continuum with superimposed line radiation from recombination reactions. Reported efficiencies range from 2-5% (Bernstein and Comisar 1970) to a measured yield of 15-20% of the incident laser pulse energy from high-Z targets (Malozzi et al. 1972). According to some estimates a 70% conversion efficiency can even be reached (Shatas et al. 1971). With pulse energies of 1-10 J and widths of 100-300 psec irradiating targets of 100 μm diamter the total x-ray output is clearly considerable. From the point of view of applications in materials analysis, the laser plasma source's main advantage seems to be its high intensity which would be useful in radiation damage studies, and possibly as a pump for an x-ray laser. Otherwise the continuum nature of the radiation has the disadvantages already mentioned in connection with synchrotron radiation, while for absorption studies its line components would be a serious drawback. The laser plasma source is also unlikely to serve as an x-ray intensity standard, an application mentioned in connection

with synchrotron radiation because of the relatively straightforward relationship between spectral output and machine parameters (Codling and Madden 1965, Lemke and Labs 1967, Pitz 1969). This is because the x-ray output of a laser plasma depends in as yet poorly understood ways on detailed knowledge of the suprathermal electron distribution which produces the hard x-ray part of the bremsstrahlung spectrum, a variety of possible plasma instabilities, input pulse form, and laser-plasma coupling physics (cf., e.g., Brueckner and Jorna 1974). It is difficult to see how these parameters could ever be sufficiently well specified, thus rendering a precise a priori determination of the x-ray output unfeasible.

2.4 X-Ray Monochromators and Spectrometers

Many of the applications of x-ray lasers to be discussed depend on the availability of highly monochromatic radiation. For a comparison of other intense sources, such as laser-produced plasmas and synchrotron radiation, with x-ray lasers it is, therefore, important to determine how the ultimate x-ray flux, collimation, and monochromaticity are affected by the interposition of monochromatizing devices. In general, high monochromaticity requires good beam collimation and there is a compromise between resolution and monochromator transmission (Azaroff 1974). Plasma-produced beams will suffer considerably more in intensity by collimation than synchrotron beams which are already well-collimated in the vertical plane (Section 2.2.1). The disadvantage of both these sources is their broad spectrum. This, as we have noted before, leads to transmission by a monochromator of sub-harmonics and overlapping orders, the elimination of which necessitates the use of additional dispersing elements causing further loss in intensity. In fact, with some monochromatized synchrotron beams the intensity at $\lambda/2$ is greater than that at the desired wavelength λ.

Monochromators and spectrometers for the x-ray region usually use either flat or bent Bragg crystals at the shorter wavelengths, and gratings (grazing or normal incidence) at wavelengths longer than approximately 10 Å; grazing incidence grating instruments work well up through at least 1200 Å, overlapping the range of Bragg crystals and normal incidence vacuum spectrometers. In grazing incidence spectrometers for the 10-400 Å region concave gratings are generally used so that the entrance slit can be imaged onto the exit slit with only one reflection to minimize losses. In analyzing wavelengths shorter than about 10 Å, Bragg crystal spectrometers give higher transmission but grazing incidence grating instruments are often used for high resolution. Both bent and flat multilayer crystals may be coated onto a substrate with interatomic plane spacings as large as 120 Å using organometallic compounds such as lead stearate (Henke 1974).

X-ray spectrometers available at the NINA synchrotron radiation facility in Daresbury, England, include a grazing-incidence monochromator and a grazing-incidence spectrograph, a normal incidence UV spectrometer, a Wadsworth-mount grating monochromator and two Bragg crystal spectrometers (one of which is used for x-ray diffraction and one for x-ray photo-electron spectroscopy work) (Marr 1976). The variety of monochromators at Daresbury are fairly typical of those currently used with either synchrotron sources or x-ray tubes.

For experimental convenience, "constant deviation" concave grating monochromators have been designed with fixed entrance and exit slits (Codling and Mitchell 1970) for use with synchrotron sources. Some progress has been made at Daresbury in overcoming the problem of transmitting overlapping orders.

Table 2.2 shows the characteristics of the far UV spectrometers and monochromators at the National Bureau of Standards electron storage ring SURF-II

Table 2.2. Summary of Spectrometer Characteristics at SURF-II*

Instrument	Wavelength Range (Å)	Dispersion (Å/mm)	Typical Bandpass (Å)	Slit Width (μm)	Horizontal Angular Acceptance (radians)	Vacuum	Comments
3 m Grazing Incidence Monochromator (3MGIM)	100-700	5.55	0.065	12	1/60	VHU	Moving exit slit, sample in front of entrance slit
2.2 m Grazing Incidence Monochromator (2MGIM)	0-800	7.57	0.76	100	1/40	UHV	Moving exit slit with attached UHV sample chamber
Toroidal Grating Monochromator (TGMV)	40-150	<0.5	∿0.5**	1000	1/450	UHV	Fixed exit slit. Stigmatic image. Sample chamber designed for gas load, chamber between 2-3 meters above floor.
	150-500	<0.7	∿1				
	400-1200	<1.0	∿1.5**				
Toroidal Grating Monochromator (TGMH)	40-150	<0.5	∿0.5	1000	1/1000-1/5000	UHV	Fixed exit slit. Stigmatic image. Chamber, provided by user, must be compatible with UHV beam line No. 8.
	150-500	<0.7	∿1				
	400-1200	<1.0	∿1.5				
3 m Grazing Incidence Spectrograph	40-620	5.55	0.06	10	1/60	VHU	Still to be converted for ring operation.

*From Ederer and Ebner (1975).
**estimated bandpass

(Ederer and Ebner 1975). The properties of the NBS toroidal-grating monochromator, designed for a modest resolution of about 1 Å with high transmission, have been described recently (Madden and Ederer 1972). It is clear from the table that the horizontal angular acceptance of most of the spectrometers listed ($\gtrsim$1 mrad) is sufficient to pass the entire r.m.s. emission cone of each electron as it sweeps by (for SURF-II, $\gamma \simeq 500$ and $\theta_{\frac{1}{2}} \simeq 2$ mrad). As most of the other presently available synchrotron sources operate at energies above 250 MeV, their angular distribution of radiation is even narrower. The SPEAR storage ring at Stanford University has a beam width of about 1 cm rather than the 1-2 mm at SURF so that the size of monochromators designed for this facility must be scaled up by a factor of about ten to achieve equivalent resolution without loss.

2.4.1 Estimate of the Transmission of a Grazing-Incidence Monochromator

To make this estimate one must know the reflectivity of the metallic grating surface (usually Al or Au) at grazing incidence and the diffraction efficiency into first order. At a grazing indidence angle of 1° for 10 Å - 100 Å radiation, experiment and theory agree (R. Giacconi et al. 1969) on a reflectivity of $\sim$90 percent for unoxidized Al and $\sim$70 percent for Au (except near the N absorption edge). For a good holographic grazing-incidence diffraction grating, one may expect a diffraction efficiency into first order of $\sim$5-10 percent. Resolution of a holographic-grating grazing incidence spectrometer can be as good as 50 meV at Ar L ($\sim$220 eV) or a resolving power $\lambda/\Delta\lambda \sim 4000$ (Nordgren et al. 1976).

For a synchrotron source with a vertical angular distribution of only 1-3 mrad out of the orbital plane the angular acceptance in the dispersion

plane is the only limitation on flux. Then the transmitted photon flux is:

F = (Incident number of synchrotron photons/sec-mrad-Å focused on the entrance slit) x (fractional grating reflectivity) x (first order diffraction efficiency) x (horizontal angular acceptance at grating from slit) x (spectrometer bandpass in Å).

(The factor F may have to be multiplied by the ratio of entrance-slit width to focal spot size if there is a loss due to too large a focal spot size when using a narrow slit at high resolution.) For example, with the parameters for the 2.2 m grazing incidence monochromator at SURF a sector of beam up to ∿10 mrad focused at unit magnification onto the entrance slit (of 100 micron width) via an external grazing incidence mirror, a fractional reflectivity of grating and mirror of 0.8 and a 0.1 diffraction efficiency into first order (optimistic), one calculates a transmission of approximately 3×10^{-3} × (bandpass in Å). This is consistent with a rough estimate given by Eastman (1972, p. 32) of 10^3 for the insertion-loss factor, using a comparable bandpass and a focused synchrotron source. Eastman's estimate probably includes some loss due to an oversize focused beam spot.

Eastman (ibid.) further calculates that for XPS (x-ray photoelectron spectroscopy) work at 0.2 eV resolution with a signal/noise ratio of 100/1 in a 1 sec integrating time, the combined insertion loss of photon monochromator and electron spectrometer with a 1 percent electron yield is a factor 10^9. This means that an incident focused synchrotron flux of 10^{13} photons/sec/eV spectral width is required, a number that happens

to coincide with the flux of the SPEAR storage ring operating at 2.2 GeV with 250 mA of circulating current and a photon energy of 25 eV. DESY can provide similar fluxes, but this flux is one or more orders of magnitude greater than that available at other U.S. installations. The quoted flux requirements for XPS are for measuring the distribution of energies of the emitted photoelectrons only. Simultaneous measurements of angular distributions and photoelectron energies will require even higher x-ray fluxes, up to the damage threshold.

With very intense sources requiring a grating monochromator, the ultimate limit to usable flux may be set not by the source but by the threshold for damage to the grating itself. In a vacuum environment one mechanism for damage would simply be radiative heating of the grating surface. The total radiation power output per electron of a synchrotron is obtained by integrating Eq. (2.9) over all wavelengths or directly from Eq. (2). The result can be expressed as

$$I = 6.7 \times 10^{-7} \, [E(\mathrm{GeV})]^4/[R(\mathrm{m})]^2 \, \mathrm{W} \, , \qquad (12)$$

corresponding to a total instantaneous output of about 100 kW for typical operating conditions of the NINA machine. A grating substending a horizontal angle of a mrad at 3 m from the radiating source is then subjected to a flux of up to 10 W/cm^2. It might be difficult to dissipate this much power without grating damage under vacuum conditions, to say nothing of the defects produced in the grating surface by broad-band x rays over long periods of time. A monochromatic x-ray laser would be flux-limited by damage to the sample not the monochromator grating and, when x-ray beam

splitters are developed (certainly possible even now), the laser could be used to illuminate an appropriate number os samples simultaneously so as not to waste the flux.

2.4.2 Bragg Crystal Monochromators for X-Rays

We now discuss the transmission and resolution of Bragg crystal monochromators suitable for the shorter wavelength region 0.1 Å - 10 Å. At the Al K_α wavelength (8.34 Å), for example, the peak reflection efficiency for a CAP crystal is ≃ 1/2 percent (Henke 1965, 1974). Lead stearate and other organometallic multilayer crystals (with a larger spacing 2d and hence a smaller Bragg angle for 8.34 Å) can have a reflection efficiency up to a few percent, but with a severe loss in resolving power (Henke 1965).

For a point source of continuum x rays, the transmitted flux of a crystal spectrometer (in photons/sec) can be approximated as $B\Delta\Omega\bar{\eta}_c(\delta\lambda/1\text{Å})$ if the source brightness B is measured in photons per unit solid angle per second per Å and where $\Delta\Omega$ is the solid angle accepted by the spectrometer. The mean crystal reflection efficiency $\bar{\eta}_c$ and the spectrometer bandwidth $\delta\lambda$ must be known. Where the geometrical angular acceptance is greater than the crystal mosaic angular spread, particularly in calculating the transmission of a line source, it is conventional to express the crystal reflectivity in terms of an integral over the "rocking curve" of the crystal in units of radians. Some of these considerations are discussed by F. W. Martin and R. K. Cacak (1975). As a numerical example, using figures from Martin and Cacak for their double-focusing

concave spherical crystal monochromator, we assume a solid angle $\Delta\Omega$ of 0.04 steradians and a resolution of 1 percent with C K_α (44.6 Å), the transmitted flux can be as high as:

$$B \times .04 \times 5\% \times (.45\text{Å}/1\text{Å}) \simeq 10^{-3}\ B$$

for a point x-ray source and using a good quality lead stearate crystal with 100 or more layers. In practice, transmissions one to two orders of magnitude less than this are more common.

Resolution of crystal monochromators is limited by the number of reflecting planes in one absorption (1/e) length (or by the total number of reflecting planes in a thin multilayer crystal such as lead stearate), the geometrical collimation used and the angular distribution of orientations of the mosaic elements composing the crystal. If very good angular resolution is needed, as in some x-ray diffraction work, pure silicon crystals are usually best. Much greater transmission at poorer resolution can be obtained by using bent mosaic pyrolytic graphite monochromators with 2d = 6.715 Å (cf., e.g., Watson and Perlman 1972).

The fractional resolution of a crystal spectrometer found by differentiating the Bragg law is

$$\frac{-dE}{E} = \frac{d\lambda}{\lambda} = \cot\ \theta\ d\theta\ , \tag{13}$$

which deteriorates badly at small Bragg angles θ with fixed $d\theta$. The dependence on wavelength is seen to be

$$\frac{d\lambda}{\lambda} = \cot\ \theta\ d\theta = \frac{\sqrt{1 - n^2\lambda^2/4d^2}}{n\lambda/2d}\ d\theta \tag{14}$$

implying that the best resolution occurs near $n\lambda = 2d$ for a particular crystal plane spacing d. Again using Al K_α as a representative example, one finds that if the Bragg crystal is quartz with $2d = 8.50$ Å and a $d\theta = 1.15° = 2.6$ mrad, the resolving power $\lambda/d\lambda \simeq 1950$ in first order, comparable to a grazing incidence spectrometer at its long wavelength limit. On the other hand, if one uses the same crystal with shorter wavelength Ar K_α radiation at 4.19 Å, the resolving power $\lambda/d\lambda$ is only $\sim$220 in first order and one must go to second order to achieve a better resolution. Overlapping orders are again a problem with a broad source such as synchrotron radiation with the use of a Bragg crystal monochromator as they are with gratings.

The trade-off between resolution and monochromator transmission is not a simple subject. In general the transmission rises rapidly as the resolving power is decreased by opening the slits, until a knee or plateau is reached. A number of examples for curved crystal spectrometers are presented in articles by T. Johansson (1933) and by Jones et al. (1963). In the 3-12 Å range, the optimum resolution for reaching this transmission plateau is at a resolving power $\lambda/d\lambda \sim 10$ Å$/0.05$ Å $= 200$, depending somewhat on the particular wavelength and crystal. An x-ray laser would, therefore, be particularly advantageous as a high intensity source in this wavelength range when a monochromaticity $>> 1/200$ is needed or when conventional source intensities are inadequate.

Reliable data on damage to analyzing crystals with broad sources are difficult to obtain. Presumably, ionic analyzing crystals of simple materials (e.g., NaCl) are less subject to radiation damage than complex

organic crystals; pure silicon crystals (2d = 3.84 Å) may be least susceptible to damage of any known crystal material (P. E. Best 1976) but they are not useful in the soft x-ray region. Some recent data taken at the Stanform SPEAR synchrotron radiation facility with protein crystals (azurin) showed little damage after a total of 28 hours of exposure to 1.376 Å radiation from the synchrotron. On the other hand, damage to other azurin crystals was detectable in x-ray diffraction data after a 100 hour exposure with nickel-filtered radiation from a Cu-anode x-ray tube operated at 700 W (Phillips 1976). More severe damage than this would be expected in a crystal monochromator exposed to the direct synchrotron beam, and a Bragg crystal might be expected to be more sensitive to x-radiation damage than a grazing incidence grating or a "passive" grazing incidence mirror.

2.4.3 New Types of Monochromators

The same techniques that are being used to make the zone plates (see Section 10.4) have recently been applied to the construction of free-standing, interferometrically formed transmission gratings with wire spacing of ∿1000 lines/mm for diffraction of x rays in the 45-275 eV (∿270-45 Å) range. Although the gold wires employed are not totally opaque to the x rays, it appears that these transmission gratings will offer substantial advantages over grazing-incidence reflection gratings in terms of throughput of soft x rays at resolutions up to about $1:10^3$ or better (Schnopper 1976). For example, one such grating (with an area 4-5 cm^2) will diffract up to 12 percent into one of the first-order peaks at the optimum wavelength. Comparing this with a commericial 2.2 m focal-

length grazing-incidence monochromator, one finds the projected grating area (onto the line of sight) to be about 4-5 times greater for the transmission grating. Diffraction efficiency into first order may also be greater for a properly designed transmission grating. The threshold for unacceptable radiation damage is probably also higher for the transmission grating, though such studies do not appear to have been made as yet.

3. X-RAY SOURCE REQUIREMENTS FOR MICROREPLICATION

3.1 Summary

For purposes of orientation we present here a review of microreplication techniques using x-ray sources commonly referred to as x-ray lithography (for a bibliography see Bernacki and Smith 1975). This is followed by a discussion of the types of microelectronic components that can in principle be manufactured by this technique, together with indications of components that could be produced if sufficiently good (<<1 μm) resolution and contrast can be achieved. The needed brightness, collimation, and monochromaticity for the production of these devices will help pinpoint those areas where an x-ray laser source has clear advantages. The survey is not intended to be exhaustive, but a substantial documentation has been provided to assist those requiring further and more detailed information.

3.2 Introduction

Shadow projection images of solid materials have been produced on sensitive films by exposure with x-rays. These microradiography techniques have been in use for the past 50 to 80 years and have traditionally used a point source of x rays, especially where image magnification is desired. Four years ago the technique of x-ray lithography was proposed for the replication of microcircuit patterns from a mask onto a semiconductor substrate in a manner analogous to photolithography (Spears and Smith 1972). Extensive research has since been undertaken to exploit x-ray technology for this application. X-ray lithography is superior to contact printing with ultraviolet light because submicron-wide lines may be replicated with no serious diffraction, scattering or reflection effects.

In order to record structures of 0.1 μm and less in size with some fidelity it becomes necessary to utilize rather novel recording media. The resolution of conventional x-ray film is set by the grain size and grain spacing. For the highest resolution conventional films the grain size is about 600 Å and the average grain spacing of the order of 2000 Å. This is clearly inadequate for recording the detail of which x-ray imaging is capable.

Microelectronics device processing then requires that the x-ray image be recorded in grainless or highly homogeneous media such as a polymer resist which, after developing, gives a relief image, i.e., the resist is removed in some areas of the image and not in others (Hatzakis 1969, Brault 1974, Thompson et al. 1974, Roberts 1975, Feit et al. 1975, Hagouel and Neureuther 1975, Gipstein et al. 1976, Taylor and Coquin 1976). This, in turn, has led to new applications of microradiography where a relief pattern is indicative of the relative x-ray absorption of various parts of the sample. Grainless recording media are, of course, not really new and their potential in microradiography was appreciated from the earliest days of the subject. For example, Ladd et al. (1956, 1957) made use of the changed solubility of ammonium dichromate crystals after exposure to x rays, obtaining a relief pattern after development in methanol. The main problem was (and is) the long exposure times required. Replicas of biological samples have been made which show details as small as 0.1 μm. The specimen is placed on a thin layer of photoresist imprinting an x-ray absorption replica of the specimen yielding a topographic profile after development (Spiller et al. 1976). These high resolution relief images have been examined in a scanning electron microscope. An expanded discussion of x-ray microscopy is contained in Section 10.

3.3 System Components

Figure 3.1 illustrates the components required for microreplication. The principal components are the source, a mask, and a resist or film.

A. Source

The source of x rays is usually a point source created by electron bombardment of a target. The x rays are emitted in all directions from this type of source. X rays may also be generated in an x-ray laser, a synchrotron or storage ring where the electrons lose energy in the form of bremsstrahlung x radiation during angular acceleration, or a high temperature plasma, e.g., laser pulse heating of a target material.

B. X-Ray Filter or Vacuum Window (Optional)

Some x-ray sources incorporate an x-ray transparent window to seal the vacuum chamber. Other sources may use a thin membrane as a filter to selectively remove certain wavelengths, and/or the filter may function as a heat shield between the source and the mask.

C. X-Ray Optics (Optional)

In most cases the degree of collimation and the area of coverage is achieved by placing the source of x rays sufficiently far from the mask. If x-ray focusing lenses or zone plates could be fabricated with sufficient accuracy, they would reduce the requirement of high intensity from the source.

D. Mask or Sample

The sample contains opaque and transparent regions which may be one material with spatial modulation of thickness or spatial variations of different materials.

E. Film or Resist

The x-ray image is reproduced in a film which must be sensitive to the x-ray wavelength emitted by the source. For high resolution images the resist is typically less than 2 μm thick.

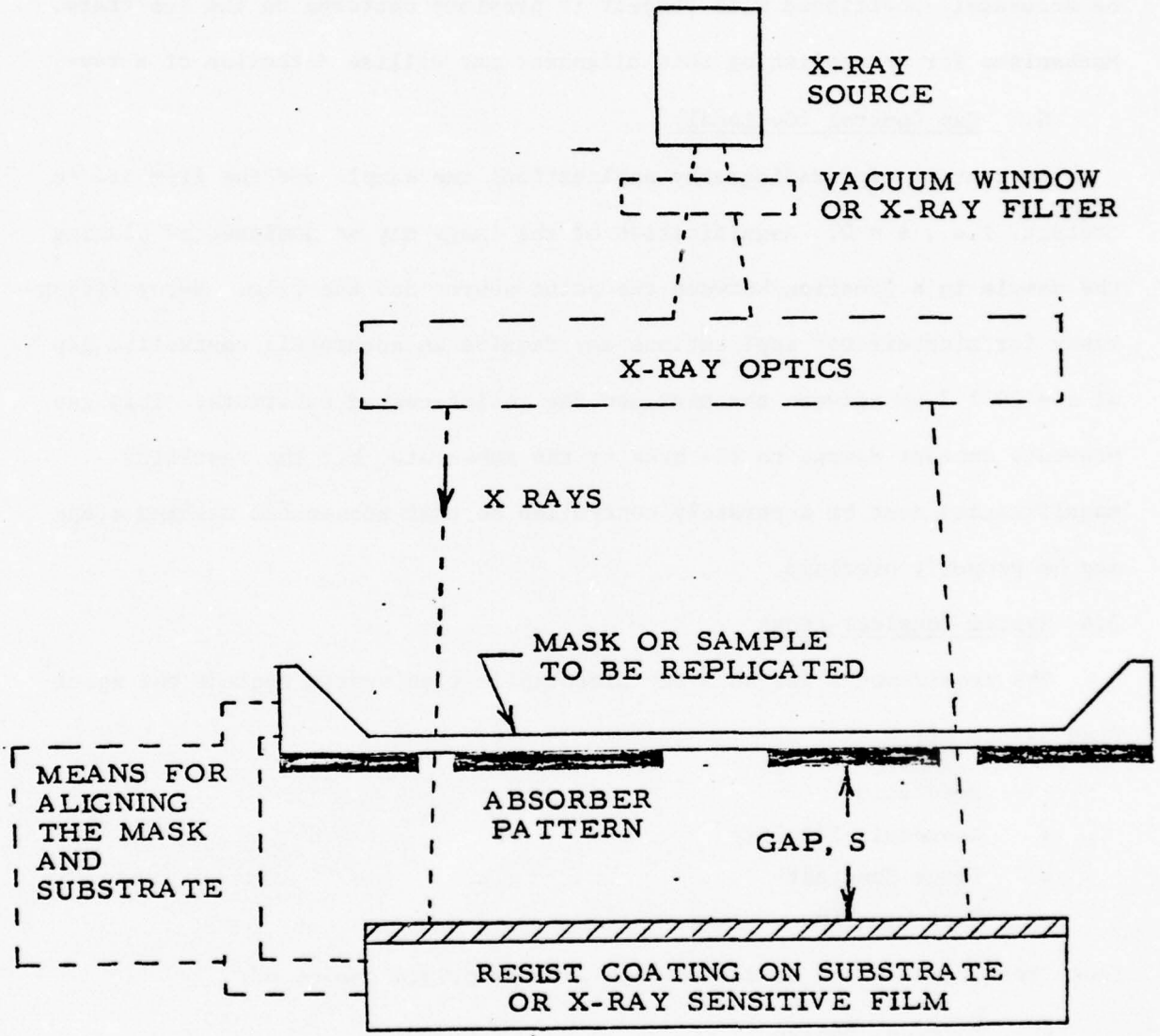

Figure 3.1. Components of a Microreplication System.

F. Alignment (Optional)

X-ray lithography for microcircuit applications requires that the mask be accurately positioned with respect to previous patterns on the substrate. Mechanisms for accomplishing this alignment may utilize detection of x rays.

G. Gap Control (Optional)

In contact microradiography applications the sample and the film are in contact, i.e., s = 0. Magnification of the image may be achieved by placing the sample in a location between the point source and the film. X-ray lithography for microcircuit applications may require an accurately controlled gap of s = 20 ± 2 μm between the mask and the resist-coated substrate. This gap prevents contact damage to the mask or the substrate, but the resulting magnification must be accurately controlled so that subsequent masking steps may be properly overlaid.

3.4 System Considerations

The requirements for an x-ray microreplication system include the specified values of:

- Resolution
- Geometric Fidelity
- Image Contrast
- Exposure Time

These requirements can be met through an appropriate choice of:

- Physical Design
  - Geometrical Layout of the Source, Sample, and Film
  - Peripheral Support Equipment
- Source
  - Spectral Intensity
  - Monochromaticity
  - Collimation
- Mask or Sample
  - Type and Thickness of Transmitting Substrate
  - Type and Thickness of Absorbing Pattern

- Resist or Film
  - Wavelength Dependent Sensitivity
  - Resolution
  - Contrast

Many of these parameters are interdependent. The following discussion considers these relevant relationships:

- The effect of the source collimation on the resolution, geometric fidelity, and exposure time.
- The effect of the source wavelength on the resolution, exposure time, and contrast.
- The means of achieving adequate contrast through the selection of the wavelength, the mask, and the resist.
- The tradeoff between resolution and sensitivity of resist materials.

3.4.1 Collimation and Beam Divergence

A particular advantage of x-ray lithography is that any desired resolution (down to 0.1 μm or less)--with any desired depth of field over any desired area (10 cm diameter or more)--can be achieved by placing a point source sufficiently far away from the mask. However, very long exposure times might be required for these extremes, even with high power x-ray sources and sensitive resist materials.

In a contact microreplication system there are no serious limitations with presently available sources of resist materials. However, if there is a gap between the mask and the substrate, there are two factors which limit the resolution and exposure area of an x-ray lithography system: penumbral shadowing and geometric distortion. The gap is maintained so that there is no contact and consequently no yield loss due to defects produced on the mask or substrate which can occur in a contact system. This gap, S,

might be typically 25 μm (Fig. 3.2). The uncertainty in this gap, due to flatness distortions or bow in the mask and/or the wafer, may be assumed to be S' = 5 μm for a properly mounted 5 cm diameter mask and substrate. In all probability S' is a function of the substrate diameter.

In order to maintain a desired resolution, the exposure time will increase in proportion to the gap between the mask and the substrate. Thus, it would be reasonable to make S as small as possible, even equal to S'. However, to ensure high yield there must be no contact. Due to the mechanical difficulties of mounting and spacing the mask and substrate, a tolerance of $S \simeq S' + 10$ μm should be allowed. Dust particles on the mask or substrate could produce defects if the spacing were less than this value. In addition, if the substrate is an epitaxial silicon wafer, it may contain epitaxial spikes which can seriously damage a mask.

Penumbral shadowing, δ, occurs due to the finite diameter, d, of the x-ray source and the distance from the source to the mask, D, as shown in Fig. 3.2.

$$\delta = S \frac{d}{D} \tag{1}$$

Because the image from the mask is projected onto the substrate by a point source, there is some slight magnification. A feature at the edge of a mask will be displaced by an amount Δ, which is termed geometric distortion.

$$\Delta = S \frac{R - d/2}{D} \tag{2}$$

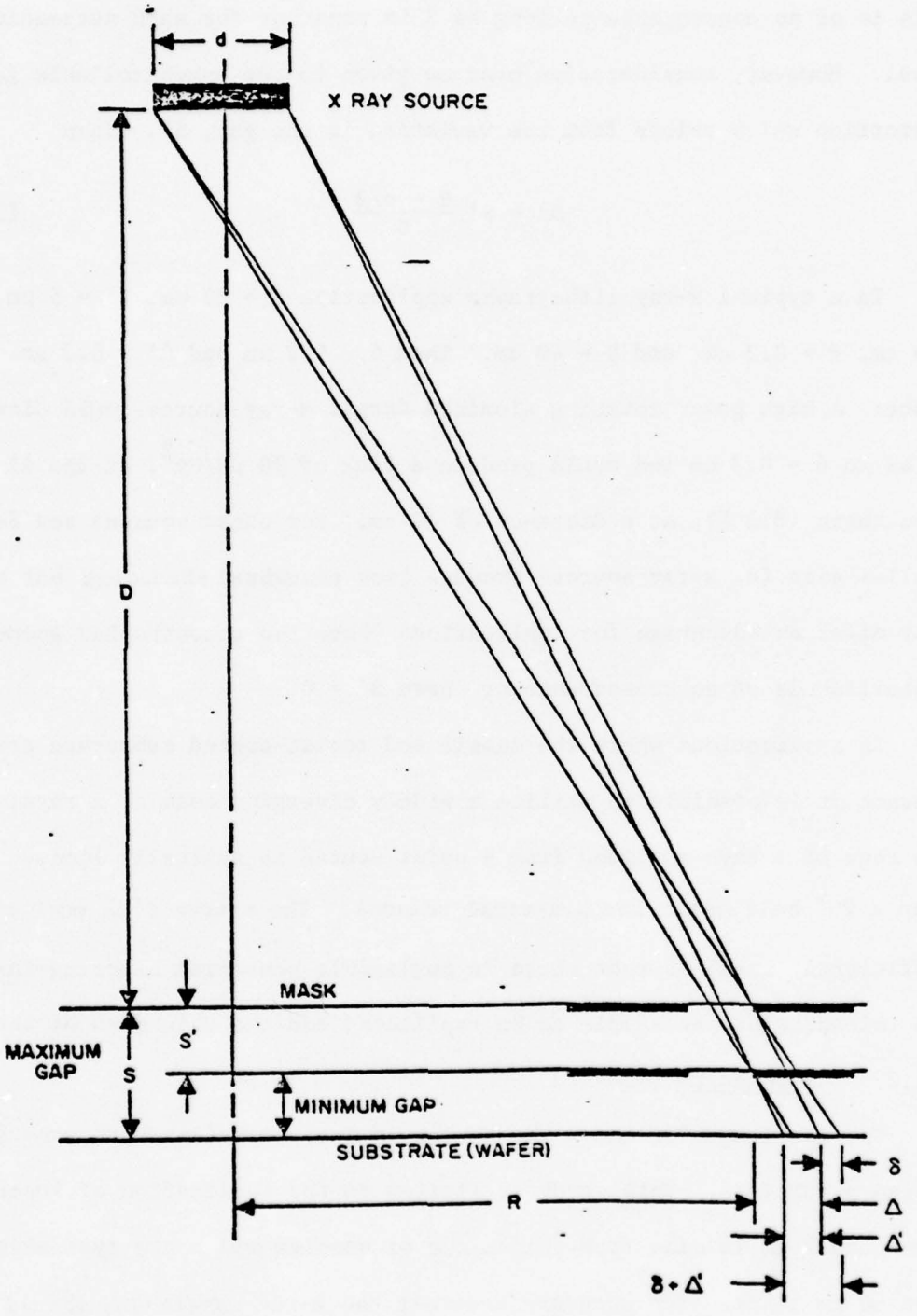

Figure 3.2. Geometrical parameters for an X-ray Lithography System

This is of no consequence so long as S is constant for each succeeding mask level. However, consideration must be given to the uncontrollable geometric distortion which arises from the variation in the gap, S'. Then

$$\Delta' = S' \frac{R - d/2}{D} \qquad (3)$$

In a typical x-ray lithography application S = 25 μm, S' = 5 μm, R = 2.5 cm, d = 0.3 cm, and D = 40 cm. Then $\delta \simeq 0.2$ μm and $\Delta' = 0.3$ μm. (Note: A high power rotating aluminum target x-ray source could dissipate 10 kW in d = 0.3 cm and would produce a flux of 70 $\mu W/cm^2$, at the Al K wavelength (8.3 Å), at a distance of 40 cm. For other sources see Section 2). Smaller size (d) x-ray sources produce less penumbral shadowing but would only offer an advantage for applications where the uncontrolled geometric distortion is of no consequence or where S' = 0.

In applications where the sample and resist-coated substrate are in contact it is possible to utilize a widely diverging beam of x rays; however, the cone of x rays utilized from a point source is typically limited to less than a 20° half angle for practical reasons. The source size must still be sufficiently small so that there is negligible penumbral blurring throughout the thickness of the sample to be replicated and the thickness of the resist.

3.4.2 Wavelength

The wavelength of the x-ray source is interdependent with many other system parameters. This study is limited to the replication of features less than 1 μm in size from thin masks or samples which are typically less than 30 μm thick. For adequate contrast the x-ray wavelength should be greater than 5 Å. Experimental and theoretical results on the efficiencies of

x-ray target materials, mask materials, and spurious effects caused by continuous radiation and photo-electrons have been presented by Maydan et al (1975). Shorter wavelength photons would not be aborbed in the thin sample or in thin resist films. Thick or highly absorbent resist films are less desirable for high resolution imaging.

The exposure time is one of the most sensitive parameters to the choice of wavelength. In many present systems the exposure time is undesirably long. Consequently, an important criterion for the choice of wavelength is that which provides the shortest exposure time in a given system. The parameters that determine this choice are discussed in detail in the paper by Sullivan and McCoy (1976) (see also Greeneich 1975) and are summarized here:

1) X-ray source brightness -- The available wavelengths may be limited from some types of sources.
2) Mask transmission -- The x-ray transmission of the mask substrate material is limited by the wavelength-dependent absorption coefficient and the thickness.
3) Vacuum window/filter transmission -- The x-ray transmission of the material used to provide radiant heat shielding, to filter out some of the continuum x rays, and/or to provide a vacuum window, is limited by the wavelength-dependent absorption coefficient and the thickness.
4) Absorption in resist -- The wavelength-dependent absorption coefficient of the polymer resist is a critical factor in selecting the exposure wavelength for minimum exposure time.

5) Resolution requirement -- Higher energy x-ray photons will produce higher energy photoelectrons that have a longer range and contribute to lower resolution. The scattering range of 1 kV photoelectrons in a polymer resist such as PMMA is about 0.05 μm; thus, for high resolution, it is desirable to limit the x-ray photon energy to less than about 2500 eV ($\lambda \gtrsim 5$ Å).

6) Contrast requirement -- The contrast is limited by the ability of the absorber pattern to effectively block the x rays. Typically, fabrication techniques require that the absorber film be less than 1 μm thick in order to define 0.5 μm geometries. If this film is gold, the wavelength must be greater than about 3 Å in order to stop 90 percent of the x rays with a 1 μm thickness. Other less absorbent substrates will be opaque only for longer wavelengths. The effectiveness of the absorber film in providing discrimination against several wavelengths emitted by the source may also be an important contribution to the contrast.

In general there is an optimum wavelength which gives the shortest exposure time. Longer wavelengths are not transmitted by the mask and shorter wavelengths, which are easily transmitted by the mask, are not absorbed in the resist film.

3.4.3 Contrast

The contrast achieved in the image is also dependent upon many factors inthe system. Imaging of biological samples, which have inherently low contrast, may require the use of a monochromatic x-ray source with the wavelength specifically selected to give maximum absorption or transmission in carbon or oxygen. In some cases it may be possible to use biological

stains which contain high atomic number elements and thus are x-ray absorbent. In cases where the source is not monochromatic it may be necessary to tailor the resist for maximum sensitivity at particular wavelengths which will produce a high contrast image. As in photographic film processing there are techniques for enhancing the contrast of resist films during development.

3.4.4 Resist Sensitivity

The fabrication of microelectronic circuits using x-ray lithography has a goal of producing submicron-wide lines over 2 to 8 cm diameter substrates with near perfect geometric fidelity. Exposure times of several minutes or less are required for this application and thus very sensitive resists and/or very intense x-ray sources are required. Exposure times up to several hours and much smaller substrates may be acceptable for the replication of patterns for discrete microelectronic devices or for imaging of biological samples.

X-ray sensitive resist materials typically require an exposure dose of 0.01 to 2 J/cm^2 at 8.3 Å wavelength. Most organic resist polymers exhibit higher sensitivity at longer wavelengths with the sensitivity proportional to λ^n where n is in the range of 2.5 to 2.9. The correlation between their sensitivity to x-ray and electron beam radiation has been discussed by Thompson et al. (1974). There are discontinuities in the spectral sensitivity, e.g., the sensitivity decreases above the oxygen absorption edge at 23.3 Å and above the carbon absorption edge at 45 Å.

The more sensitive resists are "negative", i.e., they remain on the substrate in the regions exposed by x rays. They usually have poorer resolution than positive resists because they consist of monomers which

cross-link upon irradiation and chain reactions may propagate. Positive resists are polymers which undergo chain scission upon x-ray irradiation. Solvents are used to dissolve away the lower molecular weight fragments in the exposed regions of the image. The resists which exhibit the best resolution are, in general, the ones with the poorest sensitivity. There is much room for improvement, however. The ultimate theoretical sensitivity of any imaging film is set by the shot noise. Each resolution element should receive at least 50 photons to differentiate it from an unexposed element. If the desired resolution element is 0.1 μm square then the minimum useful exposure dose must be 5×10^{11} photons/cm^2. This is 1.2×10^{-4} J/cm^2 at 8.3 Å wavelength or 2.2×10^{-5} J/cm^2 at 45 Å wavelength. This assumes that the resist film is sufficiently thick to absorb all of the x-ray photons. When an x-ray photon is absorbed in the resist it generates 1 or 2 energetic photoelectrons. There are no competing scattering or absorption processes. These electrons may possess sufficient energy to break several bonds in the polymer molecules. These gain mechanisms reduce the effect of quantum noise in the exposure process.

Much additional research will be required on resist materials before the ultimate in sensitivity can be achieved. Current applications must use very high power x-ray sources to achieve reasonable exposure time. For example, a 10 kW, rotating aluminum target x-ray source with a beryllium window has a brightness of 0.11 W/steradian. Approximately half of this flux is absorbed in the transparent regions of the mask. At a distance of 40 cm the exposure time for PMMA high resolution positive resist (2 J/cm^2) is about 16 hours. Thus, the process is generally quite inefficient with conventional sources. In addition to the

improvements already mentioned, the monochromaticity of an x-ray laser could dramtically improve recording material sensitivity by seeding the absorber with a substance with a resonance at the laser wavelength.

3.5 X-Ray Laser Sources for Microreplication

A chief requirement for x-ray lithography and microradiography is a high brightness source of x rays. Appropriate wavelength, intensity, and collimation can be obtained from several types of x-ray sources. X-ray lasers offer three unique attributes over other types of x-ray sources: they are monochromatic, collimated, and coherent.

A monochromatic source may be useful with x-ray optics for beam expansion or collimation, since some types of optics exhibit chromatic aberration. A monochromatic source could also provide enhanced contrast of specific types of samples, i.e., the x-ray source wavelength might be chosen to match the absorption edge of particular elements in the sample or in the resist for increased sensitivity.

A collimated x-ray source would give better geometric fidelity in the replicated images because it allows a larger gap between the mask and the resist-coated substrate and a reduction in the uncontrolled geometric distortion.

A coherent source may be useful for microreplication using holographic techniques or for the recording of phase contrast images of samples. Holographic methods will be discussed further in Section 7.

3.6 Application to the Fabrication of Microelectronic Components

3.6.1 Introduction

Conventional photolithography has developed into a high-level technology for the production of microelectronic devices. There are, however, two problem areas that are amenable to improvement by more sophisticated techniques. The first problem is low yield and short mask life due to the

requirement for contact between the mask and substrate during exposure. The second area for improvement is the resolution limitation caused by diffraction and multiple reflection of ultraviolet (4000 Å wavelength) light.

Off-contact techniques have been developed to improve yield; however, the resolution is degraded by diffraction and light spreading. Projection lithography is subject to lens limitations; however, resolution down to 0.8 μm can be maintained over a small field. Step and repeat techniques can be used to cover a large area substrate but the throughput is considerably lowered.

X-ray replication techniques have been proposed which use very short wavelength (<50 Å) radiation. X-ray lithography has the potential for yield improvement over conventional contact photolithography because projection or shadow printing can be used. In addition, the resolution limit due to diffraction or scattering effects is less than 0.1 μm. A list of references on work not explicitly referred to in the text follows the bibliography for this report.

In this report, various types of microelectronic components are discussed and the gain in performance or the reduction in cost which can be achieved by the application of x-ray lithography is considered. The following prime advantage becomes evident in this survey: The fabrication of microelectronic components by x-ray lithography is cost effective.

- Discrete components such as transistors, surface acoustic wave devices, etc. with less than 1 mm^2 area can be produced with high yield but their frequency of operation is limited by the linewidth of current replication processes. The smaller linewidths produced by

x-ray lithography can extend the frequency of operation by at least one order of magnitude and therefore data can be communicated and processed more rapidly. In most electronic system applications the following axiom is held in high esteem: Time is money.

- Large area components (>5 mm^2 area) such as integrated circuits, diffraction gratings and magnetic bubble circuits are limited in size by the random defects introduced in the fabrication process. The yield of some complex circuits manufactured today may be only 5 percent. X-ray lithography offers the potential to increase the yield to 50 percent, thus reducing the manufacturing cost of each circuit by an order of magnitude. Alternatively, with higher yields the chip area can be increased thus allowing a more complex electronic system function to be produced for less cost. In addition to yield improvement, the high resolution capability of x-ray lithography allows a higher packing density of components within a given chip area. This also allows a more complex electronic system function to be produced at less cost. A dramatic example of this statement is the hand-held programmable calculator containing only two large scale integrated circuits which is orders of magnitude less costly, less power consuming, lighter, smaller, and more reliable than a similar computer built with the small scale integrated circuits available 10 years ago. A high level of circuit integration on each chip leads to higher reliability and low repair costs for the overall electronic system because fewer interconnections are required.

- A third class of components cannot be fabricated at all, except by high resolution lithography. These include gratings for distributed feedback solid state lasers (3600 Å periodicity for GaAs), superconducting weak link and Josephson junction cryogenic devices (<<1 μm spacings required for tunneling phenomena), and integrated optics (500 Å edge smoothness required to reduce scattering in optical waveguides). All of these devices, if they can be economically fabricated, will displace existing components in high technology systems.

3.6.2 Advantages of X-Ray Lithography

X-ray lithography offers several important advantages over other large area replication techniques:

- < 0.2 μm resolution
- No requirement to place the mask or substrate in vacuum
- Noncontact exposure
- Insensitivity to dust and low atomic number contamination
- Uniform exposure with depth, vertical profiles in thick resist
- No reflection, scattering, or diffraction
- Linewidth independence of substrate material or resist thickness

The last five points contribute to improved yield - a primary concern in large scale integrated circuit processing.

The lithography step has traditionally been the major source of defects in the processing chain and thus presents the greatest opportunity for yield improvement. Improved photolithographic processing techniques have contributed substantially to increased yield of devices and has allowed chip areas to increase from the 10 mm^2 we could attain only 5 years ago to 25 mm^2 today. We believe this trend can be continued with x-ray lithography.

Preliminary verification of improved yield obtained with x-ray lithography has been reported by Bernacki and Smith (1975) for fabrication of discrete MOS transistors with 2.5 μm minimum linewidth.

3.6.3 Devices with Dimension-Dependent Performance

The principal areas of application of high resolution lithography lie in those classes of microelectronic devices for which the performance is dependent on the arrangement and size of surface patterns and for which device performance generally improves as these patterns are made finer. Examples of the principal resolution-dependent microelectronic devices are shown in Fig. 3.3. Other devices in this class but not shown include superconducting microstructures and bubble memories.

A quantitative indication of the increase in device performance that can be achieved by the use of higher resolution lithography is given in Figs. 3.4, 3.5, and 3.6 for two of the types of devices illustrated in Fig. 3.3. The high frequency limit of the microwave field effect transistor (Fig. 3.4) is ultimately limited by the carrier transit time between source and drain. In short gate length devices with narrow source-drain gaps, the field will be high enough that the carrier velocity is the saturated level (v_s), so that the maximum or cutoff frequency is given by $f_c = v_s/\pi L$. The symbol L is used in Fig. 3.4 to represent the length of the critical dimension for each type of device; in the case of the FET, L represents the gate length. The dependence of f_c on L is shown by the upper two lines in Fig. 3.4, corresponding to carrier velocities at the peak of the GaAs carrier velocity plot, and to the high field saturation level which is valid for both GaAs and Si. It is seen from these theoretical curves

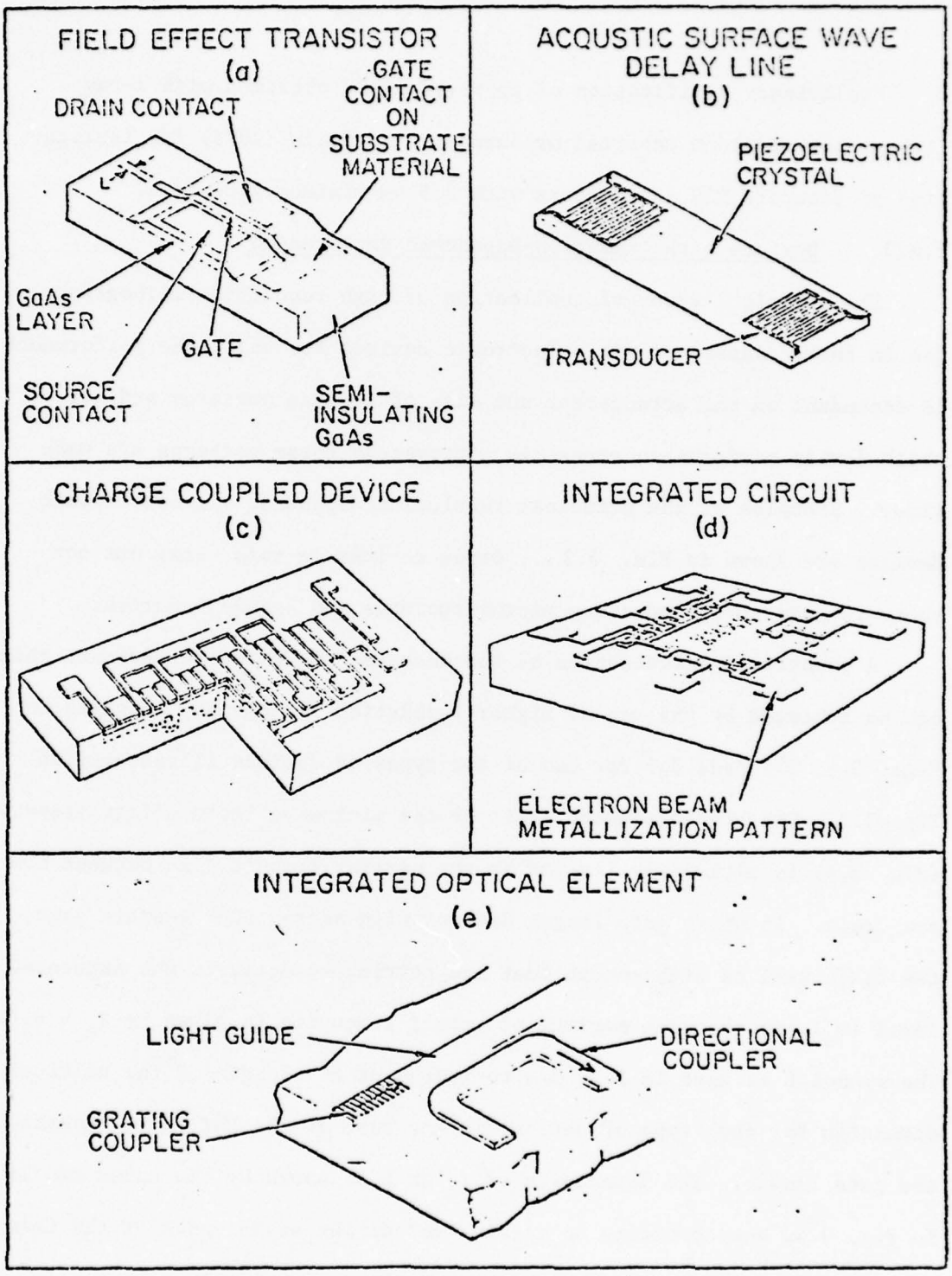

Figure 3.3. Some devices with dimension-dependent performance.

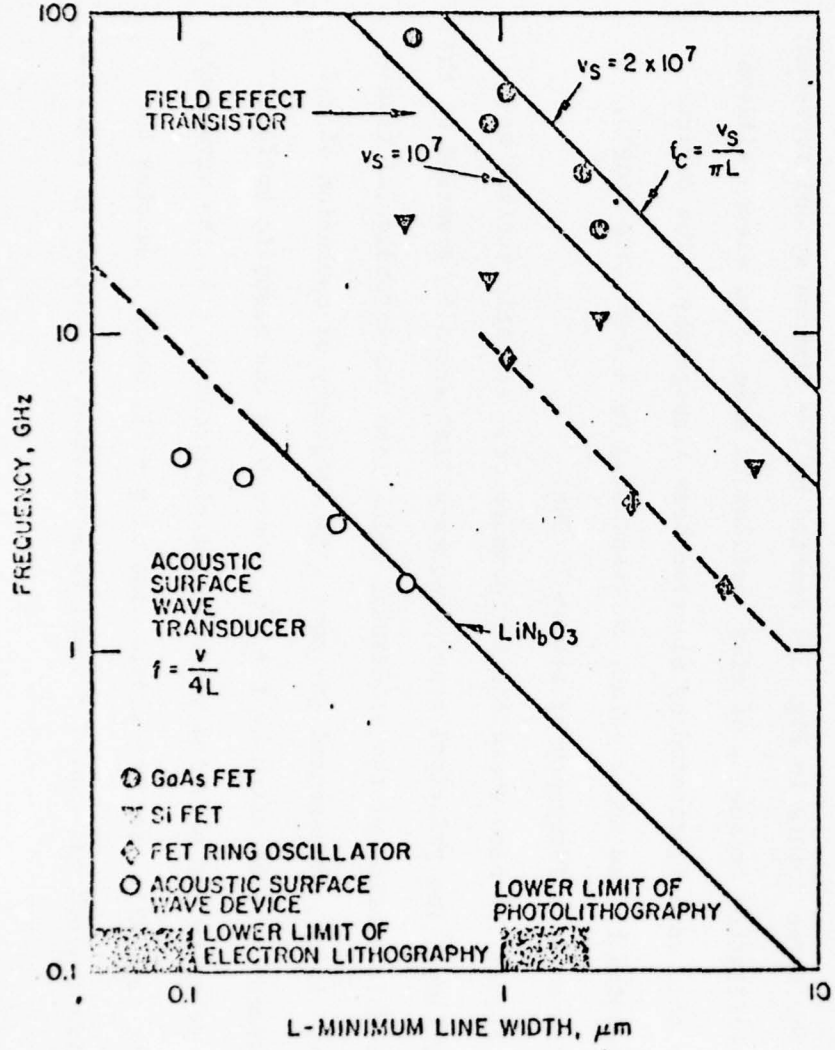

Figure 3.4. High frequency limit of a microwave FET as limited by the minimum linewidth.

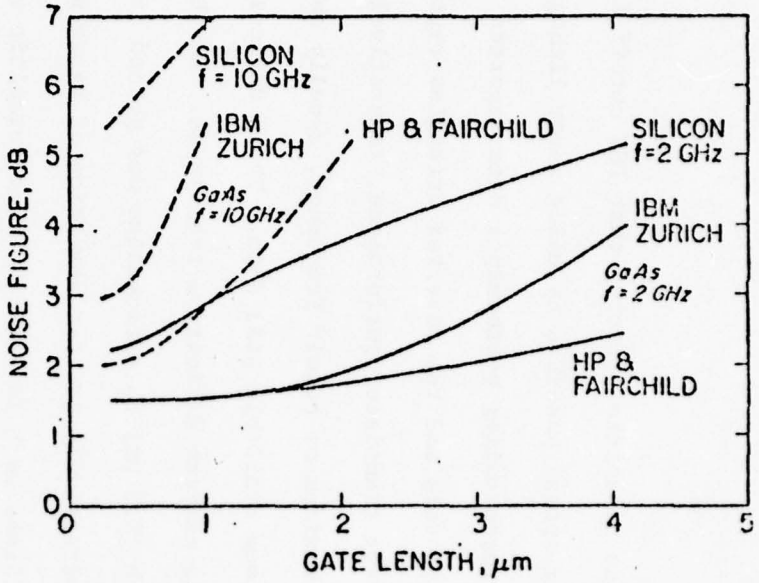

Figure 3.5. Effect of gate length on noise figure for microwave FET.

(which neglect device parasitic effects) that FET cutoff frequencies greater than 100 GHz appear possible by using x-ray lithography techniques. A number of points representing performance data reported in the literature are shown. The solid dots and the inverted triangles represent GaAs and Si microwave field effect transistor performance, respectively. The ordinate position shows the maximum or cutoff frequency, usually obtained by extrapolation of the maximum available gain data. These devices were all made by photolithographic pattern definition techniques. In the case of the smallest gate length (0.5 μm) this technique was pushed to its limit. It is seen, by the progressively greater deviation of these points from the transit time limit lines as L is reduced, that parasitic effects are also important determinants of device performance.

The three points in Fig. 3.4 denoted by the diamond symbol represent the oscillation frequency of ring oscillators made up of eleven silicon FET's that were fabricated by electron-beam lithography. The devices represented by the upper point, corresponding to a 1-μm gate length, oscillated at a frequency of almost 10 GHz.

Figure 3.4 also shows the performance of an acoustic surface wave delay line. The principal upper frequency limitation is governed by the achievable spacing of the electrodes which form the interdigital transducer. In the fundamental (π) mode, the frequency of operation of the transducer will be given by $f = v/p$, where v is the acoustic surface wave velocity and p is the pitch of the electrode ($p = \lambda$, the wavelength on the crystal). For the simple case of $p = 4L$, where L denotes the electrode width and gap, $f = v/4L$; this relation is plotted in Fig. 3.4

for wave velocities corresponding to $LiNbO_3$. The points plotted near this line represent a pulse compression filter, fabricated using serial electron beam lithography, a nondispersive 2.5 GHz delay line, and transducer patterns that were fabricated for operation at 3.5 GHz and 4.1 GHz. The points are off the straight line because the electrode width was less than a half period.

The clock rate of the charge-coupled device shift register can also be made higher by the use of higher resolution lithography. In this device the gap between electrodes should be made small for fast charge transfer. The maximum frequency can be shown to vary approximately as $1/L^2$ (where L is the electrode pitch). The power depends on the area of the CCD.

The effect of gate length on device noise figure for microwave FET's made in silicon and gallium arsenide is shown in Fig. 3.5. These curves were derived from published data and extrapolated slightly to smaller gate lengths. It is noted that the trend is strongly toward lower noise figures with shorter gates, particularly for silicon and for gallium arsenide at the higher operating frequency (10 GHz). The noise figure values at the shorter gate lengths compare favorably with the best microwave bipolar transistors. By employing x-ray lithography to fabricate FET's with submicron gate length, and with further device optimization for low noise, even lower noise figures could be obtained.

3.6.4 Theoretical Size Limits of Microelectronic Devices

The theoretical limits to the size of silicon microelectronic devices have been estimated by HOeneisen and Mead (1972). For conventional MOS

field-effect transistors and CCD shift registers the thickness of the gate oxide must be reduced as the gate length is reduced. The ultimate limit is set by electric field breakdown of the gate oxide (SiO_2); a practical limit may also be set by the oxide pinhole density. Hoeneisen and Mead give, as an example, the design for a typical minimum size MOS transistor which has 0.24 μm gate length, 140 Å gate oxide thickness, and 2.7×10^{17} cm^{-3} substrate doping concentration. Other factors which limit the device dimensions to about the same size are drain-source punch-through, drain-substrate breakdown, drain 'corner' breakdown, and statistical fluctuations in the substrate doping.

Hoeneisen and Mead (ibid.) also estimate a minimum size bipolar transistor where the smallest lateral element is the opening for the emitter contact window. In their example of a minimum size isoplanar transistor the emitter dimension is $3r \times 3r$ where r is the base thickness. The minimum base thickness is determined by punch-through, a condition where the depletion regions extending from the emitter and collector junctions overlap. The depletion depth is minimized by high base doping concentration up to the limit of collector junction breakdown. A voltage margin must be allowed for statistical fluctuations and manufacturing tolerances in the base doping concentration. The minimum collector-base voltage for logic circuit operation is assumed to be two diode drops (1.2 V for silicon). This combination of conditions results in a minimum size isoplanar transistor with r = 0.07 μm and thus a minimum geometry element of 0.21 μm square. Power dissipation requirements may limit the

packing density of such transistors to somewhat larger dimensions in fully active logic circuits. However, it should be possible to realize these theoretical limits in a low power bipolar technology such as I^2L.

Although integrated circuits have not yet been fabricated with such small dimensions, it does appear to be theoretically possible if the limitations of present-day lithography and etching can be improved. Discrete SBFETs have been fabricated with 0.5 μm channel length in both silicon and gallium arsenide (Baechtold et al. 1973). The fabrication of minimum size MOS and bipolar devices with accurate control of the 0.2 to 0.25 μm linewidths will require the use of techniques such as x-ray lithography with resolution capability on the order of 0.1 μm or better.

Other types of microelectric devices such as magnetic bubble and Josephson junction devices can also be made much smaller than the present state-of-the-art. Keyes (1975) estimates that magnetic bubbles could operate with 0.01 μm diameter bubbles. Josephson tunneling structures (Anacker 1974) operate with tunneling thicknesses of less than 100 Å and the switching energy ($< 10^{-14}$ J) is so small that the lateral dimensions could be theoretically reduced to 0.1 μm or less in order to achieve high packing density. Thus the theoretical size limits of many types of microelectronic devices are less than 1 μm and justify the development of x-ray lithography so that these devices can be fabricated.

3.6.5 Devices Fabricated with X-Ray Lithography

Although x-ray lithography is still a very new technology the following experimental work has been reported on device fabrication by this technique.

Surface acoustic wave devices were one of the earliest applications of x-ray lithography because they require only a single masking step. X-ray replication of surface acoustic wave device patterns has been reported by Spears and Smith (1972), Smith (1974), and Sullivan and McCoy (1975). In fact, a complete x-ray lithography system for the fabrication of surface acoustic wave devices has been delivered to the Air Force Cambridge Research Laboratories (Sullivan 1975). Patterns with lines as small as 0.5 μm have been replicated (Sullivan and McCoy 1975) thus extending the frequency capability of these devices above 1 GHz.

A similar component (one mask level, small area, high resolution) which has been fabricated by x-ray lithography is a Fresnel zone plate. These devices are useful for x-ray focusing. Lines as small as 1000 Å wide were x-ray replicated (Feder et al. 1976) with a carbon K source (44 Å wavelength) and with synchrotron radiation (Spiller et al. 1976).

Another application which requires only one masking step is the fabrication of magnetic bubble circuits. These circuits cover a much larger area than SAW devices. Patterns of this type have been x-ray replicated by Maydan et al. (1975), Watts et al. (1976), and Spiller et al. (1976). The small, well-defined lines obtained by x-ray lithography are advantageous in order to achieve a high packing density in the memory circuits.

A similar application (one mask level, large area) demonstrated by Spiller et al. (1976) is the x-ray replication of large quantities of submaster and working x-ray masks from a master mask.

The unique properties achieved by x-ray exposure of a high resolution resist with no scattering effects allowed Neureuther and Hagouel (1974) to fabricate blazed diffraction gratings.

In order to take advantage of the high resolution capability of x-ray lithography for silicon device and integrated circuit fabrication, a corresponding increase in the precision of mask alignment must be achieved. Some effort in this area has been reported by McCoy and Sullivan (1974, 1976). To date the only devices of this type fabricated by x-ray lithography have been limited to conventional geometries by available alignment techniques. Bernacki and Smith (1974) reported the fabrication of p-n junction diodes with minimum linewidths of 2.5 μm, bipolar transistors with minimum linewidths at 10 μm, and MOS transistors with minimum linewidth of 2.5 μm (Bernacki and Smith 1975). All of these devices performed as well as similar devices fabricated by photolithography; there was no degradation of performance due to x-ray exposure.

3.6.6 Other Small Devices Fabricated by Electron Beam Lithography

While the following microelectronic components have not yet been fabricated by x-ray lithography, performance advantages have been demonstrated in small linewidth devices fabricated by scanning electron beam lithography.

A performance comparison between devices and IC's fabricated by electron beam and by conventional lithography is given in Fig. 3.6. The two points marked EB on the right side of this figure represent the performance of the FET ring oscillator plotted in Fig. 3.4, and an FET NAND circuit. From simple scaling considerations the maximum frequency

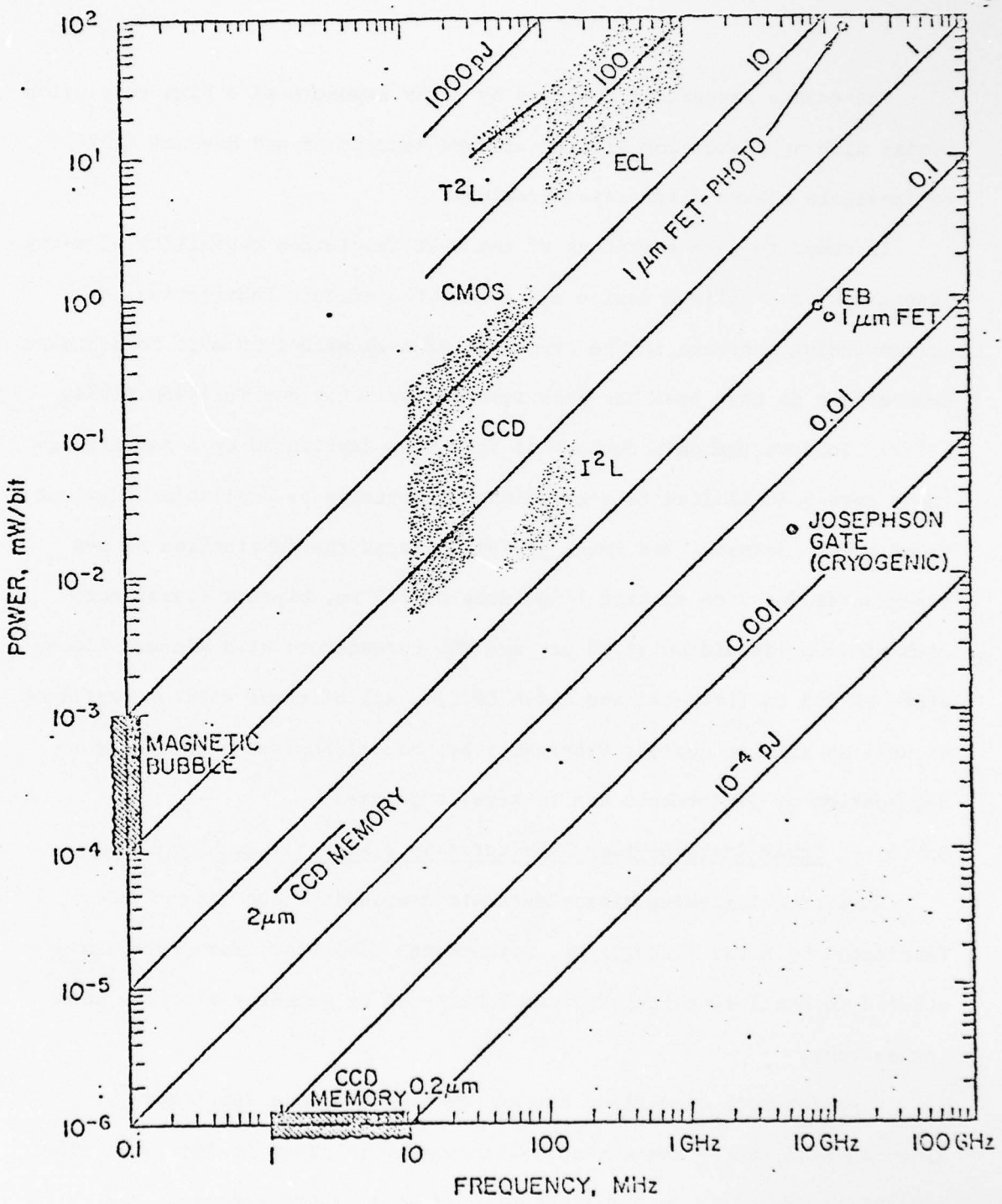

Figure 3.6. Relative performance characteristics of microcircuits fabricated by electron beam and conventional lithography.

(inverse minimum propagation delay) should vary as L (the gate length). The power per device will vary approximately as L^2Z (where Z is the gate width). Thus, the speed-power product $P \cdot t_{pd}$ will vary roughly as L^3Z. Comparing the CMOS data in Fig. 3.6 (devices made with roughly 5 μm design rules) with the electron-beam-fabricated devices, we see a decrease by a factor of $\sim 10^2$. Thus, the devices with smaller dimensions exhibit roughly the expected performance gain. Even better performance should result from devices with submicrometer gate length.

The values of propagation delay observed experimentally for the two devices made by electron beam lithography show that there is no electronic effect that will limit the frequency of an IC made with 1 μm design rules to less than 10 GHz. The power per gate can be expressed roughly as fCV^2, therefore, power will increase with operating frequency. Let us see if power dissipation will form a limit on frequency. With 1 μm design rules, a gate density of approximately $5 \times 10^6/cm^2$ is possible. Since each gate must dissipate about 0.8 mW ($\sim$0.1 pJ at 10 GHz), the power dissipation capability of the IC must be 4×10^3 W/cm^2. While this value is very high by conventional IC standards, it is less than the power density typical of microwave solid state devices. For example, the power density at the device-heat sink interface of a Ka band silicon IMPATT is $\sim 10^6$ W/cm^2. The reason that this high power density can be sustained with tolerable temperature rise is that the heat flow away from this tiny area takes place in the two lateral directions as well as the perpendicular. This well-developed technology used in microwave devices can be applied to high performance integrated circuits. It can be shown that 20,000 gates can be

made on a 2 mm × 2 mm chip and the power corresponding to an 8 GHz operating frequency dissipated without excessive temperature rise. At the lower left of Fig. 3.6 we show projections of CCD memories made with 2 μm and 0.2 μm minimum design rules. Since power in these devices varies as area, it is clear that the way to low speed-power product is through high resolution lithography.

A GaAs Schottky barrier FET has been fabricated with a 0.5 μm wide gate electrode by Ozdemir et al. (1976). This transistor had a gain of 8 dB at 18 GHz.

An X-band transistor with 1.0 μm wide emitter contacts was fabricated by scanning electron beam lithography by Kruger et al. (1975). Compared to a conventional transistor with 1.25 μm wide contacts, it exhibited a 25 percent improvement in power added efficiency at 10 GHz and the fabrication yield was improved by a factor of 10.

An 8,192 bit random access memory chip (MOS FET) has been made with 1.25 μm minimum linewidths by scanning electron beam lithography by Yu et al. (1975). It operated with an access time of only 90 nsec.

3.6.7 Benefits of X-Ray Lithography - Summary

Significant benefits to the microwave solid state and microelectronics fields by the use of x-ray lithography are seen. These benefits are summarized in the chart below.

There are two types of benefits foreseen. First: Increased device or IC performance that require the achievement of surface electrode dimensions that are unattainable, as a practical matter, by the use of photolithography. Since device and IC performance have been pushed to their limits using

contemporary techniques, and there is system demand for further performance growth, the implementation of advanced fabrication technologies is vital.

Secondly, by the use of smaller devices to form integrated circuits a higher level of integration is possible on a chip. The smaller number of contacts per function and smaller silicon area required per function should result in significant yield and therefore cost improvements. The smaller silicon area and/or the use of fewer integrated circuits per system should result in higher reliability.

It is also very important to recognize that these benefits can accrue by using this new technology well within its operational limits. The most useful region of resolution (e.g., 0.5 to 1 μm) is outside of the photolithographic regime, but is well above the ultimate limit (<0.1 μm) of x-ray lithography.

Table 3.1

- HIGHER PERFORMANCE
  - Microwave FET - Higher Frequency
    - Lower Noise
  - Integrated Circuits - Higher Speed
    - Lower Power
  - Acoustic Surface Wave Devices - Higher Frequency
    - Broader Bandwidth
- LOWER COST PER FUNCTION
  - By Higher Integration on Chip
  - By Higher Yield Without Contact Lithography
- HIGHER RELIABILITY
  - Lower Silicon Area/Function
  - Fewer System Interconnections
- NEW TECHNOLOGY
  - These Benefits Accrue Without Using X-Ray Lithography Near Its Resolution Limit

Having determined some basic parameters for the various applications of x-ray lithography, the advantages of x-ray laser radiation over conventional sources are now clear. First, the source intensity will be high enough to lead to exposure times of grainless media measured in seconds rather than hours. This is particularly important for mass-production where the advantage of x-ray lithographic methods of simultaneously producing many copies must not be counteracted by the long exposure times that presently characterize this approach. Second, as will be discussed more fully subsequently, the advantage of data storage by holography may be realized at x-ray wavelengths. The early promise of data storage by optical holography which depended on improved discrimination against dust particles, scratches on the recording material, etc., has never fully come to pass because of the concurrent improvement in orthodox optical methods. With x-ray holography, the advantage of spreading the information over areas large compared with a μm, say, becomes significant as optical methods will no longer be available at the bit densities envisaged.

Third, the inherent monochromaticity and narrow linewidth of the laser source can provide enhanced contrast by judicious utilization of absorption edges. Fourth, chromatic aberration to which most x-ray optics are prone will be absent, making it possible in particular to utilize the large gathering power of zone plates in imaging systems. Fifth, the excellent collimation of the ultimate x-ray laser will not lead to the problems of penumbral blurring and geometric distortion, which limit the resolution obtainable by conventional means, thereby yielding improved geometrical fidelity.

The most serious disadvantage with this application of x-ray lasers is, of course, the economics. But it should be appreciated that an x-ray laser facility would presumably not be used exclusively for a particular application. Rather, it would be user oriented much like the various synchrotron facilities and other particle accelerators, and the high-power infrared laser installations built in recent years. A particular facility would thus be available to a large number of research groups covering among them a large number of applications.

4. MEDICO-RADIOLOGICAL APPLICATIONS

The use of monoenergetic x rays for radiological applications has been discussed and investigated in many laboratories since the early 1950's. Practical use for these has been limited both for research and clinical applications by the lack of adequate sources.

4.1 Differential Absorption

Two important applications of monoenergetic x rays in modern diagnostic radiology and in physiological research are: the improvement of the contrast obtained in radiographs, and the quantitative determination of heavy elements in vivo. These applications were first discussed by Jacobson (1953) who termed this technique dichromography. The terminology was meant to describe a technique which uses the absorption differentials between two or more x rays of different wavelengths for the production of a roentgenogram, showing the distribution of given elements in an organ, or for the determination of the concentration of such an element in the organ of interest. One example might be the determination of the iodine content of the thyroid gland. This is easily done in principle, for example, by the measurement of the difference in absorption of two wavelengths lying close to but on different sides of the K-edge of the element of interest (Engström 1946). Because of the difficulty in measuring small density differences on film, Jacobson (1953) has suggested a slightly different approach which he called continuous dichromography. However, it has been shown recently (Bailey and Crepeau 1975) that using video techniques and simple computer processing, a differential absorption of less than 1 percent can be detected with a statistical certainty of better than

97 percent. Another approach to this problem, using a multi-wavelength technique, will be discussed below. The technique proposed by Jacobson and others would make a useful adjunctive procedure in radiology.

4.1.1 Sensitivity and Contrast

A series of applications using both animals and patients was described by Edholm and Jacobson (1959). After intravenous injection of an iodine containing contrast agent in rabbits, both the actual iodine content and its distribution in the body were studied as a function of time after injection. The method was also used to study the iodine content in the blood, bile, and urine of cholecystectomized human subjects. These experiments utilized compensating wedges to provide the required sensitivity (continuous dichromography). To improve the method these authors suggest the use of 4 wavelengths and 4 wedges (soft tissue, fat, bone, and iodine). Even with the limited intensities they had available, readings only required about 1 sec of x-ray exposure. Another major advantage which they found was that only approximately 0.1 of the normal contrast agent concentration was required. This is of major importance since both the number and severity of contrast agent reactions increase with the amount injected.

4.2 Fluoroscopy

In their original experiments a secondary x-ray beam was generated by using the 90° scatter from a target irradiated by the usual inhomogeneous beam. This results in a beam having a majority of its photons at the characteristic wavelength of the scatterer. The source(s) of monochromatic x rays used in their later work was not discussed.

Ort et al. (1973) using the same principle, have described an electronic subtraction technique for fluoroscopically generated images. They concentrated on the imaging of periodic contrast changes such as found in the lungs and the cardiovascular system. They generated quasi-monoenergetic x rays by filtration of the usual inhomogeneous clinical x-ray sources. To record these time dependent images the filters were mounted on a revolving disc driven at the proper rate.

For in vivo applications this method can only be used to detect elements which have a K-absorption edge above 20 keV since the x rays used must have sufficient penetration to make their use feasible with human subjects.

A more general paper describing the results obtained with the fluoroscopic imaging technique was published by Mistretta et al. (1973). They point out that the advantages of this approach are: it is a low cost addition to standard clinical apparatus, it eliminates the need for a scanning detector when images of the distribution of the element of interest are desired, it eliminates the need for administering radioactive drugs in certain instances, and it provides images with higher resolution. Imaging times are of the order of 1 sec. In the case of iodine they found each mg/cm^2 of concentration in soft tissue gives rise to a differential absorption signal of approximately 1 percent. The filters used in this work were composed of iodine and cerium.

Jacobson (1964) had also devised a similar technique using crystal-photomultiplier detectors and an analog computer to process the data. The system used both a reference and an object beam, each having a series of absorption wedges (3) and 3 wavelengths generated by a special x-ray tube.

This tube had secondary radiators or targets residing within the tube envelope. Using this equipment and his modified technique he was able to determine iodine content *in vivo* to an accuracy of about ±20 percent. His study also included making bone density profiles on two groups of patients, one a control group and the other osteoporotic. As he correctly points out, the method gives for the first time a technique which has application in any situation where a pathological condition may have or has resulted in a change of elementary composition.

4.3 Dosage and Sensitivity

A project designed to provide information on photon flux requirements for accurate quantitation of several elements *in vivo* was described by Atkins et al. This study utilized semiconductor detectors which gave the system the capability of responding simultaneously to several monochromatic beams. Because of the high resolution capabilities of the semiconductor detectors, they have the ability to separate beams close together in wavelength. Three beams were used (one for reference) but of course no filters were required. They were again limited by low beam intensity. They concluded that to determine concentrations of iodine in the thyroid of 1 mg/cm^2 requires 10^6 $photons/cm^2$ in each beam.

In a recent article Kelcz and Mistretta (1976) reported the results obtained with their fluoroscopic technique using a three filter method. They found that by using carefully selected filters, and logarithmic image processing they were able to present difference images in which only the element of interest was visualized.

The usefulness of monoenergetic x rays having wavelengths bracketing certain absorption edges for increasing roentgenographic contrast has also been discussed recently by Atkins et al. (1975). This work included a rather comprehensive investigation of x-ray spectra produced by diagnostic apparatus and the effects of various types of filtration using characteristic absorption edges in creating a band pass effect. They found for example that the use of gadolinium filtration increased the contrast for both iodine and barium. A further bonus found with this type of system is a decreased patient dose.

The development of computerized tomography (CT) has resulted in a new and dramatic improvement in medical imaging technology. Its impact on neuroradiological procedures has resulted in improved diagnosis, and the elimination of traumatic, complicated, and both time consuming and costly procedures while reducing morbidity and mortality statistics. It has increased the radiologist's capability to visualize structures having minimal differential attenuation between themselves and surrounding tissues. The technique is now rapidly expanding into imaging of other regions of the body. Since the resultant image is reconstructed from a matrix of attenuation coefficients, the accuracy with which each matrix element is determined and their relative values will depend on the beam quality not varying as it traverses the patient. With the usual inhomogeneous x-ray beam, even after filtering, beam hardening (preferential absorption of the low energy components) takes place. The use of a monoenergetic beam would eliminate this problem.

The above examples clearly illustrate the need and desire for monoenergetic x-ray sources having sufficient intensity and the proper

wavelengths for a number of applications of diagnostic importance in clinical medicine and for physiological studies. In the case of thyroid disease, iodine content of the thyroid ($\sim$2 mg/cm^2) and its distribution in the gland is of significance. In the case of osteoporotic patients quantitative studies of calcium or bone mineral content are highly significant as is its cross sectional distribution in the bone. A third application which uses quasi monoenergetic x rays for many diagnostic studies is mammography. Here the usual tungsten target x-ray tube is replaced by one with a molybdenum target. When used at a low potential such as that required for mammography ($\sim$35 kVp) the K_α emission ($\sim$17 keV) is a significant contributor to the total x-ray flux incident on the object to be radiographed. An obvious improvement would result if the higher energy bremsstrahlung component were completely absent as with x-ray laser radiation.

For the determination of the required flux levels one must decide on a technique, a level of accuracy, and the resolution desired. For example, if one wishes to determine whether two areas have equal densities, the flux requirements (statistical), or the number of quanta which must be terminated by the object varies inversely with the largest permissible error one wishes to tolerate. For example, if the largest permissible error is to be 1 percent, then 8×10^4 quanta must be terminated by the object. For a 0.1 percent error this number would rise to 8×10^6. To determine concentrations of 1 mg/cm^2 of iodine in the thyroid requires a flux of about 10^6 photons/cm^2. This would require a flux of about 200 times this amount incident on the patients' skin ($\sim$10 mR). For thicker body parts a flux of about 5 times this amount would be required. The resolution requirements have been calculated by Kelcz and Mistretta (1976). The following graph (Fig. 4.1) is from this publication.

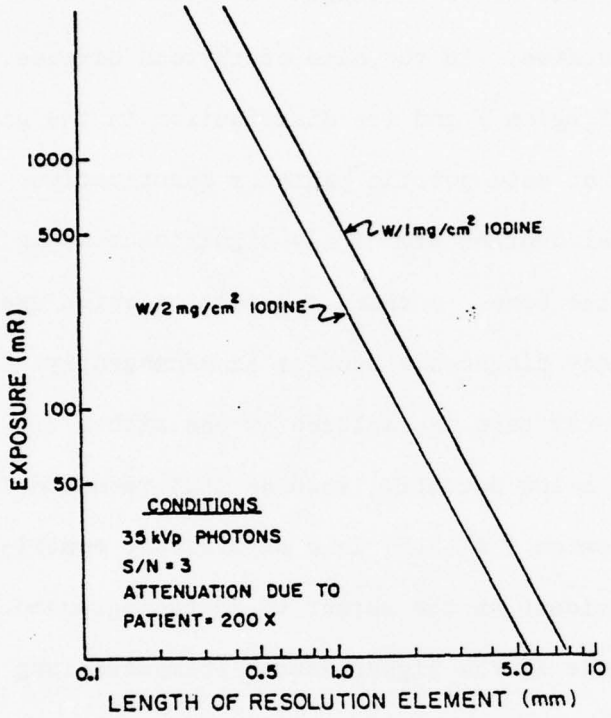

At this energy, 1 mR is approximately equal to 1.7×10^7 photons/cm^2.

Figure 4.1. Statistically limited resolution plotted as a function of patient exposure.

4.4 Holographic Imaging

Three-dimensional presentations of organs or portions of the body at depths would be useful for: diagnosis of abnormal anatomical situations produced by congenital abnormalities or disease processes, analysis of extent and geometry of tumors, the location of tumor masses with respect to normal structures, and the dynamic changes associated with the functions of the various organ systems.

A two-step method for holographically recording 3-dimensional images of incoherently illuminated objects was described by McCrickerd and George (1968). In this method, the holographic stereogram is a multiplexed plate made by holographically recording a series of ordinary

photographic transparencies on a single photographic plate. The use of this technique for producing 3-dimensional x-ray pictures was first described by Redman (1968) and later by Shuttleworth et al. (1969).

These early attempts at 3-dimensional roentgenography required special equipment and resulted in a large patient dose. Using a different concept, Baily et al. (1971) made use of tomographic sections made on conventional clinical tomographic units. Each of the body sections was multiplexed over the entire area of the holographic plate. The film-to-plate distances were made proportional to the corresponding distances of the x-ray target from the central planes of the tomographic sections. Reconstruction is effected in the usual manner. This yields a virtual image for each tomographic section hologrammed and all of these are viewed simultaneously from the emulsionless side of the plate. A steroscopic image of the object is the result. The results using two physical objects were found to be quite satisfactory for applications in radiation therapy treatment planning. A further investigation showed that the same process was applicable to the study of anatomical structures (Baily et al. 1971). These authors produced a 3-dimensional representation of the lumbar vertebrae. This holographic presentation consists of the detailed anatomical information present in each of the in-focus levels represented by the individual tomographic sections. Obviously, a truly coherent x-ray beam would result in a simplified procedure and significantly reduced patient dose. Further details on x-ray holographic techniques are given in Section 7.

4.4.1 Photon Energy and Dosage

The x-ray energy requirements for roentgenographic imaging are generally in the range of 60 to 125 kVp. The effective energy range in

terms of monoenergetic radiation is 40 to 70 keV. High speed film requires approximately 1 mR for producing a film of density = unity. The loss (absorption plus scatter) of x rays incident on the object varies from about 50 to 10^3. This therefore places a requirement on the beam intensity of approximately 10^{11} photons/cm^2. Since patient movement must be avoided, this flux must be delivered in a time of 0.1 sec or less for routine applications and in times of the order of a few millisecs for some angiographic applications.

4.5 Microprobe

There are at least two applications which the extremely small diameter of the expected x-ray laser beam would be a real asset. The first of these would be for microirradiation studies. The application of a laser beam for such studies was originally described by Bessis (1962). Since that time there have been many studies of this technique and which have been summarized in a recent review by Berns et al. (1976). There appear to be two major areas for such studies. First, we have studies that describe the effects of small beams on the cell and second, studies that use the beam as a tool to study cell function. Cell function is studied by irradiating various subcellular structures. These experiments require beam diameters as small as 0.25 μm. The studies are carried out through the use of time lapse photography. The energy densities which have been used range from 25 $\mu J/\mu m^2$ to 10^3 $\mu J/\mu m^2$. The availability of x-ray wavelengths would simplify such studies since no dyes to facilitate absorption of particular wavelengths would be required, thereby giving greater flexibility to the investigator.

The rapid growth in the use of laboratory studies for diagnostic procedures in medicine has supplied the impetus for the development of many automated procedures designed to increase speed, thereby making information available in a timely fashion, and to reduce patient cost. One of the more spectacular successes has been the development of laser flow microphotometry for the analysis and sorting of cells using a continuous flow of cells in suspension. This development was originally described by Van Dilla et al.(1969). Present systems allow quantitative measurements to be made of the optical properties of individual mammalian cells. The optical pulses are detected, etc. and analyzed using nuclear spectroscopic techniques. The availability of x-ray lasers would allow one to expand such studies so that x-ray fluorescence analysis could also be used. These might also replace some light scattering studies where the use of dyes and staining techniques are not really appropriate. Three major advantages of such systems are: rapid quantitative measurements are possible on large numbers of cells (5×10^4 cells/min); high statistical precision; measurements on individual cells within a population are now possible with this method. In addition to fluorescence measurements, light scattering studies have been used as indicators of size, internal structure, and surface detail. Monochromatic x radiation in a small diameter beam from an x-ray laser should be even more useful for such studies.

Some new areas which might be approached using x-ray wavelengths are:

1) Measurement of the distribution of angular scattering for cell identification.

2) Absorption measurements on single cells.

3) X-ray fluorescence analysis.

5. METALLURGICAL APPLICATIONS

Since x-ray techniques with conventional sources have been used for many years to study the composition, weld integrity, surface contamination, and many other properties of metals, it is to be expected that access to the intense, monochromatic, and well-collimated beam from an x-ray laser would have a large number of advantages, opening up areas of investigation previously hardly accessible. We sketch below some of the more important areas in metallurgy that will benefit from the availability of such a source. Some applications have already been realized with the aid of synchrotron radiation. In view of the drawbacks mentioned earlier (Section 2) of this source, one expects considerable improvement in resolution and exposure times with a still more intense beam of properly chosen wavelength.

5.1 X-Ray Penetration in Metals

An important aspect of metallurgical studies in the examination of the surface of metals for hardness and for the presence of wear. These properties are closely related to such surface layer parameters as crystallite size and average strain which in turn are conveniently studied by x-ray diffraction. To examine the usefulness of x rays for such surface studies it is useful to list a number of conventional sources and the degree to which their K_α radiation penetrates in various metals. This penetration depth follows readily from values for the mass absorption coefficients at various wavelengths and metal densities given, for instance, by AIP (1963, Ch. 8). From Table 5.1 given by Bienenstock (1975) it will be seen that in iron regions varying in thickness from 4 to 64 μm can be probed by a judicious choice of incident wavelengths; for Cu the range

Table 5.1. Penetration Depths in Metals

Material	1/e Penetration Depth in Microns for Various K_α Radiations - λ in Å						
	Ag-0.5608	Mo-0.7107	Cu-1.5418	Fe-1.9373	Mn-2.1031	Cr-2.2909	Ti-2.7496
Fe	64.1	32.8	4.1	19.0	15.0	11.7	6.9
Cu	42.4	22.0	21.2	10.9	8.6	6.7	4.0
Mo	22.0	77.6	8.8	4.8	3.8	3.1	2.0

is from 4 to 42 μm, while for Mo layers from 2 to 78 μm can be probed. The effective depths of material which contribute to a diffraction peak is $x/\sin\theta$ with x the depth and θ the Bragg scattering angle.

5.2 Surface Studies

There remains a controversy whether the surface of a work-hardened crystal is soft (Fourie 1968) or hard (Kramer 1968). This question is closely related to the surface microstructure. Unfortunately, probes of the surface or a cross-section of it by micro-hardness measurements are suspect because interaction effects in the tests extend over a μm range. Studies by transmission electron microscopy are of doubtful value because image stresses produce changes in dislocation structure and loss of dislocations.

The requirement of small depth gauging implies operating near an absorption edge where fluorescent decay is an undesirable concomitant which can only be removed by elaborate procedures involving pulse-height analyzer systems. Tunability of the radiation source is important as we can then work arbitrarily near the absorption edge leading to the desired small penetration depth. The use of continuous synchrotron radiation has in fact been proposed (Bienenstock 1975). This source has the further advantage of high intensity which becomes important for studying the lighter elements. However, because of the problem of fluorescence it becomes necessary to use monochromators with a loss of intensity. More seriously, perhaps, the very advantage of high intensity now becomes a disadvantage because of the production of sub-harmonic multiples by the monochromators (cf. Section 2.4). These must be filtered out, leading to

further signal degradation. A tunable x-ray laser would suffer from none of these drawbacks while retaining the advantage of high intensity.

Directly related to the hardness of a metal surface is the problem of determining wear. A new theory by Suh (1974) is based on the existence of a soft layer at worn metal surfaces. The determination of such a layer would be facilitated by accurate methods for deducing dislocation cell structures (crystallite size and average strain) in the 0.5 to 5 μm depth range. The results would be relevant to possible non-destructive evaluation of wear of engine parts, for example, by oil analysis rather than by maintenance inspection. Bienenstock (1975) has proposed to ascertain the existence of the soft layer postulated by Suh by careful measurement of diffraction line shapes from the surface. Their Fourier components to different orders of reflection are compared and the crystallite size and strain effects separated. This separation is carried out at different wavelengths such that the diffraction contribution from a depth of one surface layer can be compared with that from twice this depth. On the basis of this information it should then be possible to infer whether a soft surface layer indeed overlays a harder subsurface. It appears that resolution requirements are not severe as they are in the 100-300 eV range.

Another potential application of this method for surface characterization is for testing polished molybdenum mirrors which have been suggested for use in focusing high power infrared laser beams. It may be that the reflectivity and breakdown thresholds are set by the presence of crystallites in the skin depth ($\sim$0.1 μm). Bienenstock (1975) thus suggests correlating the linewidths of diffracted radiation with reflectivity and breakdown threshold to facilitate quality control measurements.

Ag K_α radiation ($\sim$0.56 Å) was proposed for this purpose but an x-ray laser in this wavelength range would clearly be superior because of beam size and intensity. Minimum defect structures in waveguides and heterojunctions could be similarly determined.

Special x-ray techniques have been developed for examining near-surface dislocation structures by Berg and Barrett (Barrett 1945) and for transmission through relatively thin crystals by Lang (1959). In the Berg-Barrett techniques, for example, a beam of x-rays falling on a surface at arbitrary incidence will be coherently reflected at the Bragg angles. Information about local variations in surface structure can thus be obtained by employing grazing incidence and recording the locally diffracted beams. Grain and sub-grain structures are exhibited by variations in image contrast. The high intensity x-ray laser would be an excellent source for these procedures leading to shorter exposure times with less background noise. For the Berg-Barrett technique the use of longer wavelength radiation would also have the advantage of thinner penetration.

5.3 Radiographic Nondestructive Testing

An important potential area of application of x-ray lasers is that of autoradiographic nondestructive evaluation. Quantitative elemental analysis would be greatly facilitated with tunable highly monochromatic x-ray or γ-ray lasers. With high intensity highly collimated sources (whether coherent or not) radiation gauging of small sections, i.e., detection of changes in the effective thickness of a test article, becomes feasible. Internal voids, inclusions, and changes in actual thickness can thus be determined. This would be especially useful in studying void formation in

irradiated materials (Ianniello 1972). By operating the laser near known absorption edges elemental specificity can then also be achieved. Radiography would in fact be revolutionized by the additional technique of holography, creating the possibility of generating three-dimensional images of interior flaws, with the consequent ability of determining size, shape, location, and orientation of such flaws. An important specific application would be to direct-shape, hot-isostatically compacted aircraft parts where conventional methods such as ultrasonic inspection are inapplicable.

Autoradiographic techniques with the beam normal to the crack surface would be useful in examining specimens containing fatigue cracks to determine the extent to which the crack closes on unloading and the closure pattern. More generally, such studies with various beam directions could be used to resolve defect structure in the plastic zone at the crack tip in either fatigue or static loading. At sufficient photon energy (in the MeV range) the reflective or backscattering technique can yield information about the interior of thick metal sections. This would have significant implications for the determination of the soundness of weldments where access to both sides may be impossible. The detection of the critical nucleation size of a crack in fatigued solids would also be facilitated. The requirement here is for intensity and spot size rather than monochromaticity. Zone plate focusing would aid in obtaining depth information.

X-ray lasers operating in the wavelength range appropriate for crystal lattice diffraction would be useful for lattice strain measurement and, inferentially, residual stress measurement in crystalline structural materials (cf., e.g. Tetelman and McEvily 1968). The higher intensity, improved

monochromaticity, and superior collimation would, of course, be significant improvements over presently available sources. These qualities in combination with holographic procedures would have considerable impact on the study of the role of lattice strain and disorder in plastic flow, fatigue, and stress-corrosion processes.

A highly focused, or small diameter, intense x-ray source would also be useful in the examination of second phases in metals, especially in the study of critical-sized nuclei of 20 Å approximate size (Christian 1975).

5.4 Practical Considerations

To inject a note of realism, it should be stressed that the practicality of some of the foregoing applications does not just depend on the availability of an x-ray or γ-ray laser *per se* but also on ease of operation, physical size of the needed equipment, and actual improvement in intensity and beam collimation over conventional incoherent sources. Because of the likely massive size of any x-ray laser now foreseen, it seems unlikely that the testing procedures described above will see extensive use in field measurements on actual structures such as pressure vessels, civil engineering structures, etc. On the other hand, a great deal could still be learned by taking laboratory samples to the facility for analysis.

6. ELECTRON SPECTROSCOPY FOR CHEMICAL ANALYSIS

6.1 Introduction

We present here an evaluation of the applicability of x-ray lasers, as presently conceived, to ESCA (Electron Spectroscopy for Chemical Analysis). At this writing, ESCA is already a well-developed form of spectroscopy which enjoys extensive usage for basic science studies in atomic physics, chemistry, and solid-state physics, as well as more applied usage--in an analytical context--for a wide variety of more practical problems. The classical reference on ESCA is "ESCA - Atomic, Molecular, and Solid-State Structure Studied by Means of Electron Spectroscopy", by K. Siegbahn et al. (1967). The basic science of ESCA applied to gas-phase studies is given by Siegbahn et al. (1969). More recent developments and further applications are discussed in Proceedings edited by Shirley (1972) and by Caudano and Verbist (1974), and in the general text by Carlson (1975).

The popularity of ESCA as an analytical tool is attributable to the fact that it yields an unambiguous, nondestructive elemental analysis of the surface of any specimen, including the chemical state of each element. By contrast, x-ray lasers do not yet exist. However, certain laser characteristics were assumed. They are listed below. Our philosophy has been to assess what could be achieved within these characteristics and to indicate desirable improvements. The scope of this study has been to consider only those aspects of ESCA that are radiation-source limited and to examine the ways in which x-ray lasers can improve the ESCA method. But the term ESCA will be interpreted in its broadest sense.

Radiation from an x-ray laser will interact with matter primarily through the photoelectric effect, creating vacancies in electronic states.* The observation of this process can be achieved in several ways: by kinetic-energy analysis of the photoelectrons that escape from the sample (conventional ESCA, or x-ray photoelectron spectroscopy), by kinetic-energy analysis of Auger electrons emitted as the holes are filled, or simply by monitoring absorption of the x-ray beam as it passes through the sample. This last observation could also be made in the fluorescence mode. Because the photon source--in this case the x-ray laser--is the unifying feature of all these methods, we have expanded the scope of this study to include Auger and absorption (and fluorescence) spectroscopy as well as conventional ESCA.

6.2 Relevant Parameters and Damage Thresholds

To focus this study, certain characteristics have been assumed for the x-ray laser (cf., Section 1):

1) A 1-100 Terawatt pulse would be delivered by the pumping laser, yielding, at 0.1 percent efficiency, a 10^{9}-10^{11} watt power level during the x-ray laser pulse. The pulse length is assumed to be between 10^{-15} sec and 10^{-11} sec.
2) The coherence length would be ∿1 mm, the emerging beam diameter ∿1 μ, and the beam divergence ∿1 mrad.
3) The repetition rate would be 1 sec^{-1} or less.

*The cross-section for photoemission exceeds that for other processes by orders of magnitude for x-ray energies below 10 keV. Above ∿100 keV, for example, Compton scattering has to be considered as well.

4) The photon wavelength would be somewhat tunable; e.g., over ∿5 eV by photon mixing with visible or UV laser photons.

5) Gain variation over the laser x-ray line could be used to narrow the line to 10 percent of its natural width.

Once these assumptions are made, an overview of the problem is provided by some order-of-magnitude calculations. Two initial questions that must be answered before we proceed are:

1) Can the sample stand up under the laser pulse? and

2) Considering the extremely low duty cycle of the laser, will there be enough intensity for ESCA?

The first question arises because the energy of the laser pulse is imparted to the sample in a very concentrated form in a very short time. Since the total laser energy is deposited in a time interval ranging between ca. 10^{-2} and 10^{2} atomic vibrational periods (10^{-15} sec to 10^{-11} sec for the pulse to pass through an affected volume element of the lattice versus $\omega^{-1} \sim \hbar/k\theta_D \sim 10^{-13}$ sec for $\theta_D \sim 10^{2}$ deg), phonons may or may not help in reducing the maximum temperature T(max) of the thermal spike in the ESCA-active volume. At any rate phonons propagate too slowly to carry heat away from the affected region during the pulse: at a velocity of 10^{5} cm-sec^{-1}, phonons travel only 100 Å in 10^{-11} sec. To estimate ΔT = T(max) - T(ambient), suppose that 10^{-6} to 1 joule (the limits implied by our assumptions of 1 Å radiation) is deposited instantaneously into a 1 micron^{2} cylindrical valume of a transition metal, which has C_p = 4 joules cm^{-3} deg^{-1}. The mass absorption coefficient λ of, say, iron at 1 Å is 100 cm^{2}g^{-1}, and the density is about 8 g-cm^{-3}. Thus the attenuation length is $\ell = \lambda\rho^{-1} \sim 10^{-3}$ cm. If the entire 10^{-6} - 1 joule were

dumped into the cylinder of volume 10^{-3} cm $\times$ 10^{-8} cm^2 = 10^{-11} cm^3 volume and converted to heat we would have $\Delta T = (10^{-6}$ - 1 joule$)(10^{-11}$ cm$^3)^{-1}$ (4 joules cm^{-3} deg$^{-1})^{-1}$ = 2.5×10^{4} to 10 degrees C. This temperature rise is destructive. In the worst case the active sample volume would be vaporized into a plasma and would also melt its surroundings. Little help can be expected in the form of the photoelectrons taking away energy before it is converted to heat, because the penetration depth of a 10 keV electron is only of the order of 1 micron; i.e., the width of the active cylinder. Some energy will leave in the form of x rays emitted as core holes are filled: perhaps half the energy will be removed in this way. The heating effect can be reduced somewhat by enlarging the beam size, which is most readily achieved by setting the sample back from the laser and using to advantage the 1 mrad divergence angle. At 1 cm distance the spot size would be (10 micron)^2 and the estimated temperature rise $\sim 10^2 - 10^8$ degrees. At 10 cm these figures become (100 microns)^2 and 1 - 10^6 degrees, and at 1 m, (1 mm)^2 and 10^{-4} - 10^2 degrees. This last figure--10^2 degrees--is manageable. It is quite common for ESCA samples to heat up several tens of degrees at the surface from various ambient effects*. This defocusing approach tends to obviate one of the most useful features of x-ray lasers ESCA (microprobe applications), as we shall see later. We conclude that the heat spike during a pulse presents a marginal problem that can be controlled.

*We emphasize that this is a "worst case" solution. It is by no means clear that a destructive ESCA test would not be feasible. Note that the electrons which are representative of surface properties (and the only ones that are analyzed in the full-energy ESCA peaks anyway) emanate from the first 10 - 100 Å of material at velocities of $\sim 10^9$ cm/sec; i.e., they are "free" within 10^{-15} sec.

6.3 Intensity Considerations

Let us address the second question: intensity. In one pulse there are 10^{-6} to 1 joule of laser energy. This is equivalent to 10^{9} - 10^{15} photons at 1 Å (10 keV) or to 10^{10} - 10^{16} photons at 10 Å (1 keV). Because the x-ray laser repetition rate is unlikely to exceed 1 sec^{-1}, and is more likely to be much less, we must consider the x-ray laser-ESCA experiment to be essentially a "one-shot" process. At the lower limit, this photon flux does not compare very well with conventional x-ray sources presently used in ESCA applications, which can deliver about 10^{10} photons sec^{-1} on the sample and can operate in a CW mode*, or with the <u>projected</u> (but not yet realized) performance of electron storage rings of 10^{12} photons/ $sec\text{-}cm^{2}$ on the sample (National Academy of Sciences 1976). At the upper limit, however, the x-ray laser is projected to deliver up to 10^{6} times as many photons in one pulse as a conventional set-up will provide in 1 sec; i.e., a single laser pulse is equivalent to 12 days of ordinary operation. It should be noted that the conventional sources are not appreciably focused. Even in the Hewlett-Packard 5950 ESCA machine the x-ray spot size is about 1 mm by 5 mm.

A flux of 10^{9} - 10^{16} photons $pulse^{-1}$ is eminently usable for absorption-edge studies; in fact it is much stronger at the upper limit than fluxes presently available for EXAFS research in electron storage rings, which tend to run about 10^{10} photons sec^{-1} (cf., Section 2.2). Thus one laser pulse can be equivalent to as much as 10^{5} sec of running time on a storage

---

*This is a mean figure for commericial spectrometers, estimated from observed counting rates. It is accurate to better than a factor of ten in either direction.

ring. Of course several pulses would be required to scan an absorption edge, and problems would be encountered in normalizing the pulse strengths. A beam splitter based, for instance, on the Borrmann effect might overcome the first of these objections (Section 10.7). The primary beam would be split up into many beams each of which could be tuned to a different wavelength by photon mixing.

For ESCA and Auger applications, the flux from a single pulse would be sufficient to produce a complete electron spectrum, although it would be necessary to devise new methods of electron kinetic energy analysis and data storage because of the pulse structure. Without going into details, it seems clear that these methods would be feasible with present technology. Nearly the entire 10^{16} photons pulse^{-1} would be converted into photoelectrons, but, because of inelastic scattering processes, only those electrons emitted from the first 10 - 100 Å of the sample would emerge with their full kinetic energy, i.e., with usable ESCA or Auger information. Thus about 10^{16} (10^{2} Å = 10^{-6} cm)/(10^{-3} cm penetration depth) = 10^{13} photoelectrons would emerge from the sample with full energy. Only 0.1 percent to 1 percent of these would be analyzed in a typical ESCA analyzer (although a special analyzer design would be required, as noted above, this figure would probably be about the same), yielding 10^{10} - 10^{11} counts pulse^{-1} in the full-energy peak, compared to the 10^{3} - 10^{4} counts sec^{-1} presently obtained with conventional x-ray tube sources.

These considerations lead us to conclude at the outset that the x-ray laser sources as presently conceived are well worth considering as ESCA photon sources. Even with a repetition rate of 1 sec^{-1} or less, they

could deliver more photons than conventional sources by several orders of magnitude over a short time interval: indeed they are competitive even on a "one-shot" basis. Their main attraction--a small beam size--can also be their main drawback, because of the intense thermal spike produced during the short pulse length. Until this problem is resolved, it would be difficult to project the breadth of applicability of x-ray laser ESCA. In the remainder of this report we shall concentrate on those applications that are feasible within these constraints, noting that a more optimal pulse structure would make even these applications more attractive, in addition to opening up whole new fields of research not covered in this report.

6.4 Relevant Aspects of ESCA

ESCA, or Electron Spectroscopy for Chemical Analysis, is the name given to x-ray photoelectron spectroscopy by K. Siegbahn and coworkers (1967). It was developed as a spectroscopic technique during the 1960s, following the development of high-resolution electron spectrometers by Siegbahn et al. The method consists of irradiating a sample with x rays of known energy, inducing electron emission from characteristic 1s, 2s, 2p, etc. levels. The photoelectron's kinetic energy is given by the energy balance equation

$$h\nu = E_B + K$$

where $h\nu$ is the photon energy and E_B is the binding energy of the characteristic level under study. Kinetic energy analysis yields K directly and E_B--the quantity of interest--by difference.

The initial appealing feature of ESCA is the versatility of the method: it may be applied to any element except hydrogen, with the elements present in the active sample and their approximate abundances being registered respectively by the position (E_B) and intensity of a characteristic core-level peak of each element. These peaks are reasonably narrow (FWHM $\sim$ 1 eV) and widely-spaced (E_B(C1s) = 284 eV, E_B(N1s) = 410 eV, E_B(O1s) = 540 eV, etc.). These positions are not only well-established experimentally for each element, but are also well-understood theoretically. They may be calculated from first principles, either approximately by using Koopmans' theorem together with a ground-state Hartree-Fock computation (Koopmans 1934) or more exactly by the "ΔSCF" method (Bagus 1965). Binding-energies are well-known for core levels of all the elements: binding-energy tables exist (Bearden and Burr 1967, Lotz 1968, and Appendix I of Siegbahn et al. 1967) and are being continually improved (Shirley et al. 1976). Thus elemental identification by ESCA is unambiguous.

A second feature of ESCA that distinguishes it from other "universal" methods of elemental analysis (Auger, x-ray fluorescence, SIMS, neutron activation, etc.) is the sensitivity of E_B to the chemical state. Chemical shifts of E_B to higher binding energies accompany oxidation of most elements. This is easily understood theoretically: oxidation of the parent atom gives it a positive charge, making core-electron loss (photoemission) a more endothermic process. The practical implications of this chemical-state sensitivity are profound. For example, oxidation of a metal surface on the atomic level can be followed by monitoring the growth of metal-oxide peaks beside the metal peaks (Fadley and Shirley 1968). Many applications of this feature of ESCA have been made (cf., e.g., Caudano and Verbist 1974).

Another feature of ESCA of paramount importanct to materials and technological problems is its surface sensitivity. Characteristic sampling depths for electrons in metallic samples (i.e., the distance travelled before an electron suffers an inelastic loss and is removed from the primary peak) range from 10 Å at 10 eV kinetic energy down to ∿3 Å (maximum sensitivity) over a broad minimum centered around ∿100 eV, up to ∿15 Å at 1000 eV (see, for example, Brundle 1974). Thus ESCA is a "semi-surface" technique, as is Auger spectroscopy. In fact ESCA and Auger have <u>exactly</u> the same surface sensitivity, because in both cases this sensitivity is derived from the characteristic loss properties of the outgoing electrons.

ESCA requires photon energies in excess of the E_B values of all core levels to be studied. However, this criterion can be met with 1000-eV photons, and there is no reason to use higher energies. This follows because it is sufficient to observe <u>one</u> core-level peak of any element: no significant information is obtained by observing additional core levels. The element neon has the most tightly-bound outermost core level--its 1s level is at E_B = 870 eV (Bearden and Burr 1967). Lighter elements have 1s levels at lower binding energies, while all heavier elements have outer 2s, 2p, etc. <u>core</u> levels that are less tightly bound. Thus characteristic lines such as Na K_α (1040 eV), Mg K_α (1254 eV), and Al K_α (1487 eV) (Bearden 1967) are of sufficiently high energy for ESCA purposes. It is clearly not viable to use photons of much lower energy, because the analytical capability would be lost. Moreover, it is also undesirable to use photons of much higher energy. The x-ray line width would tend to be larger at higher energy (lowering the ESCA chemical-shift resolution), the surface sensitivity would be reduced, the electron analyzing efficiency

of the spectrometer would be lowered, and the photoelectric cross-section would be smaller. Thus in every respect an Al K_α x-ray laser would be preferred to Cu K_α for ESCA applications.

Auger peaks are observed in ESCA spectra because of photon-induced holes which are filled by Auger transitions. The Auger lines appear as peaks rather than as derivative spectra because the signal/noise ratio is far higher than in conventional electron-induced Auger spectroscopy. In practice the photon-induced Auger peaks are also better resolved. Photon-induced Auger also has the distinct advantage over electron-induced Auger spectroscopy (the only type in commercial practice) that there is far less radiation damage to the sample. In fact it has been estimated that the amount of radiation damage required to yield the same amount of information is smaller by orders of magnitude in the photon-induced method (see, for example, Coad et al. 1975). This result can also be established by calculation of radiation dosage. The importance of this result for present purposes is that x-ray laser ESCA offers an alternative to the very widely used Auger method that is not only comparable, but actually superior. As one example, we note that Auger spectroscopy is not presently applicable to nonmetallic samples because of the radiation-damage problem. ESCA is applicable to all materials. In addition to the advantages given above, ESCA spectra that show both photoelectron and Auger peaks (as most do) provide a valuable reference for chemical shifts. The reason for this is rather esoteric, but essentially neither ESCA shifts nor Auger shifts alone have any absolute meaning, but their difference, a quantity called the Auger parameter (Wagner and Biloen 1973, Kowalczyk 1973), does.

Absorption-edge spectroscopy is much more sensitive than either ESCA or Auger, for a given photon flux, because all of the transmitted photons are counted. It is not surface-sensitive, however, except in special circumstances (e.g., fluorescence from adsorbates) and it requires both thin samples and highly tunable photon sources. The chemical-shift information obtainable from absorption-edge spectroscopy is similar to that obtained from ESCA shifts (Cramer et al. 1976).

6.5 Basic Spectroscopic Considerations

What can x-ray lasers do for ESCA? We address here the basic spectroscopic improvements that certain features of x-ray lasers would provide for ESCA basic research on homogeneous samples. Microprobe applications to materials are discussed in the next section.

High resolution and tunability are the two features that seem to be most promising in this context. There are, for example, no obvious ways in which coherence properties of lasers will affect ESCA, and non-linear effects are out of reach at the peak pulse intensities that can be tolerated in an ESCA sample.

6.5.1 Line Width

By making use of the variation in gain across the laser line, it should be possible to reduce the line width significantly below the natural width (another approach is to use highly-stripped ions, to suppress Auger decay). In the Al K_α line this natural width is approximately 1.0 eV. Reduction by an order of magnitude, to 0.1 eV, would provide an ESCA source sufficiently narrow to map out fine structural

details that are inaccessible using traditional x-ray tubes as sources*. The most obvious application would be in the determination of core-level chemical shifts in molecules having two or more atoms of the same element in chemical environments that differ only very slightly, a level of subtlety that is beyond the reach of present-day ESCA. For example, it would probably be possible at this resolution to differentiate directly between inequivalent carbon sites in substituted benzenes, which have been predicted to show shifts at the 0.1 to 0.5 eV level (Davis et al. 1972). Another possibility is that of measuring the difference of surface and bulk atoms' core-level binding energies, an effect that has been suspected but not observed. Still another application would be a definitive study of adsorbed molecular species on catalytically active substrates, in several inequivalent sites. Important for both fundamental and practical reasons, this area of research has been the subject of much recent attention and considerable confusion (Brundle 1974).

Line-shape studies of core levels in metals would be greatly aided by higher resolution. The subject of x-ray edge anomalies in metals has recently seen renewed interest because of asymmetries in core-level photoemission peaks that result from the same physical phenomena. Doniach and Sunjic (1970) predicted the form of the asymmetric lines to be expected from many-body effects, and these asymmetries have been observed by Citrin et al. (1975). It is difficult to separate the asymmetry arising

*However, intense monochromatized sources are presently under development in K. Siegbahn's laboratory. See, e.g., the opening paper in the Proceedings edited by Caudano and Verbist (1974). It is unlikely that these sources could produce linewidths of less than 0.25 eV, but with sufficiently high intensity they would provide competition for the x-ray laser.

from many-body origins from various spurious experimental contributions to both line width and asymmetry, however, notably finite source line width. Any further narrowing of the source line, particularly if it could be accomplished without loss of resolution, would be valuable in establishing the magnitudes of the line asymmetries more reliably and accurately.

Vibrational structure on core-level lines has actually been observed in ESCA, in the C 1s line of methane in the gas phase, by the Uppsala group (Gelius et al. 1974). They were barely able to resolve this structure, however, and it seems clear that further improvement of such spectra can be achieved only through the use of narrower lines, as might be provided by an x-ray laser. Similar effects--inhomogeneous line broadening by vibrational fine structure--show up in ESCA peaks from solid samples. In this case the phenomenon is referred to as "phonon broadening", and it shows a marked temperature dependence. Again, extraction of the true phonon-broadened line width as a function of temperature would be greatly facilitated by the use of narrow-line x-ray sources.

Another area in which high-resolution ESCA could play an important role would be in studying the details of the valence-band structures of semiconductors and metals, particularly near the Fermi energy. The electronic band structures of these materials determine their properties, and are of utmost importance from both a fundamental point of view and because much of our present technology rests on the special properties of materials. The only way to understand the electronic band structure thoroughly is to determine the state density and other properties for several eV around the Fermi energy. Both ultraviolet photoemission and

ESCA can in principle yield the state density, but they both suffer shortcomings. Ultraviolet photoemission is difficult to interpret unambiguously because of final-state effects, and ESCA does not have adequate resolution. High-resolution ESCA would combine the advantages of these two methods and provide information about state densities that is presently inaccessible.

6.5.2 Tunability

Turning now to tunability, the major advantage for electron spectroscopy is to distinguish photoelectron peaks from Auger peaks. The kinetic energy of the former will track the photon energy, while the Auger energy is of course fixed. Although this seems a rather prosaic use of tunability, it is in fact a very important feature that is not available in ESCA with fixed source energies.

Tunability is essential for absorption spectroscopy. If the central laser wavelength could be made to coincide with a given x-ray absorption edge (a condition that would not be met under our present assumptions), fine-tuning across the edge would serve both to delineate details of the edge structure and to yield chemical information rather similar to that obtained from ESCA shifts. If this experiment were done in the fluorescence mode, it could be very sensitive to dilute impurities. One would only need to collect data above and below the edge energy, in the same way that an Oak Ridge group recently sought* confirmatory evidence for the recently-reported discovery of primordial superheavy elements in nature (Gentry et al. 1976, Fox et al. 1976).

*An Oak Ridge National Laboratory group carried out absorption-edge studies in search of superheavy elements at the Stanford Synchrotron Radiation Project in July-August 1976.

6.6 Specific Materials Applications

This section is directed toward utilization of the fine-focusing characteristic of the x-ray laser--a feature which most effectively distinguishes x-ray laser ESCA from conventional ESCA. With fine focusing, the x-ray laser will make possible the development of a selected area ESCA microprobe for routine nondestructive elemental and chemical-state analysis of microscopic regions of materials surfaces.

A recent article by Pocker and Haas (1975) discusses the technical considerations that go into designing an analytical instrument that performs high-spatial-resolution Auger spectroscopy, in effect combining scanning electron microscopy (SEM) with Auger electron spectroscopy (AES). Several approaches have been implemented. Among these, scanning Auger microscopy (SAM) has been developed into successful commercial practice by Physical Electronics Industries, Edina, Minn. In this method, an electron beam from a thermionic source, with a beam diameter as small as 1 micron, is scanned or rastered across the sample, producing Auger spectra which form an elemental map of the surface composition (to the extent that this is possible with Auger spectra). This approach is not readily adaptable to an x-ray laser ESCA device because of its infrequent pulse character.

Another approach to the combination of SEM with AES, put forth by Pocker and Haas but not yet in commercial practice, is Selected Area Auger Spectroscopy (SAAS). In this method a high spatial-resolution scanning electron gun is used as a point probe to select interesting features for AES. Although this approach sacrifices the elemental mapping

capability per se, it allows the experimenter to concentrate on the areas of interest and, unlike SAM, it makes larger areas accessible. Pocker and Haas showed a $(100 \text{ micron})^2$ micrograph of the surface of a René alloy, in which the secondary electron image, while not chemically specific, is sufficiently composition-sensitive to provide good contrast for isolating relevant features for Auger studies.

An x-ray laser microprobe device would have to operate in this latter mode, because of the one-shot character of the laser. There are a number of technical problems which would be encountered in actually building such a device, but basically one could envision using scanning electron microscopy to locate an area for study, then illuminating that area with an x-ray laser pulse, observing photoelectrons and Auger electrons. The technique might be termed Selected Area Electron Spectroscopy (SAES).

One example of the way in which SAES could be applied to materials science problems would be the analysis of fracture surfaces of high-strength alloys. For example, many modern technological applications of high-strength or specialty steels require alloys that have been specially heat-treated to produce an optimum grain size and at the same time to retain an optimum concentration of austenite (the high-temperature form) in a nominal martensite matrix. The microstructure of this two-phase composite material is responsible for the properties of specialty steels. Among the most important properties is "toughness", which is a measure of the ability of the material to resist crack propagation. A good general discussion of this subject is given by G. Thomas et al. (1974).

In developing high-toughness steels, the usual approach is to vary the composition, including one or more of a number of elements (carbon, Cr,

Mn, Ni, Si, etc.) and simultaneously to vary the heat treatment, thereby refining the microstructure. Tests are then performed to determine the strength characteristics. These tests invariably involve producing fracture surfaces due to crack propagation, and the question arises, "Why did the specimen fracture along this particular surface?" Because of the many variables in these complex systems, the answer must often come from circumstantial evidence plus some rather speculative models for crack propagation. There is also an element of randomness in such an approach because one cannot be certain that two specimens have been made in exactly the same way.

Chemical analysis of the fracture surfaces should add substantially to the information available on these systems. Auger microprobes are useful in this regard, but the possibility of doing microprobe-ESCA, or SAES, as described above would be really exciting. Not only would a more reliable and complete elemental analysis be obtained than is possible with Auger, but in addition the chemical state of each element as it occurs on the fracture surface would be apparent. This could be extremely useful in designing or modifying alloy-fabrication processes. For example, if phosphorus impurities were found to be abundant on a fracture surface, steps could be taken to retard the migration of phosphorus to grain boundaries, where fracture occurs. Other benefits would accrue from the ability of ESCA to provide chemical information. For example, it would probably be possible with ESCA to distinguish austenite from martensite (through differences in core-level multiplet structure or in valence-band shapes), and it would certainly be possible to determine the degree of oxidation of iron or any other element on the fracture surface.

One more example should suffice. As the semiconductor industry produces ever-smaller microcircuitry, the importance of microprobe analysis increases accordingly. Today it is routine to fabricate a large number of densely-packed circuit components *in situ* on a single silicon wafer (Section 3.6). Failure of an inordinate number of these systems is costly. Malfunctions of such devices are frequently attributed to "surface states", a generic term for almost anything going wrong on the surface. With ESCA it is possible to study *real* surface states, by angle-resolved photoemission (Rowe et al. 1974), as well as to identify "surface states" that actually arise through reactions of impurities on the surface. If ESCA can be combined with a microprobe capability (as in SAES), this would provide valuable analytical insight into the nature of the surface states in real microcircuit systems.

6.7 Further Technical Considerations

In Section 6.1 a summary of technical considerations was given to establish feasibility. In this section we return briefly to this area of concern. It is our opinion that x-ray laser ESCA is feasible (given the laser), and that it would be a valuable and needed addition to the arsenal of the surface scientist and the materials scientist, as well as having considerable applicability in fundamental studies on homogeneous samples. It also seems clear that technological problems associated with the adaptation of x-ray lasers to ESCA are minor compared to those associated with developing the x-ray laser itself. Nevertheless a few technical observations are given below from the point of view of an ESCA "user" who would take or send a sample to an x-ray laser facility.

First, a number of accessories would be needed at the ESCA "port" of an x-ray laser. These should include the usual ultra high vacuum and sample treatment facilities, including provision for in-situ fracture studies. A crucial element that would require careful design would be the microprobe capability. It would be necessary to magnify the image of a small area and to project it on a screen, using electron microscopy. One would then want to select an area for study and to "aim" the x-ray laser beam accurately at that area.

A time-of-flight spectrometer is the natural choice for ESCA and Auger electron analysis with an x-ray laser, because of the pulse structure. In this approach, which has already been successfully employed for photoemission studies at electron storage rings, a clock is started by the laser pulse and electrons are recorded as they arrive, thereby registering their kinetic energies. The total transit time is less than 1 microsecond. Although single-electron counting has been used in the past, this approach could also be used to record current, employing any detector with a fast linear response.

Finally, the least attractive feature of the x-ray laser as presently conceived, judged from the ESCA point of view, is its one-shot nature, including in particular the intense thermal spike and the low duty cycle. Even with these features it is quite attractive, as detailed above, but a different pulse structure would be highly desirable. If the energy presently concentrated in one pulse could be spread out over many pulses, spaced one microsecond or further apart, the heating problem would vanish, the microprobe characteristics would be greatly enhanced (because a

scanning mode would be feasible), and the time-of-flight capability would be retained. Although there is presently no known scheme to effect this change, its desirability should be borne in mind as the x-ray laser is developed.

6.8 Summary and Conclusions

We have assessed the applicability of x-ray lasers to ESCA. The basic feasibility of the method was established first; then, after a brief discussion of the relevant aspects of ESCA, specific applications to basic spectroscopic problems and to materials problems were taken up. Finally, technical considerations were again briefly touched upon. The following conclusions were drawn:

1) Within the constraints of the characteristics of projected x-ray lasers, x-ray ESCA is feasible. There is enough flux in even one pulse to make this method attractive.
2) The thermal spike during a single pulse presents a problem that can be dealt with by making certain compromises.
3) For ESCA purposes, the Al K_α x-ray laser is far preferable to the Cu K_α laser. Energies below 1000 eV are less desirable.
4) X-ray laser and x-ray Auger spectroscopy have some distinct advantages over conventional Auger spectroscopy.
5) Absorption studies are feasible if the wavelength is correct and the laser is slightly tunable.
6) High resolution and tunability are attractive features of x-ray ESCA. Coherence and nonlinear effects are unlikely to be important.

7) The high resolution possible with x-ray ESCA would facilitate the study of chemical shifts, line shapes, vibrational structure including phonon broadening, and valence-band structure.

8) Tunability is essential for absorption spectroscopy, and useful in electron spectroscopy in distinguishing photoelectron lines from Auger lines.

9) Materials applications would hinge on microprobe capabilities. A selected area electron spectroscopy (SAES) mode would be most practical.

10) SAES would permit the elemental and chemical analysis of microscopic areas of fracture surfaces of specialty steels, surface states of semiconductor microcircuits, and other surfaces of importance in materials science and engineering.

11) A more frequent, somewhat less intense pulse structure would be preferable for ESCA applications.

7. HOLOGRAPHY

7.1 Introduction

The development of holography was principally motivated by a desire to improve the resolution of short-wavelength microscopy to its theoretical limits (Gabor 1948, 1949). Several workers in the 1950's (El Sum and and Kirkpatrick 1952, El Sum 1952, Rogers 1950, 1952) concerned themselves unsuccessfully with the application of the new technique to obtain image resolution of the order of the wavelength of the radiation employed without having recourse to lenses or other conventional imaging devices.

The availability of lasers as coherent sources increased interest in holography considerably in the 1960's, and powerful techniques were introduced which ultimately led to the well-known and highly publicized three-dimensional photography (Leith and Upatnieks 1962, 1964). It is not surprising, therefore, that x-ray holography ranks high among potential applications cited for x-ray lasers.

In the following we discuss the promise and some of the problems inherent in x-ray holography on the assumption that the coherence and power requirements can be met.

7.2 General Comments

We consider an arbitrary distribution of scatterers (the object field) which is illuminated by a monochromatic coherent source of radiation of wavelength λ assumed to be located in the half space $z < 0$. An opaque screen with an aperture A located in the plane $z = 0$ separates the object field and its illumination source from the source-free observation half space $z > 0$. It follows from Huygens' principle that all information about the object field which can be obtained by imaging systems of any kind,

located in the observation space $z > 0$, is contained in the complex amplitude distribution F(xy) of the wave which emanates from the illuminated object field.* F(x,y) is termed the object wavefront in the aperture. It is to a good approximation a band limited function (Mueller 1976) with a spatial bandwidth of less than $1/\lambda$ line pairs per unit length. (Such a band limited function is adequately described by a set of $4\ A/\lambda^2$ complex numbers and can in principle be recorded without loss of information on a recording medium with a resolution capability at least equal to the spatial bandwidth of F(x,y).)

The aim of holography is in essence to record the complex amplitude F(x,y) over the receiving aperture A and to reconstruct from this record either a replica of the original wavefront, or to modulate the complex amplitude F(x,y), or a suitably magnified version of it, with radiation of a different wavelength to form an image of the object field. The analog reconstruction process can be avoided by proceeding directly from the record of F(x,y) to a reconstruction by computation.

Before proceeding to a description of the holographic process, we shall briefly comment on the relationship between the object wavefront and the object field from which it originates. The object wavefront F(x,y) cannot contain complete information about an arbitrary object field as there exist an infinite number of distributions of scatterers, which can give rise to a given complex amplitude distribution. For example, the distribution of gelatin on a glass plate in a bleached optical hologram can, if suitably illuminated, trick the observer into "seeing" a nonexistant three-dimensional field of objects.

*For simplicity, we suppress the vectorial character of the wavefront F(x,y) since all features of interest can be brought out by a scalar description.

The relationship between the two distributions is, however, for all practical purposes unique if the object field is essentially two dimensional and its distance and orientation relative to the receiving aperture known, or if the object field consists of compact scatterers large compared to the wavelength with well-defined contours occupying only a small fraction of the illuminated volume.

The second case is characteristic of visually encountered object fields. There, imaging proceeds by focusing through the illuminated volume until areas with high contrast and sharp contours are encountered which are then interpreted as images of real objects seen against the background of out-of-focus images of other objects in the volume of interest.

This process of constructing a likely field of objects fails, however, if the distribution is three dimensional and lacks sharp discontinuities. This is the situation one expects when attempting to image the electron density of a non-planar molecule. In this case a true reconstruction of the object field requires a large number of complex amplitude distributions obtained by varying the illumination angle or the orientation of the object field or both relative to the aperture (Sweeney and Vest 1973). This procedure is difficult to realize with x-ray holography since it requires positioning accuracies of the order of the desired resolution which imposes enormous technical difficulties. We shall, therefore, limit our evaluation to imaging of essentially two-dimensional object fields.

7.3 The Holographic Recording Process

For light, U-V and x-ray radiation, only intensity sensitive recording media are available. To record, therefore, the complex amplitude distribution $F(x,y)$ of a given object wave one has to resort to interferometry.

A second coherent wavefront R(x,y) (the reference wave) of known amplitude and phase is made to impinge simultaneously with the unknown wavefront F(x,y) on the aperture, and the intensity I of the combined excitation is recorded. This intensity is given by:

$$I = |R + F|^2 = |R|^2 + RF^* + R^*F + |F|^2 \ . \qquad (1)$$

This "interferogram" now contains the unknown complex amplitude distribution multiplied by the known reference wave amplitude R*, together with the other three extraneous terms in Eq. (1) which have to be separated from the desired term R*F in order to recover the complex amplitude F(x,y). In all practical cases one can choose the reference wave R such that $|R|^2$ is a constant over the aperture and therefore does not seriously interfere with the desired distributions. The intensities of the wavefronts R and F can furthermore be chosen such that $|F|^2$ becomes negligibly small compared to RF* and R*F so that the problem of isolating RF* reduces to separating the term R*F from its conjugate complex F*R. This can be readily achieved (Goodman 1968) if the complex amplitude F is a band limited function with a bandwidth smaller than 1/2 the resolution capability of the recording medium. In this case the reference wave R can be chosen such that the spatial spectra of RF* and A*F are displaced enough from each other so as not to overlap and jointly occupy the full bandwidth which the recording medium is capable of handling. Simple analog or digital filtering can then be used to separate the terms and retrieve the recorded complex amplitude F(x,y) unencumbered by the other terms in the holographic recording.

The important result for our considerations here is that the spatial frequency of the complex amplitude F has to be kept less than 1/2 the

effective bandwidth of the recording medium for complete separation of the terms R*F and RF*.

We will next show (cf., Collier, Burckhardt, and Liu 1971, § 3.1) that the obtainable image resolutions of a hologram produced with a plane wave reference is equal to the resolution with which the complex amplitude F is recorded. This implies according to the above considerations that the highest resolution obtainable with a holographic system is 1/2 the resolution of the holographic recording medium.

7.3.1 The Zone Plate

Since a scattering object may be considered to consist of many point scatterers, a zone plate may be thought of as an elementary hologram. Consider then (Fig. 7.1) a point source S of wavelength λ illuminating a scattering center O. The intensity distribution I on a plane H is then given by the interference between the primary beam of complex amplitude $a_1 e^{i\phi}$ and the scattered beam of amplitude $a_2 e^{i\phi}$ so that

$$I = a_1^2 + a_a^2 + 2a_1 a_2 \cos(\phi_1 - \phi_2) . \tag{2}$$

The intensity fluctuations along H are due to the phase difference

$$\begin{aligned} \phi_1 - \phi_2 &= \left(\frac{2\pi}{\lambda}\right) (SP - SO - OP) \\ &= \left(\frac{2\pi}{\lambda}\right) \left| (v^2 + x^2)^{\frac{1}{2}} - (v - u) - (u^2 + x^2)^{\frac{1}{2}} \right| \end{aligned} \tag{3}$$

when $x \ll u,v$ we have approximately

$$\phi_1 - \phi_2 \simeq \frac{-x^2}{\lambda} \left(\frac{1}{v} - \frac{1}{u}\right) \equiv \frac{\pi x^2}{\lambda f} , \tag{4}$$

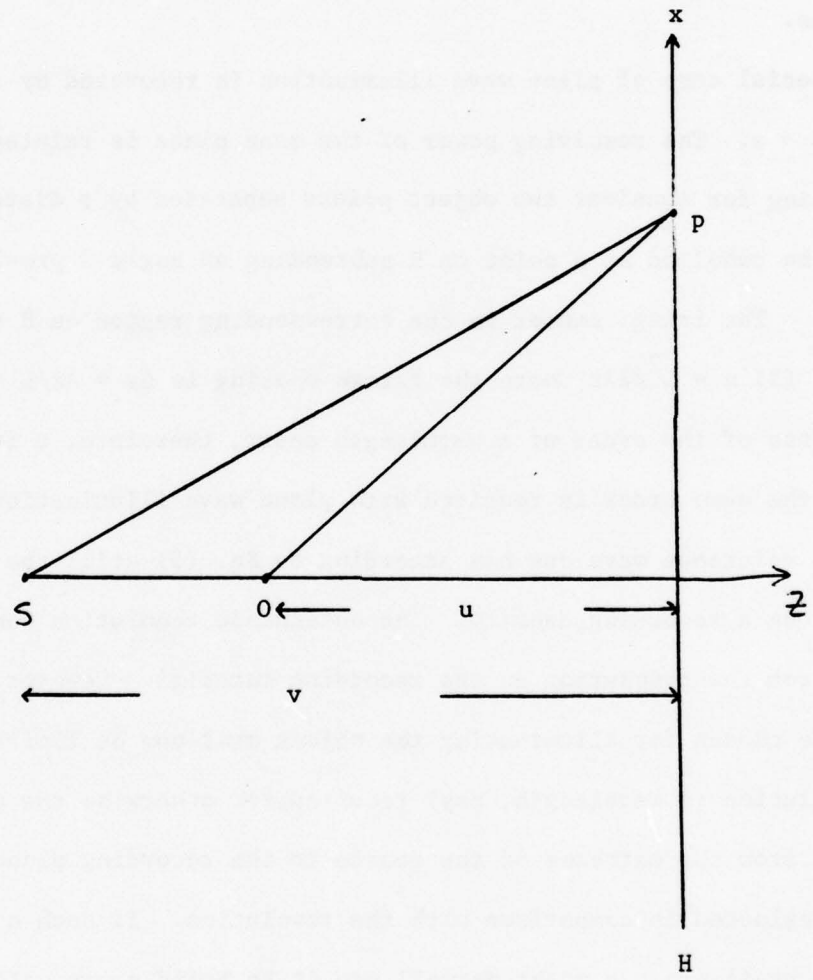

Figure 7.1. In-line hologram of a point scatterer.

where f is the effective focal length. Bright interference fringes occur whenever $(\phi_1 - \phi_2) = 2\pi n$ or when x is x_n given by

$$x_n = (2\lambda f n)^{\frac{1}{2}} , \tag{5}$$

with a fringe spacing $x_{n+1} - x_n \simeq (\lambda f/2n)^{\frac{1}{2}}$ or $(\Delta x)_{min} = \lambda f/\rho$ with ρ the zone plate radius.

The special case of plane wave illumination is recovered by letting $v \to \infty$ and $u \to z$. The resolving power of the zone plate is related to the fringe spacing for consider two object points separated by a distance d. These will be resolved at a point on H subtending an angle θ provided $d \sin \theta \simeq \lambda$. The fringe number in the corresponding region on H (at $L \simeq z\theta$) is from Eq. (5) $n = L^2/2\lambda z$ where the fringe spacing is $\Delta x = \lambda z/L \simeq d$. To resolve points of the order of a wavelength apart, therefore, a fringe spacing of the same order is required with plane wave illumination. With a spherical reference wave one has according to Eq. (5) still the freedom in f to choose a recording density. The obtainable resolution can then be decoupled from the resolution in the recording material. However, the point source chosen for illuminating the object must now be limited in size to the resolution (a wavelength, say) required, for otherwise the path differences from the extremes of the source to the recording plane can no longer be neglected in comparison with the resolution. If such a point source were available one might as well use it to build a projection microscope (cf., Section 10.2) with better resolution and with less effort than that obtained via holography with the same recording material. The utility of the holographic approach in this case clearly does not lie in the obtainable resolution. Holographic imaging might still be useful due

to the image amplification afforded by the heterodyning process of holography, but this also loses its usefulness if the dominant noise encountered in the process is the "shot noise" of the reference beam, and not additive noise from the recording medium.

7.4 Radiation Tolerance

An important problem which bears on the feasibility of holographic x-ray microscopy is the number of quanta which have to be scattered by one resolution element in the object field to obtain a hologram from which a "useful image" of this resolution element (e.g., an atom in a large organic molecule) can be derived.

To address this problem properly it will be necessary to define quantitatively what constitutes "useful image". The relationship between the obtainability of a useful image and the number of photons scattered per resolution element is a statistical one. We shall in later sections relate the critical photon number to the probability for obtaining a useful image from a hologram which we assume to be recorded on an ideal recording medium and reconstructed computationally (with a digital computer). The computer provides a noise-free environment for the reconstruction and a processing versatility not possible with analog reconstruction.

We will find that even under these idealized circumstances the number of photons required to be scattered out of one resolution element of the object distribution is of the order 10^3 to 10^4, that is, three to four orders of magnitude more than suggested in the literature (Chapline and Wood 1975, 1976; Trammell 1976). The total incident radiation intensity is then likely to exceed the damage threshold of the object under investigation.

7.5 The Gabor Hologram

We consider for the following evaluation a Gabor hologram. It was pointed out by Goodman that the recording geometry afforded by a Gabor hologram and the required transparency characteristics of the objects are ideally suited for x-ray holography. The first hologram recorded with radiation of significantly smaller wavelength than that of visible light reported in the literature was, following this suggestion, a Gabor hologram (Bjorklund et al. 1974, Bjorklund 1974).

The very simple recording geometry of a Gabor hologram is shown in Fig. 7.2. A plane wave of amplitude R illuminates a planar object occupying area O inside the object Aperture A_o. The undisturbed portion of the plane wave together with the wave scattered by the object proceed to the recording aperture A, which is of the same size as or larger than A_o and located in a plane (the hologram plane) parallel to the object plane at a distance z from it. We assume that the illuminating plane wave impinges normally to the object and hologram planes. The amplitude transmittance of the object is $t(\zeta,\xi)$ and satisfies the condition:

$$\frac{1}{O} \int_O |t(\xi,\zeta)|^2 \, d\xi \, d\zeta - 1 \ll 1 \ , \tag{6}$$

ξ and ζ are the coordinates in the object plane.

The complex amplitude F(x,y) in the hologram aperture is composed of the undisturbed plane wave amplitude R and the scattered wave amplitude a(x,y):

$$F(x,y) = R + a(x,y) \ , \tag{7}$$

where x and y are the coordinates in the hologram plane. Since the illuminating plane wave impinges normally, R is constant over the recording aperture. We can normalize the phase of F without loss of generality such that R is a real constant. The intensity distribution in the recording aperture is then

$$I(x,y) = |F(x,y)|^2 = R^2 + R[a(x,y) + a^*(x,y)] + |a(x,y)|^2 . \quad (8)$$

We neglect the term $|a|^2$ as small and of second order as mentioned before and obtain for the intensity distribution the approximation which we shall use in the following:

$$I(x,y) = R^2 \left[1 + \frac{a(x,y) + a^*(x,y)}{R}\right] . \quad (9)$$

7.5.1 Amplitude Transmission and Scatter Cross-Sections

Before proceeding to discuss the hologram recording process, we shall relate the information bearing term a(x,y) to the scattering cross-section per resolution element of the object distribution.

As shown in Fig. 7.2 the object aperture A_o which is partly occupied by the object is illuminated by the plane wave R. The complex amplitude $U(\xi,\zeta)$ in A_o (behind the planar object) is:

$$U(\xi,\zeta) = Rt_A(\xi,\zeta) , \quad (10)$$

where t_A is the amplitude transmission function defined over the full object aperture A_o. In the area O covered by the object proper t_A is equal to the object amplitude transmission function t, while over the rest of the object aperture A_o the amplitude transmission function t_A is equal to unity:

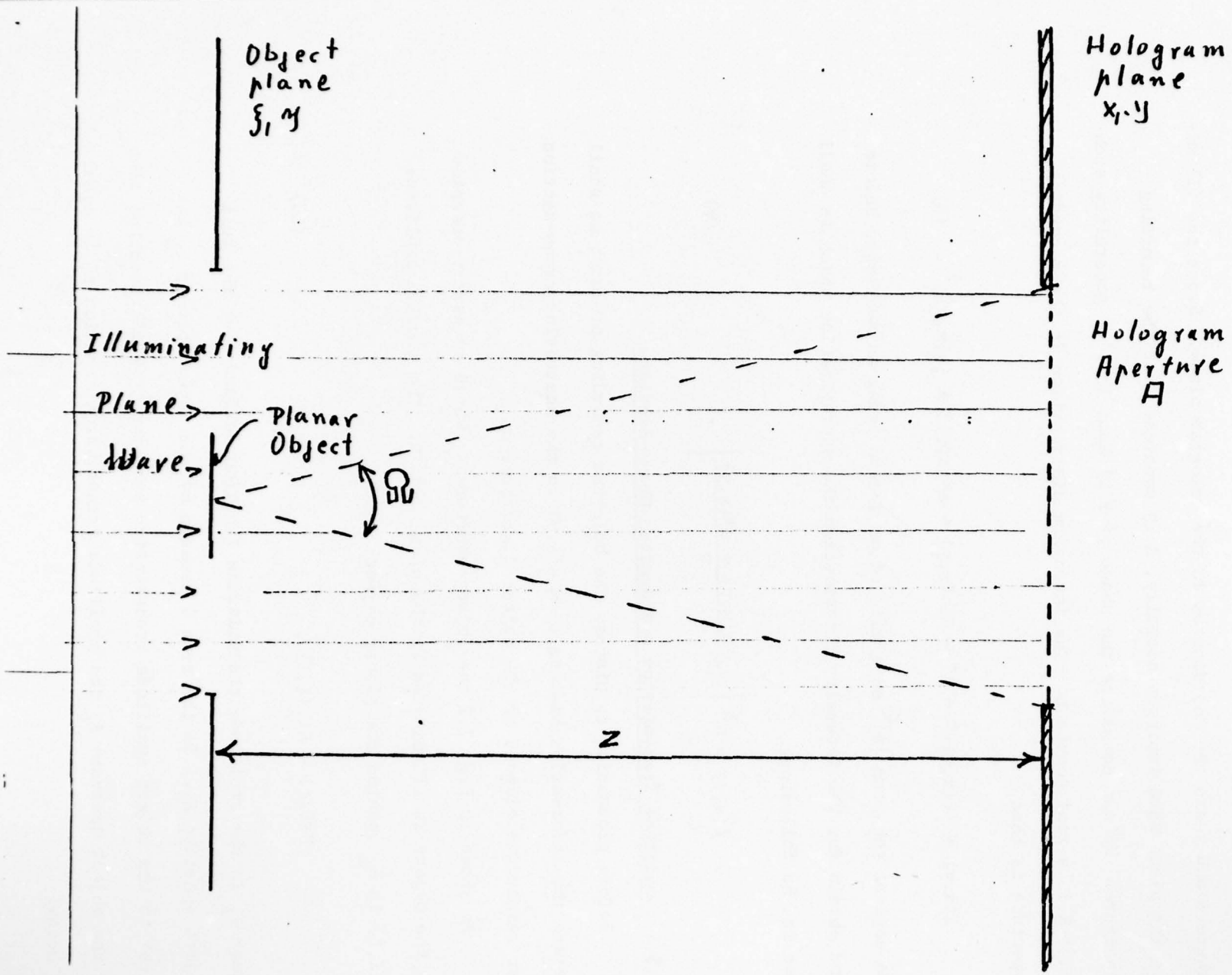

Figure 7.2. Gabor hologram recording geometry

$$t_A = \begin{cases} t & \text{in } O \\ 1 & \text{otherwise} \end{cases} \tag{11}$$

We now introduce a modified object transmission function $t' = t_A - 1$ which is defined over the full object plane:

$$t' = \begin{cases} t - 1 & \text{in } O \\ 0 & \text{otherwise} \end{cases} \tag{12}$$

Eq. (10) becomes

$$U = R + Rt' \ . \tag{13}$$

We assume that the aperture A_o is large enough so that diffraction effects due to the finite aperture size can be neglected. The plane wave term R of Eq. (13) therefore propagates unchanged to the receive aperture A. The term Rt' undergoes an integral transformation on propagating to A which we approximate in the usual way by a Kirchhoff-Fresnel diffraction integral, so that ($k = 2\pi/\lambda$)

$$a(x,y) = -\frac{iR}{\lambda} \int_{\xi=-\infty}^{\infty} \int_{\zeta=-\infty}^{\infty} \frac{t'(\xi,\zeta) \exp\{ik[(x-\zeta)^2 + (y-\zeta)^2 + z^2]^{\frac{1}{2}}\}}{[(x-\xi)^2 + (y-\zeta)^2 + z^2]^{\frac{1}{2}}} \tag{14}$$

$$\simeq -\frac{iR}{\lambda z} \exp\,[ik(x^2+y^2)/2z] \int_{-\infty}^{\infty}\int t'(\xi,\zeta) \exp\left[\frac{ik(\xi^2+\zeta^2)}{2z}\right]$$

$$\times \exp\left[-\frac{ik}{z}(x\xi + y\zeta)\right] d\xi\, d\zeta \ , \tag{15}$$

on expanding the square root and neglecting terms of second and higher powers in z, the distance between the object and hologram planes. Since the transmission function t' vanishes outside the object area O it can be expanded as a discrete Fourier series:

$$t'(\xi,\zeta) = \sum_{\mu=-\infty}^{\infty} \sum_{\nu=-\infty}^{\infty} a_{\mu\nu} \exp\left[\frac{2\pi i}{a}(\mu\xi + \nu\zeta)\right] \mathrm{rect}_a(\xi)\ \mathrm{rect}_a(\zeta)\ , \tag{16}$$

where a is the side of a square, oriented parallel to the coordinate axes ξ and ζ, which encloses the object area O (Figure 7.3), and

$$\mathrm{rect}_a(\xi) = \begin{cases} 1 & \text{for } -\tfrac{1}{2}\, a < \xi < \tfrac{1}{2}\, a \\ 0 & |\xi| > \tfrac{1}{2}\, a\ . \end{cases} \tag{17}$$

The integration over ξ and ζ can now be carried out by substitution for t' into Eq. (15). For our purposes it is sufficient to consider the far-field limit $(\xi^2+\zeta^2)_{max}/\lambda \ll |z|$, corresponding to Fraunhofer diffraction:

$$a(x,y) \simeq -\frac{iR}{z\lambda} a^2 \exp\left[ik(x^2+y^2)/2z\right] \sum_{\mu,\nu=-\infty}^{\infty} a_{\mu\nu}\ \mathrm{sinc}\left[\pi\left(\mu - \frac{xz}{\lambda z}\right)\right]$$

$$\times\ \mathrm{sinc}\left[\pi\left(\nu - \frac{ya}{\lambda z}\right)\right]\ , \tag{18}$$

where sinc $x \equiv \sin x/x$. For smaller values of z the central maximum becomes broader than the sinc function with smaller secondary maxima. We define a new function $\bar{a}$ (x,y) by cutting off the summarion in (18) at $|\mu|,\ |\nu| \leq K$ where

$$K = \frac{a\sqrt{A}}{2\lambda z}\ . \tag{19}$$

It follows from Eq. (18) and the property of the sinc function that $\bar{a}$ is a good approximation to z(x,y) inside the aperture (i.e., for $|x|,\ |y| \leq \sqrt{A}$) and contributes only insignificantly to a(x,y) outside the aperture.

The total power P scattered by the object into the aperture is therefore in good approximation:

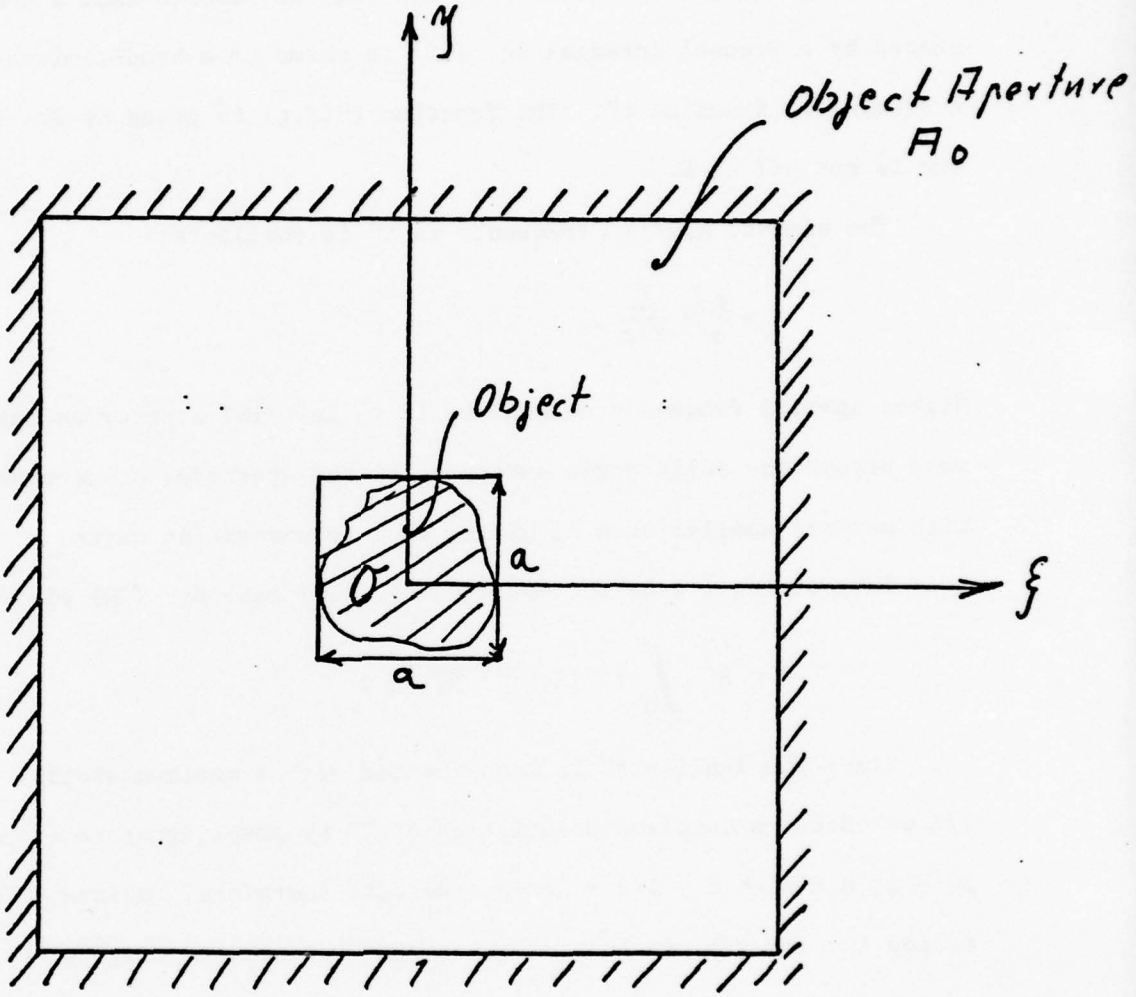

Figure 7.3. The object plane in Gabor holography.

$$P = \int_A |a(x,y)|^2 \, dx \, dy \simeq \int_{-\infty}^{+\infty} |\bar{a}(x,y)|^2 \, dx \, dy \; . \qquad (20)$$

To evaluate the second integral in Eq. (20) we observe that $\bar{a}$ can be represented by a Fresnel integral Eq. (15) in terms of a band-limited object transmission function t". The function $t''(\xi,\zeta)$ is given by Eq. (16) if the sum is cut off at K.

The highest spatial frequency in t" is therefore:

$$\frac{1}{\ell} = \frac{K}{a} = \frac{\sqrt{A}}{2\lambda z} \; . \qquad (21)$$

Higher spatial frequency components in t' Eq. (16) scatter an impinging plane wave beyond the solid angle subtended by the aperture, or represent gratings with periods smaller than λ, giving rise to evanescent waves.

Introducing $\bar{a}$ from the modified Eq. (15) into Eq. (20) yields:

$$P = R^2 \int_0 |t''(\xi,\zeta)|^2 \, d\xi \, d\zeta \; . \qquad (22)$$

Since the funtion t" is band-limited with a maximum spatial frequency $1/\ell$ we obtain a complete description of t" by sampling at intervals $\Delta\xi = \Delta\zeta = d$ with $d = \ell/2 = \lambda z/\sqrt{A}$. We can, therefore, replace in good approximation the integral in Eq. (22) by a sum over all sampling points in O:

$$P = R^2 d^2 \sum_{m,n} |t''(\xi_m,\zeta_n)|^2 \; ,$$

with $\xi_m = md$, $\xi_n = nd$; $n,m = -a/2d \ldots 0 \ldots a/2d$. d^2 is the area per sampling point (the resolution element) which corresponds to the resolution limit $d = \lambda_2/\sqrt{A}$ derived above for zone plates. We can write this equation as

$$P \simeq R^2 \sum \sigma_{mn} = R^2 \sigma_o \qquad (23)$$

where

$$\sigma_{mn} \equiv \Delta |t''(\xi_m,\zeta_n)|^2$$

is the scattering cross-section of the (m,n)th resolution element. This quantity can itself be expressed in terms of the inverse Fresnel transform of a(x,y) via Eq. (14), and we write

$$F_{mn}[a(x,y)] = \frac{1}{A} \int_A a(x,y)\, e^{-ik(x^2+y^2)/2z}\, e^{k(x\xi_m+y\zeta_n)/z}\, dx\, dy$$

$$\simeq i \left(\frac{R\lambda z}{A}\right) t''(\xi_m,\zeta_n)\, e^{ik(\xi_m^2+\zeta_n^2)/2z}\,, \qquad (24)$$

or

$$\sigma_{mn} = A\left|F_{mn}[a(x,y)]\right|^2/R^2\,. \qquad (25)$$

If the total scatter cross-section of the (m,n)th resolution element be denoted by σ^T_{mn}, we have

$$\sigma_{mn} = \gamma\, \sigma^T_{mn}\,, \qquad (26)$$

where γ is determined by the solid angle subtended by A and the spatial bandwidth of the transmittance t. For point scatterers which scatter isotropically we may simply take $\gamma = \Omega/4\pi$ or

$$\gamma = A/4\pi z^2\,. \qquad (27)$$

The maximum solid angle $\Omega = A/z^2$ is essentially set by the resolution r line points per unit length, of the recording medium which from Section 7.3.1 is given by $r = \Omega^{\frac{1}{2}}/\lambda$ or $\gamma = (\lambda r)^2/4\pi$. For a given resolution, then, the wavelength can be adjusted to obtain a practical value for Ω. But the radiation load cannot be reduced by operating at smaller wavelengths, for this results in a loss of effective aperature which is not outweighed by the gain in elastic versus inelastic scattering.

While these considerations are valid for a plane wave reference beam, we have already noted that decoupling image from object resolution requires an imaging capability which one hopes to create with holography.

7.6 The Recording Process

We assume for the purpose of this discussion an ideal recording medium. It consists of an array of quantum counters with a resolution high compared with the obtainable image resolution $r = \sqrt{A}/\lambda z$. The number of quanta registered by each counter during the holographic exposure together with the counter address x,y yields for each exposure a set of numbers $N(x,y,\xi)$ representing a stochastic process. The average number $N(x,y)$ of quanta which the counter at position x,y receives is proportional to the intensity $I(x,y)$ at the counter location in the hologram plane, and to the exposure time which we shall assume to be fixed for all trials. The numbers $N(x,y,\xi)$ are statistically independent from each other if we assume as the only known quantity the expectation n of the photon flux density of the illuminating plane wave. We define the exposure time as the unit of time. The expectation n of the flux density then corresponds to the illuminating wave intensity R^2. We assume all counters have an acceptance area α. The number of the evenly distributed counters is M. The area α of each counter can be less than or equal to A/M. The capture ratio $\kappa = \alpha M/A$ is therefore less than or equal to one. The expectation of the number of photons counted in any counter per unit time exposed to a flux of average density n is $N = \alpha n$.

We can now write in view of Eq. (9) and the above definitions:

$$E[N(x,y,\xi)] = N\left[1 + \frac{a(x,y) + a^*(x,y)}{R}\right] = \overline{N(x,y)} \quad . \qquad (28)$$

The variance of the process is:

$$\sigma^2 = E[(N(x,y,\xi) - \overline{N(x,y)})^2] = N\left[1 + \frac{a(x,y) + a^*(x,y)}{R}\right] \approx N = n\alpha \quad .(29)$$

Since a/R is very small compared to unity we can consider the variance of the process $N(x,y,\xi)$ to be independent of the location in the hologram aperture and equal to the variance of the photon flux density of the illuminating plane wave times the counter area.

7.7 Image Reconstruction

The objective of the reconstruction process is to recover the scatter strength $\sigma(\xi,\zeta)$ of the object distribution. We can, as we have seen, recover at best the distribution of scatter cross-sections σ_{mn} which is in essence an average over one resolution element Δ of the desired function $\sigma(\xi,\zeta) = |t'(\xi,\zeta)|^2$. We shall see in this section that even under ideal reconstruction conditions the recovered approximation to σ_{nm} contains a noise term which is due to the granular structure of the reference beam R.

Any analog reconstruction includes an image of the generally very intense reference beam, which focuses at a different location of the image space from that of the desired image of the object distribution. It can be removed by spatial filtering. This filtering process, however, leaves the sidelobe structure of this very strong image to interfere with the desired weak reconstructed image which represents a major contribution to the image noise. But this noise is in contrast to the noise from the granularity of the radiation a deterministic function of the average reference beam intensity, and can therefore in principle be avoided (or removed) in a digital reconstruction. One method described in the literature (Mueller 1976) is to subtract from all

numbers $N(x,y)$ the average N as the first processing step. This leads to the new set of numbers $N'(x,y,\xi)$ with unchanged variance and a mean which includes only the information bearing terms:

$$E[N'(x,y,\xi)] = N\left(\frac{a + a^*}{R}\right) ; \qquad \sigma^2 = N \tag{30}$$

The next step in the reconstruction process is to multiply each of the numbers N' with the corresponding values of $\exp [ik(x^2 + y^2)/2z] \cdot \exp [-ik(x\xi_m + y\zeta_n)/z]$ and to sum the resulting numbers to give a new set $T(\xi_m,\zeta_n,\xi)$. The coordinates ξ_m,ζ_n represent an appropriately chosen location in the object distribution. Samples ξ_m,ζ_n have to be taken as mentioned above at intervals commensurate with the size of the resolution area Δ. This operation is essentially the inverse Fresnel transform F_{mn} introduced above. The expectation of $T(\xi_m,\zeta_n)$ is therefore according to Eqs. (24) and (30)

$$\overline{T(\xi_m,\zeta_n)} = (MN/R)\left\{F_{mn}[a(x,y)] + F_{mn}[a^*(x,y)]\right\} . \tag{31}$$

The term $F_{mn}[a^*(x,y)]$ represents the out-of-focus conjugate image which contributes to the image noise but can be neglected in our approximation, especially if Ω is kept small. We have, therefore, to sufficient approximation

$$\overline{T(\xi_m,\zeta_n)} \approx (MN/R)\, F_{mn}[a(x,y)] . \tag{32}$$

The expectation $E[|T(\xi_m,\zeta_n)|^2]$ is:

$$E[|T_{mn}|^2] = \sigma_T^2 + |\overline{T_{mn}}|^2 \qquad \text{with } \sigma_T^2 = M\sigma^2 = MN . \tag{33}$$

We obtain, therefore, from Eq. (33) with Eqs. (26) and (32)

$$E|T_{mn}|^2 = MN\left(1 + \frac{M\alpha}{A} n\sigma_{mn}\right) . \tag{34}$$

Eq. (34) implies that the reconstructed image intensity in every resolution cell consists of two terms: the desired image information, which is proportional to the scatter cross-section σ_{mn} and a noise term which is in essence the 'spatial' shot-noise of the reference beam. The term $n\sigma_{nm}$ in Eq. (34) represents the number of photons scattered by the resolution element mn into the aperture. Using Eq. (26) we can express $n\sigma_{mn}$ in terms of the total number P_{mn} of photons scattered by the resolution element and obtain instead of Eq. (34):

$$E(|T|^2) = MN(1 + \kappa\gamma P_{mn}) \tag{35}$$

κ is the capture parameter introduced above. Both γ and κ are significantly smaller than unity for any conceivable holographic recording system.

We shall discuss in the following section how large the number $\kappa\gamma P_{mn}$ has to be so that the reconstruction given by Eq. (35) as an ensemble average constitutes a useful image.

7.7.1 The Useful Image

We shall consider here images of object distributions consisting of well-defined and on the average widely-separated structure elements. It is assumed that the resolution is commensurate with the size of a structure element of interest--that is, one image element represents either none or one structure element, (e.g., atoms in an organic molecule). We assume that the number of structure elements in the object distribution is K, the number of resolution elements in the image is L. We have seen above that

in a reconstructed image each image element contains a sample of the shot noise intensity, say B^2, a random variable which averages to the mean value MN. Some image elements (to be precise K of them) receive the additional intensity $\kappa\gamma PNM$, which is essentially deterministic.

The decision whether a particular image element represents a structure element of the object distribution is made on the basis of whether the intensity in this particular resolution cell is larger than a suitably defined threshold $\tau \cdot MN$, say. We can now reduce the concept of image quality to a simple probability statement. We define an image as useful if the probability is β (or less) that an image point which does not represent a structure element has an intensity greater than τMN (false alarm) and one that does represent a structure element has an intensity smaller than τMN (miss). With this definition one finds (Van Trees 1967) that the deterministic term in Eq. (35) has to be four times τMN or:

$$P_{mn} = \rho/\gamma\kappa \rightarrow 4\tau/\gamma\kappa \ . \tag{36}$$

In order to determine τ we observe that the probability β is equal to the probability that a given sample of the shot noise intensity B^2 is greater than τMN. This probability is (Steinberg 1976):

$$\beta = e^{-\tau} \ , \tag{37}$$

or

$$\tau = -\ell n \ \beta. \tag{38}$$

If we want to limit the ghost images to an average $\alpha\%$ of the expected true images, β becomes

$$\beta = \frac{\alpha K}{100\ L} \quad . \tag{39}$$

The number of image points missed is then:

$$N_m = \beta K = \frac{\alpha K^2}{100\ L} \quad , \tag{40}$$

compared to the number N_g of ghost images:

$$N_g = \frac{\alpha K}{100} \quad . \tag{41}$$

If L/K is large the number of misses and ghosts is unequally distributed. If one distributes N_m and N_g more equally one can limit the number ρ of Eq. (36) to the range:

$$\tau < \rho < 4\tau \ . \tag{42}$$

To evaluate the significance of ρ assume an image of an object with a thousand structure elements in a field of 10^6 resolution elements and require that less than 1% of the apparent image points are ghost images. This implies $\alpha = 1$, $K = 10^3$, and $L = 10^6$, or by Eq. (39) τ is 14. If we relax the requirement and allow 10% of the image points to be ghost images τ becomes 11. If half of the image points are ghost images τ becomes 8. At this point the image is probably considered useless for most applications. We see that τ is not very sensitive to changes in α. We are, therefore, reasonably safe to assume for our following discussion a value of 10 for τ, or 20 for ρ.

7.7.2 The Number of Photons Scattered per Image Element

We can now estimate the minimum number of photons which have to be scattered per resolution element to give an image with minimum acceptable quality. It is proportional to the three factors $1/\gamma$, $1/\kappa$, and ρ. The three factors are not independent of each other. The correlation is especially high between the aperture efficiency γ and the sensitivity parameter κ of the recording or detection medium. We can assume that the scattering of the radiation considered here is isotropic in the object distributions of interest. The factor $1/\gamma$ then becomes according to Eq. (27) $1/\gamma = 4\pi z^2/A$. We have discussed above one apparent limitation of this factor which is due to the coupling of the effective aperture size to the resolution r (line-pairs per unit length):

$$1/\gamma = 4\pi/(r\lambda)^2 \ . \qquad (43)$$

One can in principle increase the wavelength and make γ approach its theoretical maximum of 1/2. This implies a system with a large relative aperture A/z^2. Those systems (if at all technically possible) have a number of very severe basic problems. For example, a system with $A/z^2 = 1$ already has a depth of focus equal to the lateral resolution ($= \lambda$) and requires in our plane wave holograms a detector or recording medium of equal depth resolution to discriminate against the longitudinal interference pattern set up by the highly divergent interacting beams. This means in the case of 2 Å lateral resolution a 2 Å depth resolution, i.e., a single atomic layer of detector atoms laid out with 2 Å tolerance in depth. Even if this could be achieved the optimum value of κ would be equal to the product of the cross-section of the detector atoms for

ionizing collisions and the efficiency of the electron collecting aperture. For an image resolution element size of $\ell = 2$ Å the number of detectors in area A is $M = A/\ell^2$ and $\kappa = 2.5 \times 10^{15}\ \alpha$. For copper at 1 Å, $\alpha \sim 120\ A_{Cu}/N_A$ cm^2/atom in terms of the atomic weight $A_{Cu} = 63.5$ and Avogadro's number $N_A = 6 \times 10^{23}$/gm mole, corresponding to $\kappa \sim 2.4 \times 10^{-5}$. κ is increased with a higher-Z material with an absorption edge near 1 Å. For Au (L_{III}-edge at 1.04 Å) $\kappa \simeq 9.6 \times 10^{-5}$. Even with no allowance for a finite electron collecting aperture it appears then that $1/\kappa$ cannot be made much smaller than 10^3 at 1 Å. The minimum total number of photons scattered per atom thus reaches $P_{mn} \simeq (4\pi)(2\tau)/\kappa \sim 2.5 \times 10^5$. Since the photo-electric cross-section $\alpha \sim \lambda^3$, κ can be increased at the expense of resolution by operating at longer wavelengths reaching its maximum value of unity in the range 10-20 Å depending on the detector atoms. The volume of a resolution element then ranges from 10^3-10^4 (Å)^3 and one comes down to reasonable photon requirements. But there is a catch. Since objects of interest in this range of resolution are in general many resolution elements thick, one encounters another severe problem which is due to the large relative aperture. If one can provide the required depth resolution in the recording medium, one obtains in the image construction, which now corresponds to one resolution plane in the image space, besides the reconstructed image points an image of the intense and complex interference structure of all the out-of-focus image-amplitudes in the image plane. This speckle pattern is in the cases of interest here indistinguishable from the true images and makes three-dimensional x-ray holography with a depth resolution comparable to the lateral resolution virtually impossible. This problem can be avoided if one designs the system such that the depth of focus becomes large compared to the lateral resolution element $\Delta^{\frac{1}{2}}$. This leads to the essentially two-dimensional holographic imaging which we

considered above. If we assume a depth of focus k times the diameter of a resolution element, we obtain from the relation between depth of focus and resolution area

$$\Delta = k^2 \Delta\lambda^2 \ . \tag{44}$$

And because of the relation between the aperture and the area of the resolution element given in Eq. (20) we find:

$$1/\gamma = 4\pi k^2 \ . \tag{45}$$

This large value of $1/\gamma$ is partially offset by the increased potential detection efficiency κ afforded by the greater permissible thickness of the recording medium. The maximum gain here is a factor k with the limitations that firstly κ cannot be larger than unity and secondly that thicker recording material gives rise to more cross-talk due to secondaries, even if the primary radiation is kept in a narrow cone.

If the limitation is the radiation load per volume element of the object, one gains another factor of the order of k because of the greater object volume which participates to create the image and we, therefore, end up again (if we take everything on the extreme optimistic side) with a minimum radiation load of one to hundred quanta per atoms at a resolution of about 20 Å. The situation improves with diminishing resolution as $\Delta^{3/2}$ or Δ^2 depending upon whether one has reached already the maximum value of the detection efficiency.

7.8 Comments and Conclusion

All quantitative statements made in the foregoing pertain to plane wave holograms. If dispersive, refractive or defractive optical elements are

available, they can either be used to make magnified images or holograms with comparably lower resolution requirements than those necessary for plane wave holograms. If the detection system is a quantum counter of arbitrary sensitivity realized, for example, by a photoelectric receiver followed by an electron microscope which is not limited by detector generated image noise, then direct imaging and holography are almost at a par with a slight edge in favor of direct imaging. The image amplification due to the heterodyne process of holography is of no advantage here, since it is effective only against detector generated noise which can be reduced to relative unimportance by increasing the intensity of the reference beam. The holographic image amplifier is not effective, however, against detector insensitivity. If the recording medium is a photo-resist film or similar medium which can be expected to introduce additive noise, holography has an advantage if the detector related noise is larger than the shot noise of the reference beam.

At the high end of the resolution spectrum one cannot, however, expect the availability of optical imaging devices with the required resolution. This is the regime where imaging is only possible by plane wave holography or similar devices like Bragg diffraction reconstruction. Holography, then, is limited by the radiation tolerance of its objects to resolutions from about 20 to 100 Å. Bragg diffraction reconstruction is not limited in this manner since firstly the radiation load is distributed over the many periodically arranged identical object distributions: the unit cells of a crystal; and secondly because the beam scattered coherently by the periodic array is highly collimated and spatially separated from other coherently scattered beams. This improves the ease of detection enormously,

however, at the cost of requiring a very large number of exposures for one reconstruction accompanied by the loss of the relative phase between individual beams.

An interesting possibility is a plane wave hologram of a two-dimensional periodic structure (crystal). Here one also distributes the radiation load over a large number of identical object distributions and obtains in one shot all coherently scattered beams and preserves their relative phase relationship. This approach may well be the only holographic approach to resolutions comparable with atomic dimensions.

8. EFFECT OF LASER RADIATION ON NUCLEAR DECAY PROCESSES

Nuclear processes can be influenced by involving the electrons surrounding the nucleus as these respond directly to radiation of high intensity. Two possibilities predominate: internal conversion and K-electron capture.

8.1 Internal Conversion

In internal conversion the excited nucleus decays to a lower level by expelling a bound electron. The energy transfer is a direct coupling between the bound atomic electron and the multipole field of the nucleus. The kinetic energy of the expelled electron is then just the difference between the nuclear transition energy ΔE and the binding energy of the electron (Figure 8.1). This mode of decay which competes with radiative decay can clearly be suppressed by removal of the electrons which participate in the internal conversion process. Observation of this decrease in the number of conversion electrons would, however, be difficult due to the presence of other electrons produced by the ionization process. Also, the radiative transition may not be strongly enough affected because of parallel conversionless decay channels. It has, therefore, been suggested to inhibit series decay processes by pre-ionization of Tc^{99} with $E \sim 2$ keV. By thus diminishing the population of a lower nuclear level subject to decay by a γ transition $(1 \rightarrow 0)$ the marked decrease in the number of γ rays emitted should be readily detectable. While heating by a high-power infrared laser to a fraction of 2 keV will produce substantial ionization due to the large statistical weight of the free electron state (Zeldovich & Raizer 1966), clearly an x-ray laser at a wavelength $\lesssim 5$ Å would be more efficient and selective.

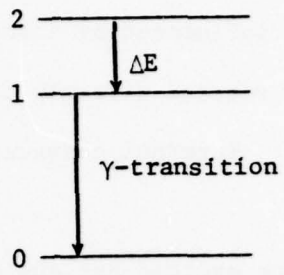

Figure 8.1. Internal conversion (2 → 1) followed by γ-ray emission (1 → 0).

8.2 K-Electron Capture

For inhibiting K-electron capture, an x-ray laser is an even more effective tool than a high temperature plasma (Accardo 1958). This process in which an atomic electron is captured by a nucleus, is important as it competes with positron β-decay. Also, prevention of K-capture which in turn decays radiatively (Figure 8.2).

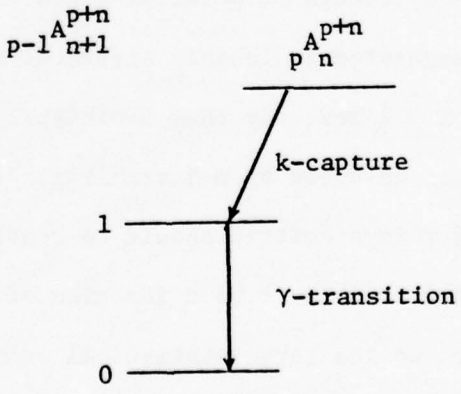

Figure 8.2. Successive transitions of K-capture followed by nuclear radiative decay.

A reduction in the rate of K-capture by the nucleus ${}_{p}A_{n}^{p+n}$ should then result in decreased γ-ray emission from the $1 \rightarrow 0$ transition of the nucleus ${}_{p-1}A_{n+1}^{p+n}$. Because of the proximity of the K-shell electrons to the nucleus, most of the vacancies are produced in the K shell (K-capture). To suppress this capture process, therefore, all atomic electrons must be removed from the atom. Complete ionization by high temperature, produced in a laser excited plasma, is limited to light elements. A typical plasma temperature obtained in this way is about 1 keV which makes Ca ($Z = 20$) with an ionization potential of the twentieth ion ($\simeq 13.6\ Z^2$ ev) of about 5 keV about the heaviest atom that can be studied. On the other hand, maximum contrast in this experiment would be obtained with high-Z nuclides as these have the largest electron capture probabilities ($\sim Z^3$). X-ray lasers can thus find useful application here. For the ${}_{4}Be^{7}$ atom[1] a 50 Å laser would be sufficient; for the higher Z nuclides one needs lasers in the $735/Z^2$ Å range. Detailed calculations must be carried out for each particular case to ensure that during the lifetime of the ionized state a measurable dose of γ-ray activity is produced.

9. PROBLEMS IN RADIATION CHEMISTRY

This section considers possible applications of an x-ray laser beam to problems in radiation chemistry. Because of the relative novelty of this field to many physicists, a broad overview of the field is presented here together with typical parameters for a number of specific processes. Some of the techniques currently in use are discussed in some detail so that the areas where x-ray laser beams could be advantageous may be more clearly signalized.

9.1 Introduction

In recent years pulsed techniques have played an important role in research in the twin fields of radiation chemistry (radiolysis) and photochemistry (photolysis). The two areas of research differ only in the energy of the radiation used to induce chemical changes. Photolysis methods usually use quanta of energy in the 5 eV or λ = 2500 Å ranges, convenience and availability of ultraviolet sources dictating the choice of exciting source. Much higher energies are used in radiolysis. Radiolysis uses typically $\sim$1 MeV γ rays from Co^{60} sources and 1 MeV, 3 MeV, 10 MeV electrons from Linac or Van de Graaff accelerators. Occasionally 50 keV x rays have been used. The energy range from $\sim$50 keV to $\sim$20 keV is rarely reported, mainly due to the lack of convenient energy sources. In spite of the large disparity in energy between the two research areas, they have nevertheless interacted, providing information beneficial to both areas (Thomas 1976). The role that a short pulsed x-ray laser could play in the aforementioned fields may be assessed from the following discussion. The discussion is mainly concerned with high energy radiation as many of the statements and conclusions

also apply to the low energy or photochemical field. On reading the subsequent discussion it is worthwhile to bear in mind that a most significant feature of the work is the observation of chemical entities at very short times. A short-pulse x-ray laser can easily extend the existing time scale by several orders of magnitude.

9.2 Time Scale of Events

The action of high energy radiation on matter eventually gives rise to chemical change, and it is suggested that the precise nature of these chemical events may also explain the course of change in biological systems. For the purposes of this report we will confine ourselves to the radiolysis of liquid systems, where most radiation chemistry has been carried out.

Speculation and experimental fact have contributed a picture of the history of the physical and chemical events in radiolysis (Allen 1961, Ausloos 1968, Matheson and Dorfman 1969, Thomas 1970a, b, 1971) which are outlined in Fig. 9.1. Both excited species and ions may be produced in the primary radiation chemical event, and the extent of these processes has been investigated theoretically by the so-called optical approximation. On experimental grounds it is found that ion chemistry predominates in the radiolysis of polar liquids like water and alcohols, while excited states predominate in the radiolysis of less polar liquids like benzene and cyclohexane. There are exceptions to this broad ruling; for example, the radiolysis of some nonpolar liquids such as tetrahydrofuran produces significant yields of ions and low yields of excited states. The radiolysis of other liquids, aniline and dioxane, produces significant yields of both excited states and ions.

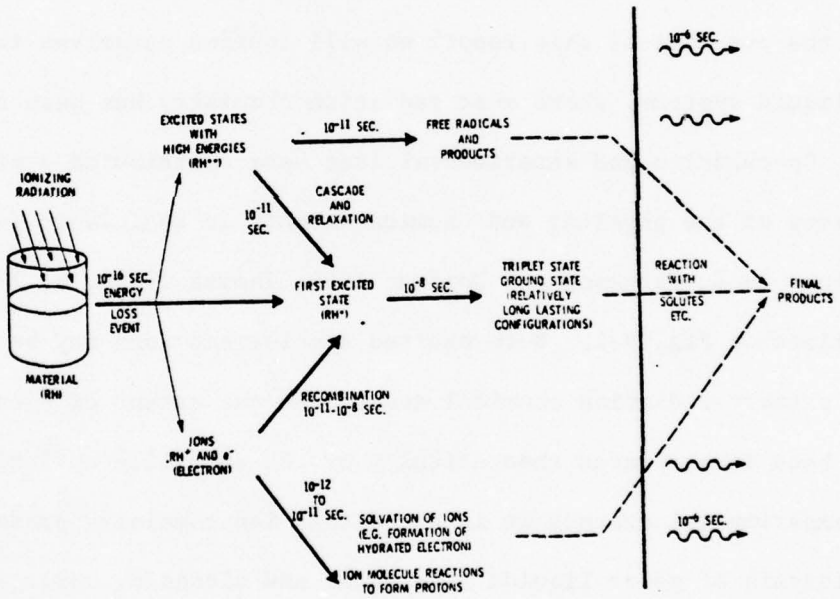

Figure 9.1. Excitation of a molecule or system with high-energy quanta.

Of course, the mere production of an excited state in radiolysis does not necessitate that a molecule has been directly excited by secondary electrons to this state, as ion neutralization processes may also lead to excited molecules, as well as to stable products or free radicals. In polar liquids such as water and alcohols, the parent positive ion is rapidly destroyed by an ion-molecule reaction involving the solvent. In water it is estimated that the lifetime of H_2O^+ is less than 10^{-14} sec. The fate of the positive ions is therefore forever sealed in these liquids. However, in less polar liquids the solvent cation may have a significant lifetime and produce a rich array of chemical processes, one of which is the formation of solute cations.

The electron which is produced along with the cation may react with a solute molecule, producing an anion; it may recombine with the cation; or it may be solvated by the solvent, forming a solvated electron. It appears that solvated electrons are formed in all solvents, and so will be formed in the radiolysis of liquids. The solvated electron again has a wide span of chemical reactions producing solute anions, etc. In the absence of suitable scavengers, some solvated electrons are stable, e.g., in ammonia.

The recombination of the ions to produce products, one of which may be excited states, is not a uniform process. The ejected electron is thermalized at various distances from the present cation, and hence results in a whole span of recombination times. From the time scale of events shown in Fig. 9.1 it is obvious that a method of rapid observation of the physical and chemical processes would greatly facilitate the description of the radiolytic events, indeed it may be well-nigh essential. To this end

various pulse radiolysis techniques have been designed, and these will be described in the forthcoming section.

9.3 Initiation of the Events

The most convenient form of high energy radiation for pulse radiolysis experiments is a fast electron. Energies of greater than 1 MeV may conveniently irradiate small, less than 0.1 ml liquid samples and produce fairly large quantities of species. A convenient energy for many experiments is 7 MeV, below the threshold for most nuclear reactions, so that the sample and surroundings do not become radioactive. Higher energies up to 40 MeV are more useful for some experiments, where the sample is in a low temperature dewar or a high pressure vessel and good penetration is needed. Also for some picosecond experiments the higher energy is required to produce Cerenkov radiation in a gas, the light being used to monitor the species. Heavy particles do not have the penetration into the sample to make convenient observations, and x rays or γ rays usually do not have a large enough linear energy transfer to give significant chemical change in the sample over a short irradiation period.

9.4 Nature of the Pulse

The advent of pulsed accelerators, both linac and Van de Graaff, has provided the necessary means of producing the radiation events in a short period of time, for subsequent rapid observation. Well defined 1 nsec pulses with peak currents up to 5 amp may be produced in Van de Graaff accelerators (Hunt and Thomas 1967), and many institutes utilize this type of machine for pulse radiolysis. Slightly longer pulses from 5 to 10 nsec may be generated in Linacs with peak currents up to 20 amps, the electron energy being larger and the sample geometry easier to achieve.

It is this last class of machine which enables the radiation chemist to push the domain of his time observations to short limits in the psec region. The fine structure of the Linac beam contains rows of pulses which for a L band machine may be 35 psec wide, full width half height separated by 770 psec, the duration of the train being 10 to 20 nsec. Indeed with selective conditions a single fine structure pulse may be extracted from the machine (Palmer and McGuire 1967). The exact shape and duration of such pulses are now known, but Fig. 9.2 shows a target measurement of two pulses from a 10 nsec row of pulses from the Notre Dame 7 MeV Linac (Beck and Thomas 1972). The fine structure pulses are observed with a transmission line target (Beck and Schutt 1972) having a rise time of 18 psec. The pulses are approximately 45 psec (FWHM) in duration and have a peak current of about 60 amps. A significant and measurable chemical change is produced by one of these fine structure pulses and the event may be observed up to the next pulse, i.e., for 770 psec. For subsequent observation it is more convenient to utilize one nsec pulses on a Van de Graaff accelerator. Shorter fine structure pulses may be produced on an s-band Linac and thus increase the time resolution of the experiments somewhat. However, the time resolution will not improve beyond $\sim$20 psec. An x-band Linac may improve the time resolution to $\sim$11 psec. The possibility of utilizing such a machine now is remote and time resolution is 20 psec or longer. The best mode locked laser experiments are then at least a factor of ten (<2 psec) better than the corresponding radiolysis experiments. The advent of a 10^{-15} sec x-ray laser pulse would immediately "set the ball rolling" again.

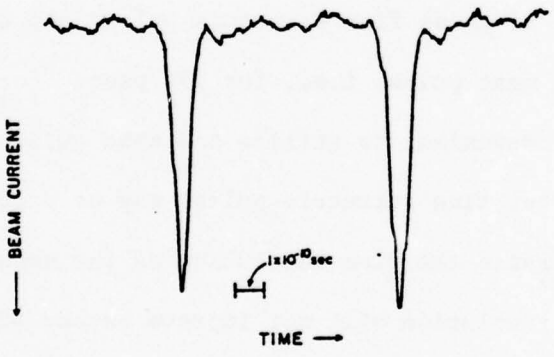

Figure 9.2. Fine structure pulses from the L-band linear accelerator as observed with a transmission line target.

However, rapid initiation is not sufficient in itself and rapid detection and observation of the resulting physical and chemical processes must be achieved. The next section presents three techniques that have been utilized and could be adapted to observe events initiated by an x-ray laser pulse.

9.5 Detection of the Intermediates--Picosecond Time Range

A schematic representation of the Notre Dame psec layout is shown in Fig. 9.3. The liquid under investigation is flowed through a 0.5 cm square suprasil sample cell, and is irradiated by 10 nsec rows of R.F. pulses. The emission or absorption spectra of the short-lived chemical intermediates are monitored by a spectrophotometric technique as shown in the figure. The light from an Osram XBO 450 watt Xenon lamp which is pulsed for 120 μsec to a current of 600 A at a repetition rate of 10 pps. or a 4 W argon ion laser (Coherent Radiation. Model 52B). is focused through the sample cell via a lens and mirror system into the entrance slit of a Bausch and Lomb monochromator (Model 33-86-02). An iris at the exit window of the cell limits the field of view of the detection system and a light chopper decreases the average light intensity falling on the cathode of an ITT F-4014 biplanar photodiode. This is mounted in a high-speed holder which is designed to match the diode to a 50 Ω system and to allow operation of the diode up to 10 kV, as the response to an increase in light level is determined by the flight time of the photoelectrons between cathode and anode. Detailed consideration of the diode performance will be given elsewhere. The linearity of the photocurrent vs. light intensity was checked with calibrated neutral density filters and by

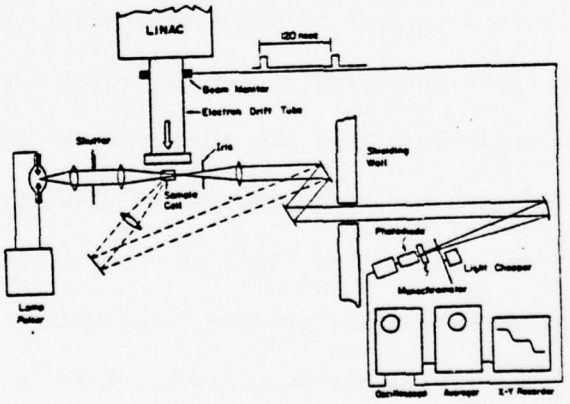

Figure 9.3. Schematic diagram of the pulse radiolysis system designed for picosecond time resolution.

observing the Cerenkov radiation from cyclohexane with the analyzing light alternately on and off. With complete illumination of the cathode current of 120 mA. It should be noted, however, that some diodes showed considerable fategue even at 4 μA mean current.

The output of the diode is fed into a Tektronix S-4 sampling head (rise time 25 psec), stored in a NS-44 digital averager (Northern Scientific), and plotted on an X-Y recorder. An advance trigger for the sampling oscilloscope is provided by operating the linear accelerator in double pulse mode which results in two 10-nsec beam pulses in one rf envelope separated by 120 nsec. These pulses are sensed by a current loop which permits the oscilloscope to be triggered by the first pulse, while the radiolysis events of the second pulse are observed. Figure 9.4 shows the response of the detection system to Cerenkov radiation from cyclohexane produced by two fine structure pulses. The diode was operated at 8 kV, corresponding to a flight time of 60 psec. The observed rise and fall times (10-90 percent) are 75 psec. The rise time in addition to the portion caused by the flight time is due to the pulse shape and trigger jitter. The overall rise time of the detection system is 60 psec.

A deconvolution technique may be used, however, so as to improve the time resolution to <5 psec (Beck and Thomas 1972). The recent development of streak cameras enables a time resolution of <2 psec to be obtained (Mavrogenet et al. 1976). Direct optical detection thus enables one to achieve a time resolution of ∿2 psec.

9.6 Stroboscopic Techniques

An alternative psec technique for absorption spectral studies has been developed by Hunt and coworkers (Bronskill et al. 1970, Wolff et al.

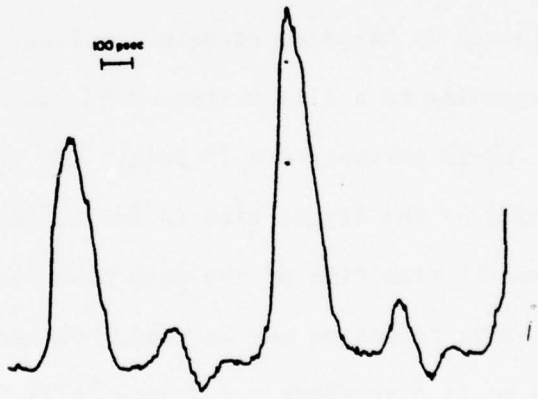

Figure 9.4. Cerenkov radition from cyclohexane produced by two fine structure pulses as observed with the picosecond detection system.

1970, Aldrich et al. 1972). The technique utilizes the Cerenkov light flash produced by the high energy radiation as a probe for the chemical species produced. The high energy radiation beam (40 MeV), initially transverses 10 cm of air and produces pulses of Cerenkov light which are identical to the initial radiation pulses. These light flashes are deflected out of the path of the radiation by the use of mirrors, the radiation beam continuing to irradiate the sample. The light flashes are then passed through the irradiated sample and the emerging light monitored both with respect to intensity and spectral distribution. By judicial choice of a mirror system the light flashes may be delayed known amounts of time after the irradiation process, the time being a fraction of the velocity of light and the light path. The intensity of the light flashes then measure the concentration of the short-lived radiation produced species. Hence the time dependence and the absorption spectrum of the species may be determined. This technique has the great advantage in that the time response of the system, which is about 10 to 20 psec, is not controlled by the response time of the detection system, but by the sample geometry and the length of the fine structure pulses. The technique is not suitable for emission studies in its present form, however. This technique has been used successfully in mode locked laser experiments to achieve response times of $\sim$1 psec. Rapid time resolution to about 1 psec has been used in pulse radiolysis studies. Similar techniques could be used in conjunction with an x-ray laser. However, it is hoped that the time resolution could be improved beyond 1 psec in order to fully utilize the "1/1000" psec pulse width of an x-ray laser.

9.7 Problems to be Solved in Radiation Chemistry

An x-ray laser would greatly improve the time resolution in pulse radiolysis studies. Three basic research areas should be investigated as indicated by Fig. 9.1:

a) Observation of very short lived species such as higher excited states with lifetimes of 10^{-13} - 10^{-12} sec.

b) Measurement of regions of higher local energy loss where the concentrations of chemical species are high and rapid initial reaction takes place. This area includes rapid geminate ion-neutralization. The tail end of this process has been measured already by Hunt et al. (loc. cit.) and Thomas et al. (1968), but more rapid time resolution is needed to observe the entire process.

c) The observation of rapid relaxation processes, in particular the reorganization of the solvent around a radiation produced species, e.g., electron. This may be termed solvation of the species involved.

9.8 Feasibility of Utilizing X-Ray Laser

An x-ray laser with the following properties would be useful in these studies:

Pulse Width	10^{-15} sec
Output	1 joule
Wavelength	1 Å (12.6 keV)

Pulse Width: The previous sections emphasized the great utility of such a short pulse of radiation.

Output: In many pulse radiolysis experiments an electron pulse of radiation will have the following properties:

Beam Energy	10 MeV (electrons), 10^{-8} sec duration
Current	2 amps
% absorption in sample	∿20 %

In other words, the energy absorbed in the sample is about 0.04 joules. The concentration of chemical species produced by such a pulse approaches a concentration of a few μmoles/l, and can be readily detected. For many studies a much lower concentration of chemical species can be monitored, especially if the species are fluorescent. The output of the x-ray laser exceeds the above limit and sufficient chemical species should be produced for detailed observation.

Wavelength: A wavelength of ∿12 keV x ray provides some problems in penetrating the sample container and irradiating a liquid sample. For 12 keV x rays the half stopping power for aluminum is 100 mgm/cm^2. This value can also be used for water. Thus 50 percent of the x ray is stopped in 1.0 mm of H_2O. The walls of a container would have to be very thin and of low density material. Special optics would be needed to observe chemical changes following irradiation. These problems could be solved, especially if the species produced were observed by luminescence techniques.

9.9 Radiolysis

It has been shown previously that the irradiation of water with high intensity light flashes (Thomas and Hart 1964) or high intensity pulses of 15 MeV electrons (Thomas and Hart 1962), leads to the production of hydrogen, hydrogen peroxide, and oxygen.

The light induced mechanism is the production of H and OH radicals from the photolysis of water with light of wavelength <2100 Å.

$$H_2O \xrightarrow{h\nu} H + OH$$

The subsequent radical reactions lead to H_2, O_2 and H_2O_2

$$H + OH \rightarrow H_2O$$

$$H + H \rightarrow H_2$$

$$OH + OH \rightarrow H_2O_2$$

$$OH + H_2O_2 \rightarrow HO_2 + H_2O$$

$$OH + HO_2 \rightarrow O_2 + H_2O$$

The higher energies of the fast electrons produce ionization of the water:

$$H_2O \rightarrow H_2O^+ + e$$

Solvation reactions of the ions produce OH and solvated ion

$$H_2O^+ + H_2O \rightarrow OH + H_3O^+ \qquad e^- + H_2O \rightarrow e^-_{aq}$$

followed by $e^-_{aq} + H^+ \rightarrow H$. The subsequent reaction of OH + H to give H_2, $O_2 + H_2O_2$ are as before.

It is anticipated that the high intensity pulse of a $\sim$1 Å laser will simulate the high intensity electron pulses, H_2, O_2 and H_2O_2 being produced. To some extent the energy of the x-ray laser is converted to chemical energy in the formation of irradiation products of H_2O viz. H_2, $O_2 + H_2O_2$. Because of the inefficiency of the eventual x-ray laser, however, it appears unlikely that this procedure will yield an economic source of fuel. However, as a tool for studying the fundamental chemistry of the process, it may prove invaluable.

10. MICROSCOPY

The potential of x rays for microscopy was appreciated already by their discoverer (Röntgen 1895). No refractory materials were found and the concept of an x-ray microscope was not discussed until several decades later when it was realized that x rays could be focused by reflection. Contact radiography, however, was almost immediately applied to the study of botanical specimens (Burch 1896, Ranwez 1896) and of alloys (Heycock and Neville 1898). The resolution was limited to the 0.2 μm set by the optical microscope needed for enlarging the microradiography. This has been reduced to about 0.1 μm by viewing with the electron microscope and by the use of grainless recording materials. Recent indications are (Spiller et al. 1976) that a resolution down to 0.01 μm is achievable in this way. Point projection, in which a narrow beam of x-rays is produced by a finely focused electron beam impinging on a thin target and magnification is obtained by placing the object close to the source, has also been practiced for decades (Ardenne 1939, Cosslett and Nixon 1951, 1953). In this procedure the x-ray beam can, of course, also be used as a scanning microscope where the object is examined point by point. The electron beam, itself, can be used in this mode but then examination is limited to the surface of the specimen because of the limited range of the electrons.

In the following we will briefly examine these methods to determine how the properties of x-ray laser can aid in their application. Details may be found in the comprehensive text of Cosslett and Nixon (1960).

10.1 Contact Microradiography

In this procedure the object is placed essentially in contact with the recording material and illuminated with x-rays. Apart from its purpose - the examination of detail in the specimen - it corresponds closely to the technique of lithography described in some detail in Section 3. The ultimate aim is to produce on film or on a grainless recording medium a shadowgraph of the specimen with the highest resolution compatible with a high degree of contrast and the least amount of geometrical distortion.

10.1.1 Resolution

We have already pointed out in Section 3 the importance of penumbral blurring in limiting resolution. The penumbra in terms of the parameters of Figure 3.2 is $\delta \simeq S\ d/D$. Thus, δ can be reduced by minumizing the angular size of the source d/D, with the minimum value of S ultimately limited by the total thickness of the specimen and the emulsion. From geometrical considerations the effective angular width for a given intensity can be reduced either by selecting a smaller source or by increasing D, the limit being finally set by the intensity required for a reasonably short exposure time. If this factor can be sufficiently controlled, the resolution then depends on unsharpness due to Fresnel diffraction. For a wavelength λ the minimum fringe width $f \simeq (t\lambda)^{1/2}$ where t is the specimen thickness. Radiation of 1 Å thus limits the resolution to 0.1 μm with a specimen 100 μm thick, and the same resolution is obtained for a 10 μm thick specimen at the biologically more useful wavelength of 10 Å.

A serious lower limit on possible resolution is due to the finite range of photo-electrons ejected from the atoms by x radiation falling on the recording medium. In conventional film this can range from more than

20 μm for 35 kV electrons to about 0.1 μm for 1.5 kV electrons (Bellman and Engström 1952), varying as the square of the electron energy (Eq. 3). If a resolution better than 0.1 μm is sought, it becomes necessary to work at wavelengths longer than about 10 Å. Similar results apply to most photo-resists. Since the grain separation of high-resolution emulsions is in any case of order 0.1 μm, these considerations are particularly important for grainless media, especially for the negative photo-resists where the photo-electrons can cause polymerization beyond the edges of the desired image boundaries.

For maximum resolution, then, a source is required of high intensity and small angular divergence in the soft x-ray wavelength region.

10.1.2 Contrast

The contrast achieved depends on the relative absorption by the object in comparison with the adjacent region. If we denote by μ_o the object linear absorption coefficient and by μ_a the absorption coefficient of the adjacent region, the discrimination is measured by the ratio of the transmitted intensities

$$I_o/I_a = e^{-(\mu_o - \mu_a)t} , \qquad (1)$$

for specimen thickness t. For a detection sensitivity of 5% this means $(\mu_o - \mu_a)t$ must be of the same order since for small differences in absorption the differential contrast $(I_a - I_o)/I_a \simeq (\mu_o - \mu_a)t$. Imposition of a given discrimination, therefore, imposes minimum thickness requirements for the various elements making up the sample; some examples are given in Table 10.1 for a number of wavelengths (Cosslett and Nixon 1960). Figure 10.1 exhibits the penetration of x-rays ranging in wavelength from less than 1 Å to 10 Å

Table 10.1

Element	Z	λ = 2.5 Å		λ = 10 Å		λ = 20 Å	
		$\mu(cm^{-1})$	t(μm)	$\mu(cm^{-1})$	t(μm)	$\mu(cm^{-1})$	t(μm)
C	12	42.8	11.5	2.52×10^{3}	0.2	1.64×10^{4}	0.031
Cu	29	1780	0.28	4.54×10^{4}	0.011	4.36×10^{4}	0.012
Os	76	1.24×10^{4}	0.040	4.95×10^{4}	0.010	-	-
U	92	1.59×10^{4}	0.031	6.36×10^{4}	0.008	-	-

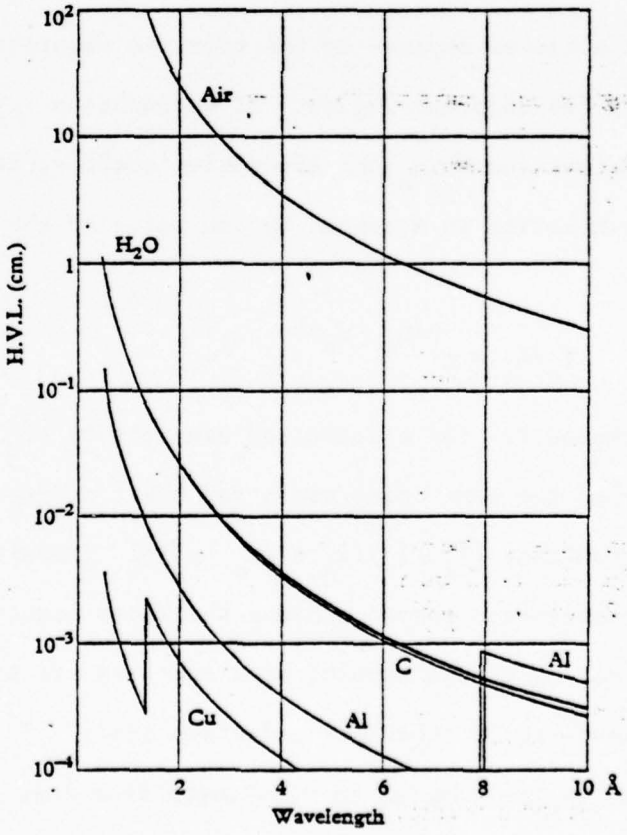

Figure 10.1. Half-value layer (H.V.L.) of various absorbers as a function of wavelength. (Engström 1956)

for some common elements and substances. The ordinate is in terms of the half-value layer or the thickness reducing by two the incident intensity.

The limitations on biological materials are particularly severe due to their low value of Z. Taking carbon as a typical constituent, we obtain a thickness requirement of 2000 Å for 10 Å radiation. Details much smaller than this dimension can only be seen by using longer wavelengths, or by staining with high-Z elements, or, of course, by lowering the detection threshold.

An exception to these general considerations occurs when radiation is available of wavelength above absorption edges. For example, working at the high wavelength side of the Cu K-edge (1.38 Å) can yield a differential absorption of at least 3000 cm^{-1} with respect to platinum (Figure 10.2). Also, quantitative measurements of element concentrations can frequently be optimized by using two wavelengths straddling an absorption edge (cf. Section 4.1). For highly accurate work in which the absorption coefficients are precisely known as a function of wavelength it is clearly important to have available radiation of narrow linewidth and sufficient intensity, such as that provided by a laser, to yield short exposure times.

10.2 Point Projection

In point projection the object is placed close to a small source and magnification is obtained as in a pinhole camera. The main differences between this method and contact microscopy are, therefore, the large object-recording medium distance and the more stringent intensity requirements on the source which, for equal resolution, must be reduced by the magnification factor. Useful source size is not limited by the spot size of the focused electron beam but rather by the heat dissipation limitations of the target

material, and the scattering range of the electrons. These factors ultimately limit the attainable brightness and x-ray spot size, particularly at short wavelengths.

10.2.1 Resolution

The achievable resolution is given as for contact microscopy by penumbral blurring and, finally, by Fresnel diffraction. In the notation of Section 3, the object-photo-resist distance is S, the source-object distance is D, and the source dimension is d. The width of the penumbra is

$$\delta = S\, d/D \quad . \tag{2}$$

The magnification $M = 1 + S/D$, and the resolution in the object plane is essentially $\delta/M \simeq d$ because in point projection microscopy $D \ll S$. The resolution is thus directly related to the dimension of the source for high magnification.

Fresnel diffraction effects may become significant at the longer wavelengths. From diffraction results for an opaque straight edge it follows that the width of the first fringe is approximately given by $(MS\lambda)^{1/2}$. For small S this leads back to the result already given in Section 10.1.1. For high magnification, however, the reduced fringe width in the object plane becomes $(S\lambda/M)^{1/2} \simeq (D\lambda)^{1/2}$. When this is compared with the geometric resolution limit given above it appears that Fresnel diffraction becomes the more important limiting factor unless $\lambda \lesssim d^2/D$. At a resolution of 0.1 μm and a wavelength of 10Å needed for reasonable contrast in biological specimens - this limits D to 10 μm or less, a serious restriction.

10.2.2 Electron Scattering

We have seen that a small spot size is crucial if the point projection technique is to yield high magnification and minimal penumbral blurring.

The spot produced by focusing electrons on a target will spread beyond the focus by the outward diffusion of electrons. To compensate for this by making the target thinner only results in serious loss of intensity.

The effect of electron scattering on spot size is expressed by the following approximate result for the range x_r of the electrons (Whiddington 1912, 1914; Lane and Zaffarano 1954; Paul and Steinwedel 1955).

$$x_r \simeq (A/a_2 \rho Z)V^2 \qquad (3)$$

in terms of the tube voltage V, atomic weight A, atomic number Z and density ρ of the target material, and a constant a_2 which is of order 10^{12} for high-Z elements. For an aluminum target the range x_r at 10 kV is then of order 1 μm, in reasonable agreement with the measurements of Young (1956, 1957). This expression is sufficient as a rough indication of spot size, although the actual diffusion disk may be up to a factor two smaller because the scattered electrons that emit most of the radiation remain confined to a forward cone of half-angle 30^o (Langner 1957). For a given target material, then, the spot size varies as V^2 while the intensity from targets comparable in thickness to the electron range is proportional to their thickness. Consequently, a typical optimum target thickness is of the order of a μm at 10 kV and only 0.01 μm at 1 kV. The increased resolution for soft x-rays can, however, only be obtained at very low intensities, while higher intensities can only be produced at poorer resolution. Typical operating conditions for a fine focus tube are: beam current 25 μA, anode voltage 10 kV and specific loading 100 kW/mm^2. The conversion efficiency from electron to x-ray power is approximately given by 1.3×10^{-9} ZV (Compton and Allison 1935, Dyson 1959) so that the power in the x-ray beam is

$$P \simeq 1.3 \times 10^{-9} ZV^2 I \quad , \qquad (4)$$

with V in volts and I in amperes. For a copper target the conversion efficiency is $\sim 3.8 \times 10^{-4}$ at 10 kV, corresponding to a total x-ray power of 95 μw at I = 25 μA. The characteristic line intensity is always less than this continuum power; at 10 kV for the copper K_α line the fraction is only about 1%, though the relative number of quanta of characteristic radi- radiation rises with excitation voltage: to 25% at 25 kV and to 40% at 45 kV (Worthington and Tomlin 1956).

10.3 Imaging by Refraction and Reflection

X-rays can be focused by refraction or by reflection off curved surfaces. We will see, however, that refraction involves excessively long optical paths, while reflection is limited by narrow field of view and loss of intensity if high resolution is to be achieved.

10.3.1 Refraction

Far from optical resonances, the refractive index, n, at x-ray wavelengths is determined primarily by the electron density, as for a plasma. Away from absorption edges we have

$$n = 1 - \frac{4\pi NZe^2}{m\omega^2} \quad , \tag{5}$$

where ω is the frequency of the incident raditaion, Z the atomic number, N the electron density, and m the electron mass. A useful quantity is the deviation δ of n from 1:

$$\delta \equiv 1 - n = 2.70 \times 10^{10}\ Z\rho\lambda^2/A \ , \tag{6}$$

in terms of the wavelength λ and the material density ρ. The refractive index for x rays is thus less than unity, and, typically, δ ranges from 10^{-5} to 10^{-6} for medium-Z elements at 1 Å. The refractive power of materials for

x rays is therefore five to six orders of magnitude smaller than that for visible light.

Focusing by refracting optics is nevertheless still possible, but with the roles of concave and convex lenses reversed from their functions for visible light; a concave lens is focusing for x rays. As an example of the magnitudes involved, consider the focal length, f, of a biconcave lens of radii of curvature R. By the lensmaker's formula $f = R/2\delta$ or $f \simeq 100$ m with R = 1 cm and $\delta = 5 \times 10^{-5}$. The focal length decreases as $1/\lambda^2$ so that at 10 Å f could be brought down to about a meter which begins to be useful. Unfortunately, the absorption increases as λ^3 which again limits the optical path to excessively long lengths. Finally, for refractory techniques to be useful at all it is essential to use highly monochromatic radiation because of the strong λ-dependence of δ.

10.3.2 Reflection

To obtain magnification in acceptable distances it is necessary to rely on total reflection of x rays. This occurs when x rays are incident on a material at angles less than some critical angle θ_c given by $\theta_c = \cos^{-1} n$ or, because of the smallness of δ, $\theta_c \simeq (2\delta)^{\frac{1}{2}}$ which typically ranges from 1-10 mrad. Table 10.2 gives some typical values (Cosslett and Nixon 1960) for δ and θ_c. When absorption is also taken into account it is found (Hildenbrand 1956) that the reflection efficiency drops to as little as 10 percent near θ_c so that the useful angle of incidence is actually much less than θ_c.

Table 10.2

	Z	λ = 0.708 Å		λ = 2.28 Å		λ = 8.3 Å	
		$\delta\times10^{6}$	$\theta_c\times10^{3}$	$\delta\times10^{5}$	$\theta_c\times10^{3}$	$\delta\times10^{4}$	$\theta_c\times10^{2}$
Al	13	1.75	1.87	1.83	6.05	2.41	2.19
Ag	47	6.35	3.55	6.60	11.5	8.75	4.18
Au	79	10.5	4.55	10.9	14.7	14.4	5.35

Focusing by total reflection from curved surfaces has been studied for many years beginning with Jentzsch (1929) and developed further by Kirkpatrick and Baez (1948). Even cursory examination of the geometry with the necessarily small incident angles involved leads to the presence of severe aberrations in non-paraxial systems if any magnification at all is to be realized. Astigmatism may be overcome to some extent by adopting a crossed-cylinder geometry, but this gives rise to considerable distortion due to the different magnifications resulting from varying distances for meridian and sagittal reflections. To compensate for the other aberrations stops and aspherical surfaces must be used (see, for example, Wolter 1952; Baez 1957). All of these involve two reflections or more, resulting in considerable intensity loss for angles near θ_c. The paraxial design mentioned and analyzed extensively by Wolter (1952) involves combining paraboloids, ellipsoids, and hyperboloid surfaces which enable the Abbe sine condition to be satisfied to first order, thereby reducing both coma and spherical aberration. However, the tolerances required for a grazing incidence angle θ are of order $\lambda/10\,\theta$, or close to an order of

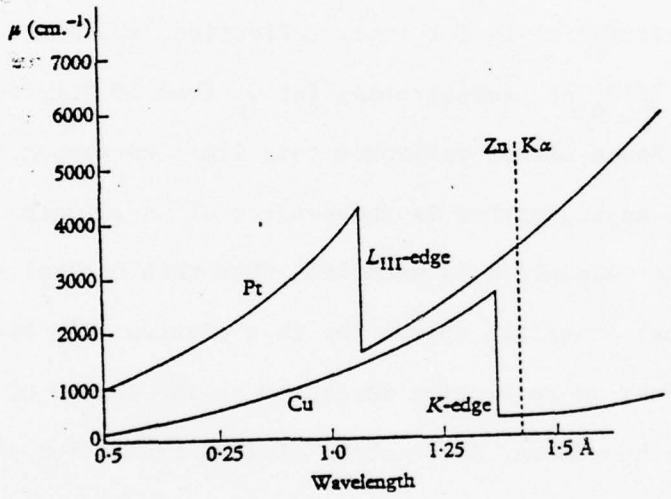

Figure 10.2. Variation in absorption coefficient with wavelength for copper and platinum, in the neighbourhood of the CU-K and Pt-L_{III} absorption edges. (Cosslett and Nixon 1960)

magnitude less than the one-tenth wavelength used for visible light. The testing for tolerances in the 10-20 Å range has been carried out by means of multiple beam interferometry (Tolanski 1948, Koehler 1953). The availability of a coherent x-ray source in this wavelength range would, of course, render such testing routine (cf., Section 5.3), making paraxial x-ray imaging systems a realizable possibility.

10.3.3 Resolution

The resolution of a system with a beam of semi-angular aperture θ is limited by diffraction to $d_D \simeq \lambda/2\theta$. Since the maximum value of θ is limited by θ_c, the critical angle for total reflection, d_D cannot be reduced to less than $\lambda/2\theta_c$ or, substituting for θ_c from 10.3.1, to less than $215\ (\rho A/Z)^{\frac{1}{2}}$ Å. For a silver reflector this limit corresponds to about 100 Å, which to first approximation is independent of wavelength. The practically achievable resolution is much less than this optimal value because of aberrations; spherical aberration is a particularly serious limitation as its effect on resolution increases as the square of the angular aperture while, as we have seen, diffraction limited resolution varies inversely with the first power of θ. Correction of spherical aberration is then particularly important if high resolution is required.

10.4 Zone Plates

We have already mentioned zone plates and their resolution in Section 7. These devices offer the intriguing possibility of focusing monochromatic x rays so that x-ray imagery with magnification would become possible with simple and efficient optics. We have also observed that the holographic production of such plates cannot be carried out down to resolutions of the order of x-ray wavelengths. Recent progress has, however, led to the

production of free-standing, partially transmitting, zone plates of gold and other heavy metals by means of electron beam machining and fabrication techniques well-established in the manufacture of integrated circuits (Dÿkstra et al. 1971). Some have been used with monochromatized synchrotron radiation (cf., e.g., Pfeifer et al. 1973, Niemann et al. 1974).

The considerable advantage of radiation from an x-ray laser is its high degree of monochromaticity coupled with high intensity (short exposure times). Monochromatic radiation must be used because the focal length of a zone plate varies linearly with the wavelength [Eq. (7.5)] so that zone plates have severe chromatic aberration.

10.5 Image Intensification

The need for minimizing penumbral blurring in contact microscopy and for optimal focusing a projection microscope leads to intensity requirements not normally met by conventional sources. It then becomes necessary to employ image intensification procedures. The most promising of these is the focusing of photo-electrons produced when x rays passed by the object impinge on a foil which emits photo-electrons in proportion to the incident x-ray intensity. The recorded image can then be further magnified by conventional means (Möllenstedt and Huang 1957). The resolution is, however, limited by the chromatic aberration of the electron lens, since the energy spread of the photo-electrons is comparable to that of the incident x-ray beam.

The beam from an x-ray laser has then at least two advantages for those applications (primarily in the study of biological materials) where the full intensity of the laser beam cannot be used because of radiation damage to the specimen. One is the highly collimated nature of the beam leading to minimal

geometric distortion. The second is the high spectral purity of the radiation resulting in reduced energy spread of the photo-electrons and hence higher resolution by the electron microscope.

10.6 Field Ion Microscopy

In field ion microscopy the material to be examined is ionized by the high electric field existing near a point electrode. The ions are then accelerated to a screen some distance away from the tip and imaged. High resolution of 2-3 Å is feasible, but the corresponding fields have to be of order 5×10^8 V/cm which can cause the molecules to be examined to vaporize (Müller and Tsong 1969). Letokhov (1975) has suggested pre-excitation of the atoms or molecules to states near the ionization limit by laser radiation. The advantage of this procedure would be a reduction in the required fields by one to two orders of magnitude. In particular, it is suggested that the lower triplet state $^3S_1$ of HeI can be populated by excitation of the $^3P_{2,1}$ states with 591.4 Å radiation from a He source.

It would appear that an x-ray laser operating at the appropriate excitation wavelength could be directly used in this scheme as it has both the required intensity and the spatial localization of the radiation needed in this application. This should allow an even greater reduction in field strength. A possible difficulty may, however, be the localization of the object sufficiently near the charged tip to prevent recombination.

10.7 Phase Contrast Techniques

The phase contrast method of Zernike (1935, 1942) is useful for examining phase objects which alter the phase but not the amplitude of the incident wave. If the transmission function of such an object is represented by $t(x)$, we have for small phase changes ϕ, $t(x) \simeq 1 + i\phi(x)$. If now the phase of

the central order of the diffraction image is retarded or advanced by $\pi/2$, the light distribution in the image plane is represented by $\pm i + i\phi(x)$ and the image intensity is proportional to $1 \pm 2\phi(x)$. By this procedure (analogous to holography) phase changes are recorded as intensity variations in direct proportionality. This technique is of particular interest at wave lengths below 10 Å, especially for biological specimens where diminished absorption occurs. The narrow beam from an x-ray laser could be used in the microprobe mode.

The splitting of the incident beam might be carried out by the use of the Borrmann effect. This can occur when an x-ray beam is incident at the Bragg angle on a perfect crystal whose thickness is many half-value layers so that passage of undiffracted light is suppressed. Dynamical diffraction theory predicts the excitation of a standing wave pattern with its nodes or its anti-nodes passing through the atomic planes. The Borrmann effect of reduced absorption occurs in the former case leading to two diffracted beams separated by twice the Bragg angle. Bonse and Hart (1965) have already shown the feasibility of constructing x-ray interferometers based on this effect. An additional important feature is the preservation of the collimation (to within fractions of a mrad) of the incident beam.

This last point raises the possibility of producing many highly collimated beams from a single laser beam, each useful for a particular experiment, apparently solving the problem of reducing the laser beam's intensity without degrading its collimation. The extent to which the radiation tolerance of the Borrmann crystal is raised by spreading the energy over many modes remains to be calculated.

10.8 Advantages of X-Ray Lasers

We are now in a position to enumerate the advantages of an x-ray laser source for the above techniques. In all three cases intensity is a prime requirement. This is particularly true when high resolution ($\lesssim 0.1$ μm) is sought. Grainless recording media then become necessary which require typically energy fluxes in the 100 mJ/cm^2 range. If conventional sources are used, this energy requirement leads to exposure times as long as ten hours and an extremely low data rate. The use of x-ray laser beams could cut these times by several orders of magnitude, although in these estimates one must ultimately reckon with the loading the recording material can withstand without being destroyed (cf., Section 6.2). High intensity levels are particularly difficult to achieve with conventional sources at the higher wavelengths (10-20 Å) which as we have indicated should be used for high resolution work in medium-Z samples such as biological specimens.

Point projection and scanning microscopy impose the further requirement of μm sized beam diameters, a condition satisfied with some x-ray laser schemes, though not by all (Section 1). Because of its large angular divergence in the orbit-plane a synchrotron source loses some of its attractiveness here because of intensity loss (cf., Section 2.2). Reflection x-ray microscopy is to first order achromatic, but a narrow beam is still imperative to suppress aberrations and to achieve high resolution.

For quantitative studies of high accuracy it becomes important to employ monochromatic radiation, for the absorption coefficient depends sensitively on wavelength. The usual characteristic line source has then in addition to its inefficiency at the important longer wavelengths the further disadvantage of a 1 eV linewidth. Synchrotron radiation, being continuous, must be

filtered or monochromatized by crystals. This leads not only to large energy losses but also to the inevitable appearance of sub-harmonic multiples. X-ray laser radiation should in this respect be ideal because of gain narrowing of the characteristic line. Its intensity further holds out the possibility of efficient mixing with narrow band optical radiation from lasers. A neodymium laser, for instance, would yield a shift of about an eV, which is sufficient to take advantage of the sharp drop in absorptivity on the long wavelength side of an absorption edge.

The property of coherence, except insofar as it is related to line-width, has not been stressed as it appears unlikely that x-ray lasers when produced will exhibit any marked degree of coherence. In any event, even for reflection microscopy a coherent source does not dramatically improve resolution, effecting at most a 1 percent improvement (cf., e.g., Born and Wolf 1959). As an early demonstration of x-ray microscopy at VUV wavelengths, Kompfner (1976) has put forward the idea of using the coherent radiation obtained by parametric up-conversion by Harris et al. (1971), Young et al. (1971), and Kung et al. (1972, 1973). He proposes to produce a diffraction limited spot at wavelengths of 1000 Å and less by reflection optics, to scan the object across the spot and then convert the scattered radiation from the instantaneous object point to a parallel beam by returning the beam through the focusing optics. A photon counter is suggested as a detector whose output is displayed on an oscilloscope synchronized with the mechanical scan. Among the optics suggested is a Fresnel zone plate which if made at a wavelength of n times the wavelength would have an efficiency varying as $1/n^2$. Since a zone plate with resolution λ must have λ as its finest zone spacing,

the production of an efficient Fresnel lens at x-ray wavelengths is clearly no easy task. For preliminary work in the VUV range, however, this might be accomplished by means of electron beam machining or by holography (cf., Section 7). There is actually little advantage to be gained from x-ray microscopy by zone plate if this plate is to be produced as an x-ray hologram of a point source. The reason for this is simply that the resolution of such a zone plate is determined by the smallest fringe spacing which in turn is set by the size of the scattering point. The recording of the diffraction pattern of this point source requires a beam of comparable dimension in which case one might as well proceed by direct contact imaging of the object. There may, however, be some advantage if the object is not suited to contact microscopy.

The main difficulty with the use of coherent radiation obtained by parametric conversion is the lack of intensity resulting from extremely low ($\sim 10^{-7}$) efficiency at the shorter wavelengths. This will again lead to excessively long exposure times of photo resists, and poor modulation.

11. INELASTIC SCATTERING STUDIES IN SOLIDS

Within the past ten years, primarily because of the availability of more powerful sources of monochromatic x rays, there has been considerable research on inelastic x-ray scattering in metals (cf., e.g., Platzmann 1976, Eisenberger 1972). In copper, for example, where the K-shell binding energies are in the keV range and the L-shell electrons are bound by hundreds of eV, inelastic scattering of monochromatized Cu K_α radiation at 8.04 keV (1.54 Å) is observed with energy losses corresponding to the energy of the Cu L absorption edges. Similar effects are observed with other metals (Sparks 1974, Eisenberger et al. 1976). X rays scattering inelastically from metals leave the material in various states of excitation. The phenomenon just described leads to excitation of the L (and, in principle, the K) shell electrons and has been described as x-ray Raman scattering by analogy with similar effects in optical spectroscopy of atoms and molecules. Inelastic plasmon and Compton scattering have been studied for a long time but the intensive study of these second-order Raman-type processes is relatively new. The high-resolution experiments of Eisenberger et al. on copper just referred to were performed with a monochromatized synchrotron radiation beam from SPEAR having about 0.9 eV bandwidth and a flux of 10^{10} photons/second. The signals were very weak (2 counts/second at the peak of the K_{α_1} at resonance) even with the strongest synchrotron source available. The data appear to give very accurate information on the location of Fermi surfaces in metals, and the method promises to be an important alternative to measuring extended fine structure and edge singularities by x-ray absorption in metals (Bannett and Freund 1975). An

increase in the average monochromatic x-ray flux by two or more orders of magnitude over the SPEAR storage ring such as might be expected from a laser source could make this a generally useful technique in the study of metals.

12. ATOMIC PHYSICS - USE OF INTENSE, MONOCHROMATIC X RAYS TO PRODUCE HIGHLY STRIPPED IONS AT LOW VELOCITIES FOR SPECTROSCOPIC STUDIES AND HEAVY ION ACCELERATORS

Photoionization of inner-shell electrons at or just above an absorption edge ($h\nu \gtrsim |E_{edge}|$) with monochromatic x rays will produce an Auger-cascade. A vacancy produced in the innermost shell of an atom (the K-shell) will be filled with high probability by a two-electron Auger process in low-Z to medium-Z elements. An electron from a higher shell (usually the next higher shell) will fill the K vacancy and a second electron will be ejected (usually from the same higher shell) from the atom, increasing the charge-state of the parent ion by one unit. In a medium-Z element with full K, L, M, and N shells, for example, a total of seven electrons will be ejected from the atom per initial K vacancy, leading to an ionic charge + 8. The ionic charge doubles at each step because each K vacancy leads to two L vacancies each of which produce two M vacancies, and so forth. In higher-Z elements which have a large K fluorescence yield, the mean final ionic charge will tend to be reduced since some of the excitation energy needed to produce the initial vacancy will be recovered in the form of x rays rather than autoionized (Auger) electrons. On the other hand, electron "shake-off" processes will substantially increase the final charge state and average charge (Carlson et al. 1966 and references therein). For example, in Hg (Z = 80) the production of an initial L-vacancy gives rise to significant production of ions up to charge +17, with a mean charge of +9.8. The article by Carlson et al. (1966) gives additional data for rare gases with initial vacancies in various shells. The double Auger process (Åberg 1975) also plays an important role in increasing the ionization.

The production of high charge states of heavy ions is important in the design of heavy ion accelerators since, crudely, the maximum energy attained by an ion for a given acceleration potential is proportional to its degree of ionization. Further, for beams of high beam quality (low divergence) the process of ion formation must be such that the transverse velocity of the ions is as small as possible. This is not achieved when one relies on high temperatures to produce a Saha equilibrium because of the isotropic nature of the velocity distribution. Rather, one wishes to produce cold ions in a high charge state. This is precisely what happens when an intense x-ray laser source is used of sufficiently short wavelength. The ultimate beam quality achieved is then set by the impulse received from the expelled electrons by the ion. High beam quality is required in applications where propagation over long distances is anticipated and in the new area of ion beam fusion where the beam must be accurately focused from an initial 10 cm size to hit a target of the order of mm across.

Spectroscopic and collision studies on such ions are also of considerable practical importance in astrophysics, in analyzing laser-driven plasmas, and in studying the role of impurities in thermonuclear plasmas. The spectroscopy of highly stripped ions has been studied extensively (cf., e.g., Sellin and Pegg 1976). Practical applications of stripped ions have been given in various proceedings (e.g., Brenn and Mehlhorn 1976).

REFERENCES

Åberg, T., Atomic Inner-Shell Processes, Vol. I, Ed. B. Crasemann (Academic Press, New York, 1975), p. 368ff.

Accardo, C. A., Phys. Rev. Lett. 1, 180 (1958)

Aldrich, J. E., P. Foldvery, J. W. Hunt, W. B. Taylor, and R. K. Wolff, Rev. Sci. Instr. 43, 991 (1972).

Allen, A. O., Radiation Chemistry of Water (Van Nostrand, New York, 1961).

Allen, L. and G. I. Peters, Phys. Lett. 31A, 95 (1970).

Allen, L. and G. I. Peters, J. Phys. A4, 238, 377, 561 (1971).

Allen, L. and G. I. Peters, J. Phys. A5, 546 (1972).

Anacker, W., Proc. 1974 Int'l. Electron Devices Meeting (December 1974), p. 5.

Andrews, R. A., "Soft X-Ray Lasers Via Electron-Collisional Pumping," in Progress in Lasers and Laser Fusion, A. Perlmutter and S. M. Widayer, Eds. (Plenum Press, New York, 1975), p. 235.

Ardenne, M. von, Naturwissenschaften 27, 485 (1939).

Atkins, H. L., R. G. Fairchild, J. S. Robertson, and D. Greenberg, Radiology 115, 431 (1975)

Atkins, H. L., W. Hauser, and H. W. Kraner, "Absorption Edge Transmission Scanning," Brookhaven Natl. Lab. Rpt. No. R-BNL-15347.

Ausloos, P., Ed., Fundamental Processes in Radiation Chemistry (Interscience, New York, 1968).

Azaroff, L. V., Ed., X-Ray Spectroscopy (McGraw-Hill, New York, 1974), Chs. 2, 3.

Baechtold, W., et al., Electronics Lett. 9, 232 (1974).

Baez, A. V., X-Ray Microscopy and Microradiography (Academic Press, New York, 1957), p. 186.

Bagus, P. S., Phys. Rev. 139A, 619 (1965).

Baily, N. A., E. C. Lasser, and R. L. Crepeau, Invest. Radiol. 6, 221 (1971).

Baily, N. A., R. L. Crepeau, and E. C. Lasser, Radiology 103, 197 (1972).

Baily, N. A. and R. L. Crepeau, Radiology 115, 439 (1975).

Balloffet, G., J. Romand and B. Vodar, C. R. Acad. Sci., Paris 252, 4139 (1961).

Bammes, P., R. Klucker, E. E. Koch and T. Tuomi, Phys. Stat. Solidi 49, 561 (1972).

Bannett, Y. and I. Freund, Phys. Rev. Lett. 34, 372 (1975).

Barrett, C. S., Trans. AIME 161, 15 (1945).

Basov, N. G., V. A. Boiko, Yu. P. Voinov, E. Ya. Kononov, S. L. Mandelshtam, and G. V. Sklizkov, Zh ETF Pis'ma Red. 5, 177 (1967) [English Transl.: JETP Lett. 5, 141 (1967)].

Basov, N. G., V. A. Boiko, V. A. Gribkov, S. M. Zakharov, O. N. Krokhin, and G. V. Sklizkov, Zh ETF Pis'ma Red. 9, 520 (1969) [Engl. Transl.: JETP Lett. 9, 315 (1969)].

Bathow, G., E. Freytag and R. Haensel, J. Appl. Phys. 37, 3449 (1966).

Bearden, J. A., Rev. Mod. Phys. 39, 78 (1967).

Bearden, J. A. and A. F. Burr, Rev. Mod. Phys. 39, 125 (1967).

Beck, G. and J. K. Thomas, J. Phys. Chem. 76, 3856 (1972).

Beck, G. and J. K. Thomas, J. Chem. Phys. 57, 3643 (1972).

Beck, G. and D. W. Schutt, Rev. Sci. Instrum. 43, 341 (1972).

Bellman, S. and A. Engström, Acta Radiol. (Stockh.) 38, 98 (1952).

Berkowitz, J., Adv. High Temp. Chem. 3, 123 (1971).

Bernacki, S. E. and H. I. Smith,"X-Ray Lithography Applied to Silicon Device Fabrication,"Proc. Sixth Int'l. Conf. on Electron and Ion Beam Science and Technology, Ed. R. Bakish (Electrochemical Society, Princeton, N.J., 1974) p. 34.

Bernacki, S. E. and H. I. Smith, IEEE Trans. Electron Devices ED-22, 421 (1975).

Berns, M. W., J. B. Rattner, S. Meredith, and M. Witter, Annals of the N.Y. Acad. Sci. 267, 160 (1976).

Bernstein, M. J. and G. G. Comisar, J. Appl. Phys. 41, 729 (1970).

Bessis, M., G. Gires, L. Mayer, and G. Nomarski, C. R. Acad. Sci. 225, 1010 (1962).

Best, P. E., private communication (1976).

Bienenstock, A., "Wear, Polishing and the Study of Surface Layers by X-Ray Diffraction," Rept. of ARPA Materials Research Council, July 1975.

Bjorklund, C. G., "Vacuum Ultraviolet Holography," Microwave Laboratory Rpt. 2339, Stanford University (1974).

Bjorklund, G. C., S. E. Harris, and J. F. Young, Appl. Phys. Lett. 25, 451 (1974).

Bloom, D. M., G. W. Bekkers, J. F. Young, and S. E. Harris, Appl. Phys. Lett. 26, 687 (1975).

Bloom, D. M., J. F. Young, and S. E. Harris, Appl. Phys. Lett. 27, 390 (1975).

Bonse, U. and M. Hart, Appl. Phys. Lett. 6, 155 (1965).

Born, M. and E. Wolf, Principles of Optics (Pergamon Press, London, 1959), §8.6.

Brault, R. G., Proc. Sixth International Conference on Electron and Ion Beam Science and Technology, Ed. R. Bakish (Electrochemical Society, Princeton, N.J., 1974), p. 63.

Brenn, R. and W. Mehlhorn, Eds., Proc. of the Second Int'l. Conference on Inner-Shell Ionization Phenomena (Freiburg, 1976).

Bristow, T. C., M. J. Lubin, J. M. Forsyth, E. B. Goldman, and J. M. Soures, Opt. Commun. 5, 315 (1972).

Bronskill, M. J., R. K. Wolff, and J. W. Hunt, J. Chem. Phys. 53, 4201 (1970).

Brueckner, K. A. and S. Jorna, Rev. Mod. Phys. 46, 325 (1974).

Brundle, C. R., J. Vac. Sci. Technol. 11, 212 (1974).

Burch, G. J., Nature (London) 54, 111 (1896).

Burhop, E.H.S., The Auger Effect and Other Radiationless Transitions (Cambridge University Press, Cambridge, 1952).

Carlson, T. A., Photoelectron and Auger Spectroscopy (Plenum Press, New York, 1975).

Carlson, T. A., W. E. Hunt, and M. O. Krause, Phys. Rev. 151, 41 (1966).

Caudano, R. and J. Verbist, Eds., Electron Spectroscopy (Elsevier, Amsterdam 1974).

Chapline, G. and L. Wood, Physics Today 40, (June 1975).

Chapline, G. and L. Wood, Physics Today, 57, (July 1976).

Christian, J. W., Transformations in Solids, 2nd ed. (Pergamon Press, New York, 1975).

Citrin, P., G. K. Wertheim, and Y. Baer, Phys. Rev. Lett. 35, 885 (1975).

Coad, J. P., M. Gettings, and J. C. Riviere, J. Chem. Faraday Discussion 60, paper 21 (1975).

Codling, K., Rep. Prog. Phys. 36, 541 (1973).

Codling, K. and R. P. Madden, J. Appl. Phys. 36, 380 (1965).

Codling, K. and P. Mitchell, J. Phys. E 3, 685 (1970).

Collier, R. J., C. B. Burckhardt, and L. H. Lin, Optical Holography (Academic Press, New York, 1971).

Compton, A. H. and S. K. Allison, X-Rays in Theory and Experiment, 2nd ed. (MacMillan, London, 1935).

Connerade, J. P.; W.R.S. Garton, and M.W.D. Mansfield, Astrophys. J. 165, 203 (1971).

Cosslett, V. E. and W. C. Nixon, Nature (London) 168, 24 (1951).

Cosslett, V. E. and W. C. Nixon, J. Appl. Phys. 24, 616 (1953).

Cosslett, V. E. and W. C. Nixon, X-Ray Microscopy (Cambridge Univ. Press, Cambridge, 1960).

Cramer, S. P., T. K. Eccles, F. W. Kutzler, K. O. Hodgson, and L. E. Mortenson, J. Amer. Chem. Soc. 98, 1287 (1976).

Davis, D. W., D. A. Shirley, and T. D. Thomas, J. Amer. Chem. Soc. 94, 6565 (1972).

Dicke, R. H., Phys. Rev. 93, 99 (1954).

Dicke, R. H., "The Coherence Brightened Laser," Quantum Electronics, Proc. of the Third Int'l. Conference on Quantum Electronics, Eds. Grivet and Bloembergen, Vol. I (Columbia Univ. Press, New York, 1964), p. 35.

Doniach, S. and M. Sunjic, J. Phys. C3, 285 (1970).

Drake, G.W.F., G. A. Victor, and A. Dalgarno, Phys. Rev. 180, 25 (1969).

Duguay, M. A., Laser Focus, 41 (November 1973).

Duguay, M. A. and P. M. Rentzepis, Appl. Phys. Lett. 10, 350 (1967).

Dijkstra, J. A., W. de Graaff, and L. J. Lantward, New Techniques in Space Astronomy, Eds. F. Labuhn and R. Lüst (I.A.U., 1971), p. 207.

Dyson, N. A., Proc. Phys. Soc. 73, 924 (1959).

Eastman, D. E., in "Research Applications of Synchrotron Radiation," Eds. R. E. Watson and M. L. Perlman, Rept. No. BNL 50381 (Brookhaven National Laboratory, Upton, N.Y., Sept. 25-28, 1972).

Ederer, D. L. and S. C. Ebner, A User Guide to SURF (N.B.S., Washington, D.C., 1975).

Edholm, P. and B. Jacobson, Acta Radiologica 52, 337 (1959).

Eisenberger, P. and S. L. McCall, Phys. Rev. Lett. 26, 684 (1971).

Eisenberger, P., X-Ray Physics and Radiation Sources in "Research Applications of Synchrotron Radiation," Eds. R. E. Watson and M. L. Perlman, Rpt. No. BNL 50381 (Brookhaven National Laboratory, Upton, N.Y., Sept. 25-28, 1972).

Eisenberger, P., P. M. Platzman, and H. Winick, Phys. Rev. Lett. 36, 623 (1976).

Ejiri, A. and T. Sasaki, J. Phys. Soc. (Japan) 20, 876 (1965).

Elango, M., C. Gälwiller, and F. C. Brown, Solid St. Commun. 8, 893 (1970).

El-Sum, H.M.A., "Reconstructed Wavefront Microscopy," Ph.D. thesis (Stanford University, 1952).

El-Sum, H.M.A. and P. Kirkpatrick, Phys. Rev. 85, 763 (1952).

Elton, R. C., Appl. Opt. 14, 97 (1975).

Engström, A., Acta Radiologica, Suppl. 63 (1946).

Evans, R. D., in American Institute of Physics Handbook, Ed. D. E. Gray (McGraw-Hill, New York, 1963, 2nd. ed.).

Fadley, C. S. and S.A.L. Bergström, Phys. Lett. 35A, 375 (1971).

Fadley, C. S. and D. A. Shirley, Phys. Rev. Lett. 21, 980 (1968).

Fawcett, B. C., A. H. Gabriel, F. E. Irons, N. J. Peacock, and P.A.H. Saunders, Proc. Phys. Soc. (London) 88, 1051 (1966).

Fay, B. and J. Trotel, Appl. Phys. Lett. 29, 370 (1976).

Feder, R., E. Spiller, J. Topalian, and M. Hatzakis, "High Resolution X-Ray Lithography with Carbon K_α Radiation," Abstr. 185, Seventh Int'l. Conf. on Electron and Ion Beam Science and Technology (Washington, D.C., May 2-7, 1976), Extended Abstracts 76-1, 472, Electrochemical Society (Princeton, N.J., 1976).

Feit, E. D., L. F. Thompson, and L. E. Stillwagon, Coatings and Plastics Preprints, 35-2, American Chemical Soc. (170th Meeting, Chicago, August 25-29, 1975), p. 287.

Ferrell, R. A. and E. A. Stern, Am. J. Phys. 30, 810 (1962).

Feser, K., J. Müller, G. Wiech, and A. Faessler, J. de Phys. Colloq. 32, 331 (1971).

Fourie, J. T., Phil. Mag. 17, 735 (1968).

Fox, J. D., W. J. Courtney, K. W. Kemper, A. H. Lumpkin, N. R. Fletcher, and L. R. Medsker, Phys. Rev. Lett. 37, 629 (1976).

Gabor, D. A., Nature 161, 777 (1948).

Gabor, D. A., Proc. Roy. Soc. A197, 454 (1949).

Garton, W.R.S., J. Sci. Instrum. 36, 11 (1959).

Garton, W.R.S., in Adv. Atom. Molec. Phys., Vol. 2., Eds. D. R. Bates and I. Estermann (Academic Press, New York, 1966), p. 93.

Gelius, U., et al., Chem. Phys. Lett. 28, 1 (1974).

Gentry, R. V., T. A. Cahill, N. R. Fletcher, H. C. Kaufmann, L. R. Medsker, J. W. Nelson, and R. G. Flocchini, Phys. Rev. Lett. 37, 11 (1976).

Giacconi, R., W. P. Reidy, G. S. Vaiana, L. P. Van Speybroeck, and T. F. Zehnpfennig, Space Science Rev. 9, 3 (1969).

Gipstein, E., W. Moreau, and O. Need, J. Electrochem. Soc. 123, 1105 (1976).

Godwin, R. P., Springer Tracts in Modern Physics, Vol. 51 (Springer Verlag, Berlin, 1969).

Goldanskii, V. I. and V. S. Letokhov, Zh. Eksp. Teor. Fiz. 67, 513 (1974) [English Transl.: Sov. Phys.-JETP 40, 254 (1975)].

Goodman, J. W., Introduction to Fourier Optics (McGraw-Hill, New York, 1968).

Greeneich, J. S., IEEE Trans. Electron. Devices, ED-22, 434 (1975).

Griem, H. R., Plasma Spectroscopy (McGraw-Hill, New York, 1964), Ch. 4.

Griem, H. R., Spectral Line Broadening by Plasmas (Academic Press, New York, 1974).

Hagouel, P. I. and A. R. Neureuther, Coatings and Plastic Preprints, 35-2, American Chemical Soc. (170th Meeting, Chicago, August 25-29, 1975), p. 289.

Harris, S. E., Phys. Rev. Lett. 31, 341 (1973).

Harris, S. E. and R. B. Miles, Appl. Phys. Lett. 19, 385 (1971).

Hatzakis, M., J. Electrochem. Soc. 116, 1033 (1969).

Henke, B. L., "Some Notes on Ultrasoft X-Ray Analysis," Adv. in X-Ray Analysis, Vol. 8 (Plenum Press, New York, 1965), p. 269ff.

Henke, B. L., "Techniques of Low Energy X-Ray Spectroscopy - 0.1-2 keV Region," Advances in X-Ray Analysis (Plenum Press, New York, 1974), p. 76.

Herzenberg, A. and H.S.M. Lau, Acta Crystallogr. 22, 24 (1967).

Herzog, R. F., J. S. Greeneich, T. E. Everhardt, and T. van Duzer, IEEE Trans. Electron. Devices ED-19, 635 (1972).

Heycock, C. T. and F. H. Neville, J. Chem. Soc. 73, 714 (1898).

Hildenbrand, G., Fortschr. d. Phys. 4, 1 (1956).

Hoeneisen, B. and C. A. Mead, Solid State Electron. 15, 819, 891 (1972).

Horowitz, P. and J. A. Howell, Science 178, 608 (1972).

Hunt, J. W. and J. K. Thomas, Radiation Res. 32, 149 (1967).

Ianniello, L. C. "Radiation-Induced Voids in Metals," USAEC Symposium Ser. 26 (1972).

Jacobson, B., Acta Radiologica 39, 437 (1953).

Jacobson, B., Amer. J. of Roentgenol. Rad. Ther. and Nucl. Med. 91, 202 (1964).

Jaeglé, P., A. Carrillon, P. Dhez, G. Jamelot, A. Sureau, and M. Cukier, Phys. Lett. A36, 167 (1971).

Jentzsch, F., Phys. Z. 30, 268 (1929).

Johansson, T., Z. Physik 82, 507 (1933).

Jones, J. L., K. W. Paschen, and T. B. Nicholson, Appl. Opt. 2, 955 (1963).

Kelcz, F. and C. A. Mistretta, Med. Phys. 3, 159 (1976).

Keyes, R. W., Proc. IEEE 63, 740 (1975).

Kincaid, B., Bell Labs. preprint (1976), submitted to J. Appl. Phys.

Kirkpatrick, P. And A. V. Baez, J. Opt. Soc. Am. 38, 766 (1948).

Kliwer, J. K., J. Appl. Phys. 44, 490 (1973).

Klucker, R., H. Nelkowski, Y. S. Park, M. Skibowski, and T. S. Wagner, Phys. Stat. Solidi 45, 265 (1971).

Koehler, W. F., J. Opt. Soc. Amer. 43, 743 (1953).

Kompfner, R., private communication (1976).

Koopmans, T., Physica 1, 104 (1934).

Kowalczyk, S. P., R. A. Pollak, F. R. McFeely, L. Ley, and D. A. Shirley, Phys. Rev. B8, 2387 (1973).

Kramer, I. R., Trans. Met. Soc. AIME 233, 1462 (1968).

Kroll, N., "High-Energy Visible and Ultraviolet Lasers," Stanford Research Institute Rpt. JSR-74-1 (1975), p. 69.

Kruger, J. B., Y. Wu, and H. Yuan, J. Vac. Sci. Technol. 12, 1301 (1975).

Kung, A. H., J. F. Young, G. C. Bjorklund, and S. E. Harris, Phys. Rev. Lett. 29, 985 (1972).

Kung, A. H., J. F. Young, and S. E. Harris, Appl. Phys. Lett. 22, 301 (1973).

Ladd, W. A., W. M. Hess, and M. W. Ladd, Science 123, 370 (1956).

Ladd, W. A. and M. W. Ladd, X-Ray Microscopy and Microradiography (Academic Press, New York, 1957), p. 383.

Lane, R. O. and D. J. Zaffarano, Phys. Rev. 94, 960 (1954).

Lang, J., Appl. Phys. 30, 1748 (1959).

Langner, G., X-Ray Microscopy and Microradiography (Academic Press, New York 1957), p. 293.

Leith, E. N. and J. Upatneiks, J. Opt. Soc. Amer. 52, 1123 (1962).

Leith, E. N. and J. Upatnieks, J. Opt. Soc. Amer. 54, 1295 (1964).

Lemke, D. and D. Labs, Appl. Optics 6, 1043 (1967).

Letokhov, V. S., Phys. Lett. 51A, 231 (1975).

Liénard, A., L'Eclairage Elect. 16, 5 (1898).

Lorents, D. C., Radiation Research 59, 438 (1974).

Lotz, W., J. Opt. Soc. Am. 58, 915 (1968).

Louisell, W. H., M. O. Scully, and W. B. McKnight, Phys. Rev. A11, 989 (1975).

McCoy, J. H. and P. A. Sullivan, "Progress in X-Ray Lithography," Proc. Sixth Int'l. Conference on Electron. and Ion Beam Science and Technology, Ed. R. Bakish (Electrochemical Society, Princeton, N.J., 1974), p. 3.

McCoy, J. M. and P. A. Sullivan, Solid State Techn. 19 (1976).

McCoy, J. M. and P. A. Sullivan, "Precision Mask Alignment for X-Ray Lithography," Abstr. 183, Seventh Int'l. Conference on Electron and Ion Beam Science and Technology (Washington, D.C., May 2-7, 1976), Extended Abstracts 76-1 (Electrochemical Society, Princeton, N.J., 1976), p. 468.

McCrickerd, J. T. and N. George, Appl. Phys. Lett. 12, 10 (1968).

Madden, R. P., D. L. Ederer, and K. Codling, Appl. Opt. 6, 31 (1967).

Madden, R. P. and D. L. Ederer, J. Opt. Soc. Am. 62, 772 (1972).

Madey, J.M.J, J. Appl. Phys. 42, 1906 (1971).

Madey, J.M.J., H. A. Schwettman, and W. M. Fairbank, "A Free-Electron Laser," 1973 Particle Accelerator Conference, San Francisco, California, Rpt. HEPL-704 (Stanford University, Stanford, California, 1973).

Mahrand, H. and U. Roeder, Opt. Commun. 10, 227 (1974).

Malozzi, P. J., H. M. Epstein, R. G. Jung, D. C. Applebaum, B. P. Fairand, and W. J. Gallagher, Battelle Memorial Institute Report (Columbus, Ohio, 1972).

Malozzi, P. J., H. M. Epstein, R. G. Jung, D. C. Applebaum, B. P. Fairand, and W. J. Gallagher, "Fundamental and Applied Laser Physics," Proc. Esfahan Symposium, Eds. A. Jaram and M. S. Field (J. Wiley, New York, 1973).

Marr, G. V., Electron and Photon Interactions with Atoms, Eds. H. Kleinpoppen and M.R.C. McDowell (Plenum Press, New York, 1976) p. 46.

Martin, F. W. and R. K. Cacak, "A Double-Focussing Soft X-Ray Spectrometer," Tech. Rpt. No. 75-092 (Univ. of Maryland, 1975).

Matheson, M. S. and L. M. Dorfman, Pulse Radiolysis (MIT Press, Mass., 1969).

Mavrogenet, G. S., C. Jonah, K. H. Schmidt, S. Gordon, G. R. Tripp, and L. W. Coleman, Res. Sci. Instr. 47, 187 (1976).

Maydan, D., G. A. Coquin, J. R. Maldonado, S. Somekh, D. Y. Lou, and G. N. Taylor, IEEE Proc. Electron. Devices, ED-22, 429 (1975).

Mead, S. W., R. E. Kidder, J. C. Swain, F. Ranier, and J. Petruzzi, Appl. Opt. 11, 345 (1972).

Miles, R. B. and S. E. Harris, IEEE J. Qu. Electr. QE-9, 470 (1973).

Missoni, G. and A. Ruggiero, Atta Acad. Naz. Lincei, Re. (Sci. Fis. Mat. Nat.) 38, 677 (1965).

Mistretta, C. A., M. G. Ort, F. Kelcz, J. R. Cameron, M. P. Siedband, and A. B. Crummy, Invest. Radiol. 8, 402 (1973).

Molchanov, A. G., Usp. Fiz. Nauk. 106, 165 (1972) [English Transl.: Sov. Phys. Uspekhi 15, 124 (1972)].

Möllenstedt, G. and L. Y. Huang, X-Ray Microscopy and Microradiography (Academic Press, New York, 1957), p. 392.

Motz, H. and M. Nalsurnura, Proceedings of the Symposium on Millimeter Waves, Microwave Research Institute Symposium Series, Vol. IX (Interscience, New York, 1960), p. 155.

Mueller, R. K., Advances in Holography, Ed. N. Farhat, Vol. 1 (Dekker, New York, 1975).

Müller, E. M. and T. T. Tsong, Field Ion Microscopy (Amer. Elsevier Publ., New York, 1969).

National Academy of Sciences, "An Assessment of the National Need for Facilities Dedicated to the Production of Synchrotron Radiation" (Washington, D.C., 1976), Table 6, p. 70.

Neuteuther, A. R., and P. I. Haguel, "X-Ray Lithographic Fabrication of Blazed Diffraction Gratings," Proc. Sixth Int'l. Conference on Electron and Ion Beam Science and Technology, Ed. R. Bakish (Electrochemical Society, Princeton, N.J., 1974) p. 23.

Niemann, B, D. Rudolph, and G. Schmahl, Opt. Commun. 12, 160 (1974).

Nordgren, J., H. Ågren, C. Nordling, and K. Siegbahn, "High Resolution X-Ray Emission Spectrum of Argon," Int'l. Conference on the Physics of X-Ray Spectra, Ed. R. D. Deslattes (N.B.S., Gaithersburg, Md., Aug. 30-Sept. 2, 1976), p. 250.

Ort, M. G., C. A. Mistretta, and F. Kelcz, Optical Eng. 12, 169 (1973).

Ozdemir, F. S.. G. O. Ladd, D. D. Loper, F. W. Cleary, and N. Hirsch, "Electron Beam Microfabrication of GaAs SBFET's," Abstract 198, Seventh Int'l. Conference on Electron and Ion Beam Science and Technology (Washington, D.C., May 2-7, 1976), Extended Abstracts 76-1, 501 (Electrochemical Society, Princeton, N.J., 1976).

Palmer, R. C. and R. L. McGuire, Trans. IEEE on Nuclear Science NS-14 (No. 1), 217 (1967).

Pantell, R. H ., G. Soncini, and H. E. Puthoff, IEEE J. Quant. Elec. QE-4, 905 (1968).

Parratt, L. G., Rev. Sci. Instrum. 30, 297 (1959).

Paul, W. and H. Steinwedel, Beta and Gamma-Ray Spectroscopy, Ed. K. Siegbahn (N. Holland Publ. Co., Amsterdam, 1955), p. 1.

Peavey, J. and D. Lichtman, Surface Sci. 27, 649 (1971).

Perlman, M. L., E. M. Rowe, and R. E. Watson, Physics Today, 30, (July 1974).

Pfeifer, C. D., L. D. Ferris, and W. M. Yen, J. Opt. Soc. Amer. 63, 91 (1973).

Phillips, J. C., A. Wlodawer, M. M. Yevitz, and K. O. Hodgson, Proc. Nat. Acad. Sci. USA 73, 128 (1976).

Pitz, E., Appl. Optics 8, 255 (1969).

Platzman, P. M., "Resonant X-Ray Raman Scattering from Solids," in Program and Extended Abstracts, Int'l. Conf. of the Physics of X-Ray Spectra (N.B.S., Gaithersburg, Md., Aug. 30-Sept. 2, 1976), p. 67.

Pocker, D. W. and T. W. Haas, J. Vac. Sci. Technol. 12, 370 (1975).

Ranwez, F., C. R. Acad. Sci. (Paris) 122, 841 (1896).

Redman, J. D., J. Sci. Instr. 1, 821 (1968).

Reid, N. W., Int. J. Mass Spectrom. Ion Phys. 6, 1 (1971).

Rhodes, C. K., IEEE J. Quant. Electr. QE-10, 153 (1974).

Roberts. E. D., Philips Tech. Rev. 35, 41 (1975).

Rogers, G. L., Nature 166, 237 (1950).

Rogers, G. L., Proc. Roy. Soc. (Edinb.) 63A, 193 (1952).

Röntgen, W. C., Sitzungber. Phys.-Med. Ges. Würzburg, 137 (1895).

Rosenbaum, G., K. C. Holmes, and J. Witz, Nature (London) 230, 434 (1971).

Rowe, J. E., M. M. Traum, and N. V. Smith, Phys. Rev. Lett. 33, 1333 (1974).

Samson, J.A.R., Techniques in Vacuum Ultraviolet Spectroscopy (Wiley, New York, 1967).

Schawlow, A. L. and C. H. Townes, Phys. Rev. 112, 1940 (1958).

Schnopper, H. W., private communication (1976).

Schnopper, H. W., submitted to Appl. Opt. (1976).

Schwinger, J., Phys. Rev. 70, 798 (1946).

Schwinger, J., Phys. Rev. 75, 1912 (1949).

Scully, M. O., W. H. Louisell, and W. B. McKnight, Opt. Commun. 9, 246 (1973).

Sellin, I. A. and D. J. Pegg, Eds., Beam-Foil Spectroscopy, Vol. 2 (Plenum Press, New York, 1976).

Shatas, R. A., J. D. Stettler, H. C. Meyer, and T. G. Roberts, J. Appl. Phys. 42, 5884 (1971).

Shipman, J. D., Appl. Phys. Lett. 10, 3 (1967).

Shirley, D. A., Ed., Electron Spectroscopy (North Holland, Amsterdam, 1972).

Shirley, D. A., et al., "Core-Level Binding Energies of the First Thirty Elements," Lawrence Berkeley Report LBL-4065 (Phys. Rev. B, to be published, 1976).

Shuttleworth, E., A. Wilson, J. D. Redman, and W. P. Walton, Brit. J. Radiol. 42, 152 (1969).

Siegbahn, K., et al., Nova Acta Regiae Soc. Sci. Upsaliensis Ser. IV, 20 (1967).

Siegbahn, K., et al., ESCA-Atomic, Molecular and Solid State Structure Studied by Means of Electron Spectroscopy (North-Holland Publ. Co., Amsterdam, 1967).

Siegbahn, K., et al., ESCA Applied to Free Molecules (North-Holland Publ. Co., Amsterdam, 1969).

Siegbahn, K., in Electron Spectroscopy, D. A. Shirley, Ed., Proc. Int'l. Conference, Asilomar (North-Holland Publ. Co., Amsterdam, 1972), p. 15.

Sinclair, C. K., J. J. Murray, P. R. Klein, and M. Rabin, IEEE Trans. Nuclear Science 16, 1065 (1969).

Skibowski, M., B. Feuerbacher, and W. Steinmann, Z. Physik 211, 329 (1968).

Smith, H. I., Proc. IEEE 62, 1361 (1974).

Sokolov, A. A. and I. M. Ternov, Synchrotron Radiation (Academic Verlag, Berlin, 1968).

Sparks, C. L., Phys. Rev. Lett. 33, 262 (1974).

Spears, D. L. and H. I. Smith, Electronics Lett. 8, 102 (1972).

Spiller, E., R. Feder, J. Topalian, E. Castellani, L. Romankiw, and M. Heritage, Solid State Techn. 19, 62 (1976).

Spiller, E., R. Feder, J. Topalian, W. Gudat, and D. Eastman, "X-Ray Lithography with Synchrotron Radiation," Abstract 186, Seventh Int'l. Conference on Electron and Ion Beam Science and Technology (Washington D.C., May 2-7, 1976), Extended Abstracts 76-1, 474 (Electrochemical Society, Princeton, N.J., 1976), p. 233.

Spiller, E., et al., Science 191, 1172 (1976).

Stankevich, Yu. L., Dokl. Akad. Nauk SSSR 191, 805 (1970)[English Transl.: Sov. Phys.-Doklady 15, 356 (1970)].

Steinberg, B. D., Principles of Aperture and Array Systems Design (Wiley, New York, 1976).

Steinmann, W. and M. Skibowski, Phys. Rev. Lett. 16, 989 (1966).

Suh, N. P., Wear 25, 11 (1973).

Suh, N. P., Wear 28, 235 (1974).

Sullivan, P. A., "X-Ray Lithography System Complete with Interdigital Transducer Master," Final Report on Contract No. F19628-75-C-0105, Report No. AFCRL-TR-0573, Nov. 1975.

Sullivan, P. A. and J. M. McCoy, J. Vac. Sci. Technol. 12, 1325 (1975).

Sullivan, P. A. and J. M. McCoy, IEEE Trans. Electron. Devices, ED-23, 412 (1976).

Sweeney, D. and C. Vest, Appl. Opt. 12, 2649 (1973).

Taylor, G. N. and G. A. Coquin, "Sensitive Chlorine-Containing Resists for X-Ray Lithography," to be presented at the Fourth Int'l. Conference on Photopolymers (Ellenville, N.Y., October 13-15, 1976).

Tetelman, A. S, and A. J. McEvily, Introduction to Fundamentals of Fracture in Engineering Materials (McGraw-Hill, New York, 1968).

Thomas, J. K., Int. J. Rad. Phys. Chem. 8, 1 (1976).

Thomas, J. K., Am. Rev. Phys. Chem. 21, 17 (1970a).

Thomas, J. K., "Charged Particle Tracks in Solids and Liquids" (The Institute of Physics and the Physical Society Conference, Ser. No. 8, 1970b).

Thomas, J. K., Rec. Chem. Progr. 32, 145 (1971).

Thomas, J. K. and E. J. Hart, Rad. Res. 17, 408 (1962).

Thomas, J. K. and E. J. Hart, J. Phys. Chem. 68, 2414 (1964).

Thomas, J. K., K. Johnson, T. Klippert, and R. Lowers, J. Chem. Phys. 48, 1608 (1968).

Thomas, G., et al., J. Mat. Sci. Engineering 16, 201 (1974).

Thompson, L. F., E. D. Feit, M. J. Bowden, P. V. Lenzo, and E. G. Spencer, J. Electrochemical Soc. 121, 1500 (1974).

Tolanski, S., Multiple-Beam Interferometry (Clarendon Press, Oxford, 1948).

Tomboulian, D. H. and P. L. Hartman, Phys. Rev. 102, 1423 (1956).

Trammell, G. T., Physics Today, 57 (July 1976).

Van Dilla, M. A., T. T. Trujillo, P. F. Mullaney, and J. R. Coulter, Science 163, 1213 (1969).

Van Trees, H. L., Detection and Modulation Theory, Part 1 (J. Wiley, New York 1967).

Vekhov, A. A., V. N. Makhov, F. A. Nikolaev, and V. B. Rozanov, Kvant. Electron. (Moscva) 2, 1318 (1975)[English Transl.: Sov. J. Quant. Electron. 5, 718 (1975)].

Vinogradov, A. V. and I. I. Sobel'man, Sov. Phys.-JETP 36, 1115 (1973).

Wagner, C. D. and P. Biloeu, Surface Sci. 35, 82 (1973).

Watson, R. E. and M. L. Perlman, Eds., "Research Applications of Synchrotron Radiation," Report No. BNL 50381 (Brookhaven National Laboratory, Upton, N.Y., Sept. 25-28, 1972).

Watts, R. K., H. M. Darley, J. B. Kruger, T. G. Blocker, D. C. Guterman, J. T. Carlo, D. C. Bullock, and M. S. Shaikh, Appl. Phys. Lett. 28, 355 (1976).

Waynant, R. W. and R. C. Elton, Proc. IEEE 64, 1059 (1976).

West, J. B., K. Codling, and G. V. Marr, J. Phys. E7, 137 (1974).

Wheaton, J.E.G., Appl. Optics 3, 1247 (1964).

Whiddington, R., Proc. Roy. Soc. (London) A86, 365 (1912).

Whiddington, R., Proc. Roy. Soc. (London) A89, 554 (1914).

Wolff, R. K., M. J. Bronskill, and J. W. Hunt, J. Chem. Phys. 53, 4211 (1970).

Wolter, H.,Am. Phys., Lpz. 10, 94 and 286 (1952).

Wood, L., G. Chapline, S. Slutz, and G. Zimmerman, UCRL-75184, Rev. I, Lawrence Livermore Laboratory, California (1973).

Wood, L. and G. Chapline, UCRL-75255 Rev. II, Lawrence Livermore Laboratory, California (1974).

Worthington, C. R. and S. G. Tomlin, Proc. Phys. Soc. A69, 401 (1956).

Yamanaka, C, T. Yamanaka, H. Kang, K. Yoshida, M. Waki, and T. Shimamura, Phys. Lett. A38, 495 (1972).

Young, J. F., G. C. Bjorklund, A. H. Kung, R. B. Miles, and S. E. Harris, Phys. Rev. Lett. 27, 1551 (1971).

Young, J. R., J. Appl. Phys. 27, 1 (1956).

Young, J. R., J. Appl. Phys. 28, 524 (1957).

Yu, H. N., R. H. Dennard, T. H. P. Chang, C. M. Osburn, V. Dilonardo, and H. E. Luhn, J. Vac. Sci. Technol. 12, 1297 (1975).

Zeldovich, Ya. B. and Yu. P. Raizer, Physics of Shock Waves and High-Temperature Hydrodynamic Phenomena, Vol. I, (Academic Press, New York, 1966), § III.5.

Zernike, F., Z. Tech. Phys. 16, 454 (1935).

Zernike, F., Physica 9, 686, 974 (1942).

X-RAY SOURCE REQUIREMENTS FOR MICROREPLICATION

ADDITIONAL BIBLIOGRAPHY

Bernacki, S. E. and H. I. Smith, "X-Ray Lithography Applied to Silicon Device Fabrication," Proc. Sixth International Conference on Electron and Ion Beam Science and Technology, Ed. R. Bakish (Electrochemical Society, Princeton, N.J., 1974), p. 34.

Bernacki, S. E. and H. I. Smith, J. Vac. Sci. Technol. 12, 1321 (1975).

Feder, R., E. Spiller and J. Topalian, J. Vac. Sci. Technol. 12, 1332 (1975).

Greeneich, J. S., Appl. Phys. Lett. 27, 579 (1975).

McCoy, J. H. and P. A. Sullivan, "Progress in X-Ray Lithography," Proc. Sixth International Conference on Electron and Ion Beam Science and Technology, Ed. R. Bakish (Electrochemical Society, Princeton, N.J., 1974), p. 3

Maldonado, J. R., G. A. Coquin, D. Maydan, and S. Somekh, J. Vac. Sci. Technol. 12, 1329 (1975).

Smith, H. I., D. L. Spears, and S. E. Bernacki, J. Vac. Sci. and Technol. 10, 913 (1973).

Smith, H. I., D. L. Spears, and E. Stern, "Soft X-Ray Lithographic Apparatus and Process," U. S. Patent 3,743,842, July 3, 1973.

Spears. D. L. and H. I. Smith, Solid State Technology 15, 21 (1972).

Spears, D. L., H. I. Smith, and E. Stern, "Soft X-Ray Mask Support Substrate," U. S. Patent 3,742,230, June 26, 1973.

Spiller, E., R. Feder, J. Topalian, D. Eastman, W. Gudat, and D. Sayre, Science 191, 1172 (March 19, 1976).